Università degli Studi di Cagliari

Dipartimento di Ingegneria Elettrica ed Elettronica
Dottorato di Ricerca in Ingegneria Elettrica ed Informatica
Ciclo XXXI

Ph.D. Thesis

Planning and Management of Energy Storage in Microgrids according to Complex Network Approach

S.S.D. ING-IND 32

Author
Saman Korjani

Supervisor
Prof. Alfonso Damiano

PhD Coordinator
Prof. Fabio Roli

February 2019

Dedicated to *Why and Answer of It*

Abstract

This PhD dissertation deals with planning and management of Energy Storage System (ESS) in power systems. **Chapter 1** is devoted to the State of the Art of ESS technologies, discussing them according to their structure and physical and chemical proprieties. For each class, the most relevant ESSs are presented and briefly portrayed, featuring their main advantages and drawbacks. In this way, a general comparison is performed with regards of different characterization of ESSs. **Chapter 2** refers to planning and management of ESSs in a power system and presents the genetic algorithm-based multi-period optimal power flow (GA-MPOPF) a management method that includes degradation costs in the economic optimization of ESS. The GA-MPOPF includes complex aging function taking into account cycle and calendar degradation costs. This is still an open issue, mainly due to the difficult estimation of cycle aging in presence of high penetration of intermittent Renewable Energy Sources (RESs). The proposed method has been exploited in two different microgrid applications based on real load and generation data: (1) planning of the optimal position of a Li-ion battery ESS (BESS) in the standard 69 IEEE bus network with high RES penetration; (2) the economic management of BESS including cycle and calendar costs. Results demonstrate that GA-MPOPF can optimize the BESS use for one month, notwithstanding the complex operative costs functions, guaranteeing in the meantime excellent convergence properties. **Chapter 3** deals with Real-Time planning and management of ESSs in the power systems. The presented GA-MPOPF has been extended to the case of Real-Time aging cost management by including a prediction algorithm based on system identification methods.Two main goals are considered: first, to have a correct BESS size within planning approach; real-time management of the BESS State of Charge (SoC) by taking into account the its degradation costs minimizing the total costs for the whole microgrid. Results show that the accuracy of cost optimization in real time is comparable with the ideal case of a perfect knowledge of the future (i.e. using for Real-Time optimization the actual data). Results also confirm that the method is able to optimize complex cost functions highlighting that a careful sizing of BESS is need to avoid economic losses due to BESS aging costs. **Chapter 4** introduces a criterion for the optimal placement of active and reactive power compensator (i.e. ESS) based on complex networks centrality metrics aiming at voltage regulation. The chapter shows the relation between centrality measures and voltage fluctuations in power networks with high penetration of RESs and ESSs. In fact, the correlation between network node centrality (namely Eigenvector, Closeness, Pagerank, Betweenness) and voltage fluctuations is sta-

tistically significant implying that the topological characteristics of the power networks are enough to find the optimal positioning of active and reactive power compensators. The results demonstrate that eigenvector centrality shows a statistically significant exponential correlation as the voltage stability increases. This finding provides a quick and easy way to position reactive power compensators in complex networks without the need to compute the traditional Optimal Power Flow (OPF).

Acknowledgements

This work was developed within the project NETfficient, Energy and Economic Efficiency for Today's Smart Communities through Integrated Multi Storage Technologies. This project has received funding from the European Unionfis Horizon 2020 research and innovation programme under grant agreement No. 646463.

Firstly, I would like to express my sincere gratitude to my advisor Prof. Alfonso Damiano for the continuous support of my PhD study and related research, for his patience, motivation, and immense knowledge. His guidance helped me in all the time of research and writing of this thesis. I could not have imagined having a better advisor and mentor for my Ph.D study.

Besides my advisor, my sincere thanks also goes to Dr. Mario Mureddu, and Dr. Angelo Facchini, for their insightful comments and encouragement, but also for the hard question which incented me to widen my research from various perspectives.

Last but not the least, I would like to thank my family and my friends for supporting me spiritually throughout writing this thesis and my my life in general.

Contents

List of Figures

List of Tables

Introduction

Recently, power systems are transformed in new concept because of wide usage of RESs. RESs experienced a quick development in recent decades because of technological enhancements that have continuously decreased their capital expenses and expanded their effectiveness in the meantime. However, RESs challenge the power system stability due to their intermittent nature. Indeed, RESs utilization in power systems requires an accurate planning and real-time control strategies, which need to deal with estimating errors and energy market necessities. In the meantime, ESSs grab the distribution system operators attention because of their ability to moderate power systems issues caused by RESs such as frequency and voltage instabilities. In fact, ESSs can be used as RES energy market buffers, thus, storing energy when the price of energy is low and delivering it when the price is high. Along these lines, ESSs ought to be appropriately sized and managed with the specific end goal to accomplish an ideal balance between increased performances and operational and capital expenses.

The present PhD dissertation deals with planning and management of ESSs in microgrids. **Chapter 1** is a review covering the State of the Art of ESS and their applications: here different technical and market characteristic of ESSs are discussed showing their most important advantages and drawbacks. **Chapter 2** presents the GA-MPOPF method, a novel multi-period OPF methodology based on Genetic Algorithm (GA) and traditional OPF. GA-MPOPF considers a complex cost functions defined over an arbitrary time period (e.g. the ESS operative costs), considering the ESSs degradation as an optimization item, likewise recognizing the optimal usage strategy of ESSs in a power system from the cost point of view. The GA-MPOPF procedure can enhance both planning and unit-commitment issues in presence of different types of RES and Fossil-Fuel generators, loads and ESSs. As test case, the GA-MPOPF method has been applied to a Virtual Power Planet (VPP) following a specific power profile during the 24 hours and a deviation from such profile implies an extra cost for the VPP aggregator under the form of a fine. The role of installed ESS in VPP is to mitigate the VPP fluctuations in order to reduce the total fines in a specific timeframe. The proposed method is applied from both management and planning viewpoint while management consists in the optimization of ESS by reducing the operational costs considering both cycle and calendar aging costs, tested on a monthly timeframe. The planning process consists in finding the optimal position of the ESS from electric perspective. **Chapter 3** deals with Real-Time planning and management of ESS in microgrids.An improved version of the GA-MPOPF

method presented and called Real-Time GA-MPOPF. The Real-Time GA-MPOPF allows for the optimization of complex cost functions over an extend time period considering ESS degradation costs and optimizing its usage in the power system taking into account energy market costs. Real-time optimization requires an optimization in each phase of real-time step and must be performed over an extended time period. The Real-Time GA-MPOPF method is able to optimize both Multi-Period and real-time aging costs of ESS. As test the ESS is installed in a VPP whose goal in each real time interval is to follow a specific power profile defined for the next 24 hours. Any aberration from such profile produces an extra cost for the VPP aggregator under the form of a fine. **Chapter 4** presents a novel criterion for the optimal placement of ESS based on complex network theory, finding a statistically significant correlation between the node eigenvector centrality and the optimal position of ESS, with a positive impacts on their voltage regulation abilities, and a overall reduction of the voltage fluctuations by a value up to 50%, significantly increasing the power quality. Each section is categorized by introduction, methods and study case, results and conclusions.

This work was developed within the project NETfficient, Energy and Economic Efficiency for Today's Smart Communities through Integrated Multi Storage Technologies. This project has received funding from the European Unionfis Horizon 2020 research and innovation programme under grant agreement No. 646463.

Chapter 1

Applications of Energy Storage Systems

The storage of energy sources has been a common pattern in human history. The ability to master and store ready-to-use energy sources for needing times has been proven to be a valuable resource for human survival. In recent times, due to spread of usage of Renewable Energies Sources (RES) in the power networks, the importance of Energy Storage Systems (ESS) is growing [7, 8].

ESSs are seen as a solution to the above mentioned challenge by facilitating the increase in the penetration of renewable energy sources, reducing the load curve [9, 10], helping to control the frequency [11, 12, 13], reducing voltage fluctuations [14, 15, 16], improving the quality of power [17, 18] reliability [18, 19]and delaying the development of transmission lines [20].

Currently, more than 176 GWh of large scale ESSs are installed on power systems around the world. The vast majority (96%) of this capacity includes pumped hydroelectric energy storage (PHES). The other 4% includes a combination of battery technologies with 1.9 GWh (1.1%) , thermal storage with 3.3 GWh (1.9%) and other mechanical storage with 1.6 GWh (0.9%) [21]. Fig. 1.1 shows the shared installed capacities of ESSs around the world [21].

This Chapter presents a short overview of the most important ESSs mentioned in the literature. In section 1.1 most important application of ESSs is described. Different type of ESSs and subsequently, their technical and market characteristic and their most important advantages and disadvantages has been presented in section 1.2.

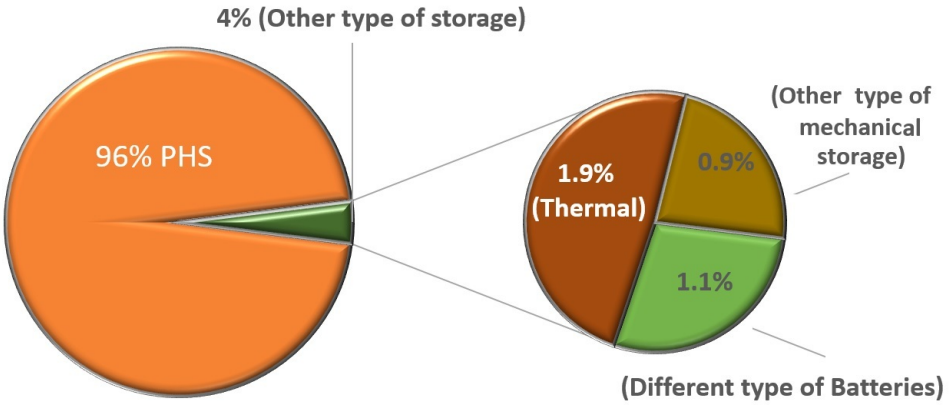

Figure 1.1: Different installed ESS around the world.

1.1 Applications of energy storage

The value of energy storage technologies is to provide different services in energy systems, providing infrastructure services in the supply, transmission, distribution and consumption parts of energy systems. These technologies are used in heat and cooling units, some other non-electric appliance applications, as well as electricity distribution and transmission systems.

By extending the usage of RESs in the power systems the role of ESSs are more important than before, due to their application to cope the unexpected fluctuations generated by RESs. Large-scale electrical energy storage technologies have many applications. In fact, different ESSs can be used for different applications, regarding of their energy and power density, response time. For example, for applications of power system stabilization such as power quality and emergency power resources, they can provide non-stop energy with ability of the depletion of energy in a fraction of a second, energy stabilization applications like energy storing with ability of providing energy within a minute (short-term), around an hour (medium-term) and days (long-term) for the aim of energy management, load curve balancing and peak shaving. Here some key applications of ESSs are mentioned;

- Seasonal Storage;
  The ability of storing energy for the duration of day, week, month in order to compensate the deficiencies in the long-term supply of electricity and/or the seasonal variation which can be happen in supply and demand of the energy systems [22, 23].

- Arbitrage - Energy Trades;

In this case, cheap energy is stored during a period in which demand is low prices and then sold at a time when demand is high prices. Generally, this type of energy trade has been expressed between two different energy markets. However, it sometimes is energy trade between costumers and energy providers within the concept of the smart grid [24, 25].

- Frequency Regulation;
  In the power systems, consumption and generation of energy must be in balance amid all circumstances. The frequency of system is a value which can be used as a measurement option to check if the consumption and generation are equal. When the supply is more than consumption, the frequency goes higher, and when the consumption is more than supply, the frequency goes lower. ESSs are often used to provide flexibility to the network by acting as a buffer, when ESSs start to be charged the demand is rising and when ESSs start to be discharged the supply is increasing. In this manner ESSs can adjust demand and supply which is a way to control frequency [26, 27].

- Load Following Power Planets;
  The load following power planets commonly are keep running amid the day and early evening. They either shut down or enormously diminish to supply energy amid the night and early morning, when the demand for power is low. Nowadays, ESSs modify the output of the load following power planets. This is obtained by properly managing ESSs charge and discharge properties in order to reduce the unbalanced peaks [28].

- Voltage Regulation;
  Supporting the voltage, injecting, or absorbing reactive power to maintain the voltage levels of the transmission and distribution system in normal conditions, Especially, regulating the voltage for system with high penetration of RESs is necessary. By using both active and reactive power control, it is possible to have a regular voltage profile [29, 30]. Since, ESSs can provide active and reactive power, they are used for reducing the voltage fluctuations [31, 32].

- Deferral Transmission and Distribution Infrastructure Investment;
  Energy storage technologies are being used widely to eliminate congestions in transmission and distribution networks and postponing the need for large investments in the infrastructure of transmission and distribution networks [33, 8].

- Peak Shaving;
  In order to match demand and supply of electricity, and to help integrate various RESs to the power systems, energy demand can be transferred and shifted. ESSs have a significant role to facilitate performing of peak demand shift [34, 35].

- Off-the-Grid;
  The application of ESSs, increase the reliability of energy supply for self consumer

power grids and support to increase of usage of local resources. ESSs fill the gap between diverse supply and demand. Recently, optimal and simultaneous placement of distributed generators (DG) and the role ESSs in stand-alone power systems is one of the most important issues in power system studies [36, 37].

- Variable RES Integration to Power Systems;
  The use of ESSs bring big opportunity to employ various RESs to the power systems. ESSs are used to encounter uncertainties which are provided by RESs. They reduce the rapid and seasonal output of RESs, and they help to decrease geographical and time gap between both demand and supply in order to increase the quality and quantity of supply [38, 4].

1.1.1 Characteristic of ESS

Here the parameter of ESSs is shortly described. These characteristics are different for each ESS. So, for special application of power system, ESS should be selected with suitable characteristic. Since, investors are looking for economical and technical advantage of usage of ESSs, it is important to have a ESS with suitable properties. These parameters are Energy (E), Power (P), Energy to power ratio, Energy density, Power density, Storage capacity, Depth of Discharge (DoD), State of Charge (SoC), Efficiency (ζ), Self-Discharge, Full Cycle, Cycle Life and Calendar Life [39, 40, 41].

- Energy (E)
  Energy is basis element of power systems. Electrical energy can be generated in conversion of other kind of energies such as chemical, thermal, mechanical and nuclear. Energy unit is joule (J). In place of storage systems the energy concept can be described as capacity or the quantity of energy when it is charging into storage or when it is discharging from the storage. The common unit of energy for ESSs is Watt-hour (Wh).

- Power (P)
  The rate of energy in unit of time is the electric power. In the case of ESSs, power meaning is the amount of energy which can be supplied from ESS or can be charged into ESS in a unit of a time. For example, an ESS with high power capability can be charged or discharged the amount of energy in shorter time and an ESS with low power can be charged or discharged the amount of energy in longer time. The unit of power is Watt (W).

- Energy to power ratio
  Energy to power ratio is a common term for ESSs and it shows the rate of installed capacity in means of energy to installed power. An ESS with small energy to power rate can deliver power for shorter time than an ESS with high energy to power rate which it can provide power for long time[39, 40, 41].

- Energy density;
  The rate of installed energy capacity of ESS to its volume is energy density and the common used unit is $kWh/liter$ or kWh/m^3 or specific energy density can be described as rate of installed energy capacity of ESS to its weight with unit of kWh/kg. Lower energy density means the ESS installation space is bigger and high energy density occupies less space for its installation [39, 40, 41].

- Power density;
  The rate of power delivered by ESS to its volume is power density and the common unit is $kW/liter$ or kW/m^3 or specific power density can be described as rate of power delivered by ESS to its weight with unit of kW/kg. Lower power density means the ESS installation space is bigger and heavier than high power density which it has low wight and volume [39, 40, 41].

- Depth of Discharge (DoD);
  DoD is the quantity of discharged energy in comparison to the nominal capacity of storage. ESSs can be totally discharged which it is called 100% DoD matching to a full energy delivered by ESS or completely discharged. Some ESSs have own limits and they do not have 100% DoD capability regarding of their technologies.

- State of Charge (SoC) ;
  SoC is the ratio of remaining amount of energy from total capacity of ESS in percentage. When the ESS is fully charged the SoC corresponding 100% and when the ESS is completely discharged, SoC is 0% [39, 40, 41].

- Efficiency (ζ);
  Efficiency is the rate of discharged energy to the charged energy. In the ESS with high efficiency, the loss of energy is low. In particular, an ESS with high efficiency is important for a system with high fluctuations since for balancing of fluctuations, the ESS needs more cycles. [39, 40, 41].

- Self-Discharge;
  Self-discharge is the loss of energy due to internal technology of ESS. Self-discharge depends on ESS type can be effected with SoC, ambient temperature, internal structure, chemical reaction and other factors. For example, for the batteries the internal chemical reaction is the reason of the reduction of connectivity of the electrodes and this causes to faster self-discharge [39, 40, 41].

- Full Cycle;
  Full cycle for an ESS is called when an ESS fully charged and then fully discharged between its available capacity [42].

- Cycle Life;
  Cycle life for an ESS described as number of full cycles which can be performed

before the available capacity of ESS reaches to below of 80% of its nominal capacity [42].

- Calendar Life;
  Calendar life can be called the life time for an ESS. All the ESSs have their own lifetime and even if they are not active after some times, they will be degraded. For example in case of batteries when the capacity rate reaches to below 80% of its nominal capacity the so-called battery is degraded. It is noted that the usage of an ESS (cycle life) consequently effects the calendar life negatively and it causes the ESS degrade earlier [42]. For example, a battery life time is 10 years or 6000 cycles and it is introduced by manufacturer considering the 6000 cycles can be done in an earlier period than 10 years. On the other hand, if the 6000 cycles is not performed within 10 years again it will be degraded after 10 years because of the calendar life of the battery.

1.2 Different type of energy storage systems

ESSs can be categorized based on their technologies and the common classification of ESSs can be described as Electrical, Mechanical, Thermal and Chemical. Fig. 1.2 demonstrates an order of various ESS technologies arranged by their work basis and ordinary time scale of application [1]. The time scale demonstrates the regular ratio of energy to power of each type of ESS and also coincides to the regular time of charge and discharge.

A smooth review on the fundamental characteristics and specifics of the various ESSs is introduced in the accompanying subsections. In the following section, the characteristics of advanced storage technology such as Compressed Air Energy Storage (CAES), Pumped Hydro Storage (PHS), Flywheel Energy Storage (FES), Lead-acid battery, NaS battery, Li-ion battery, Flow battery, Super-Capacitor, and Superconductive Magnet Coil Energy Storage(SMES). For each ESS the advantage and disadvantages has been introduced. The properties of each of them has been given in a table which is taken from available data in 2016 and an estimation of possible development in 2030 [21].

1.2.1 Mechanical Energy Storage

Mechanical ESSs store energy in type of mechanical then this energy, depends on type of storage system, can be used as mechanical energy or conversed energy such as electrical energy, heat energy or both as hybrid energy. The mechanical energy storage systems which are commonly used in power system applications are Pumped Hydroelectric Storage (PHS), Compressed Air Energy Storage (CAES) and Flywheel Energy Storage (FES) [1, 43].

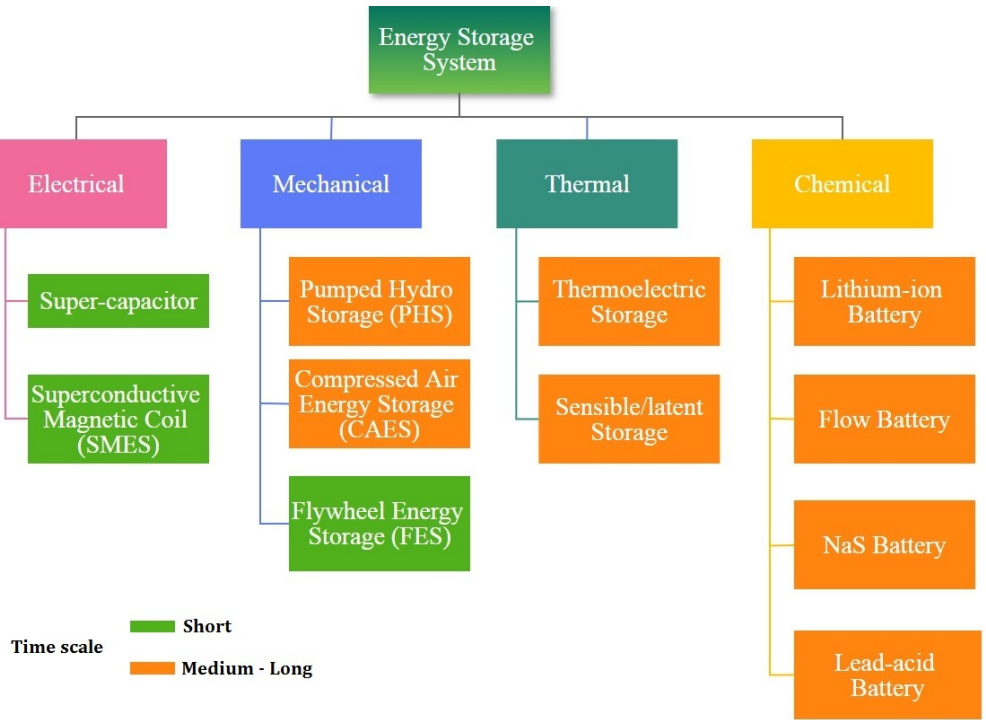

Figure 1.2: ESS category and some example of each technology [1].

1.2.1.1 Pumped Hydroelectric Storage (PHS)

A pumped hydro energy storage system includes of two interconnected water supplies situated at various heights, for example, a mountain and a valley reservoirs. An electric pump draw up water from the lower to the upper water deposits amid the charging procedure and a water turbine is fueled by releasing water from top to down reservoir amid the discharging procedure. Fig.1.3 originally reported in [1] shows a typical layout of a PHS. This water, when demand is high or there is needed for stored electricity, is injected into the rotating turbines in order to generate the needed power [1, 44, 45, 43].

The stored energy capacity relies upon the height distinction between the two water deposits and the volume of stored water at each reservoir [1, 46, 47, 44]. The power rate of PHS plants depends on the pressure of water and water flow rate among the turbines and power rate of the pump-turbine and generator-engine units [48]. PHS is the world leading storage innovation and has been utilized since the mid twentieth century [49] with in excess of 150 Gwh installed capacity till end of 2016 [21].

The most particular advantages and disadvantages of PHSs can be categorized as following [50, 49, 51, 43, 44].

- Advantages;
  - Established technology
  - Very long life-time

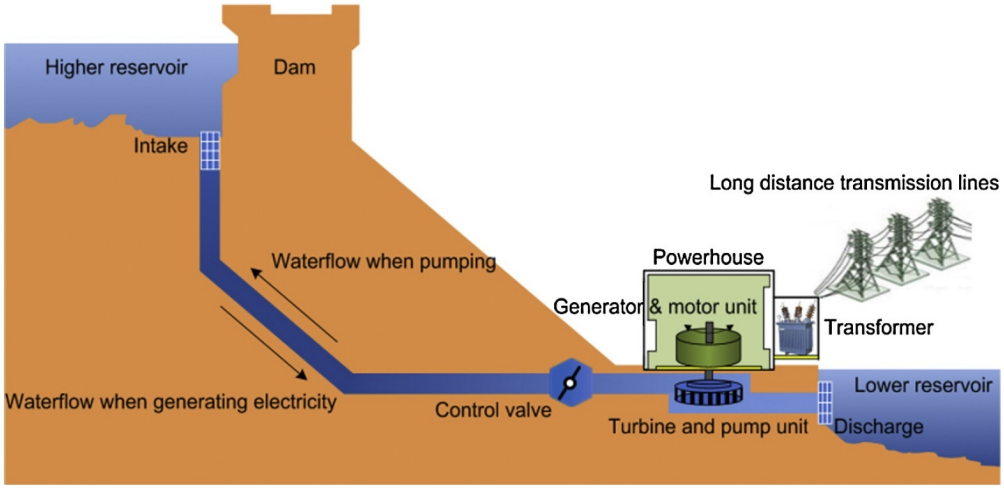

Figure 1.3: A PHS layout. Originally reported in [1].

Table 1.1: PHS properties in 2016 and 2030

Parameters for PHS	2016	2030
Energy density (Wh/L)	$0-2$	$0-2$
Energy installation cost (USD/kWh)	$5-100$	$5-100$
Cycle life (equivalent full-cycles)	$12000-100000$	$12000-100000$
Calendar life (years)	$30-100$	$30-100$
Depth of discharge (%)	$80-100$	$80-100$
Round-trip efficiency (%)	80	80

  - Low self-discharge
  - Good efficiency

- Disadvantages;

  - Low energy density
  - Geographical restriction
  - High investment costs
  - Long return of investment
  - Only large units connected to the transmission grid are economical

Table 1.1 describes some important properties of PHS in 2016 and 2030 [21].

1.2.1.2 Compressed Air Energy Storage (CAES)

A CAES has an electric motor which compresses the air and stores energy by means of compacted air. Usually, the air is stored in natural or artificial caverns. The compressing procedure is done in the least demand periods. After that the air is pressurized to around 75 bar. In case of need of electricity , the air is expelled from the cavern. Primary heating procedure is done by the recuperator then again recuperator uses the energy from the coolers of compressor. Small amount of gas is injected to the hot air in the combustor then they are burnt inside of the combustor. After that, the mixed hot gas and air pass through turbine to produce electricity . In the other word, when the load demand is higher than generation, the compressed air is discharged. After heating and compressing procedure, the energy is converted to electricity by turbine [2, 1, 43]. Fig. 1.4 illustrates a CAES reported in [2].

The first CAES plant in large scale was in the Huntorf-Germany control plant, in 1978. This planet is used to bring facilities such as; black-start power for power planet, back-up to the regional utilities and producing additional energy to balance demand and generation [52].

In principle, diabatic CAES method are essentially just conventional gas turbines, but where the compression of the combustion air is separated from and independent to the actual gas turbine process. This gives rise to the two main benefits of this method. Because the compression stage normally uses up about 2/3 of the turbine capacity, the CAES turbine unhindered by the compression work can generate 3 times the output for the same natural gas input. This reduces the specific gas consumption and slashes the associated CO_2 emissions by around 40 to 60%, depending on whether the waste heat is used to warm up the air in a recuperator. The power-to-power efficiency is approx. 42% without, and 55% with waste heat utilization [53].

Adiabatic method a much higher efficiency of up to 70% can be achieved if the heat of compression is recovered and used to reheat the compressed air during turbine operations because there is no longer any need to burn extra natural gas to warm up the decompressed air. An international consortium headed by the German energy company RWE is currently working on the development of the necessary components and the heat storage. The pilot plant is scheduled to start operations in 2018. Thermal oil and molten salt storage is being investigated in the US [53].

The most significant advantages and disadvantages of CAESs is described as following [50, 4, 54, 55, 43, 56, 1, 44].

- Advantages;
  - Relatively low cost for the energy storage (caverns)
  - Small footprint on surface due to underground storage
  - Long life of the air reservoir (cavern) and the power systems (compressors, turbine)
  - Low self-discharge of compressed air

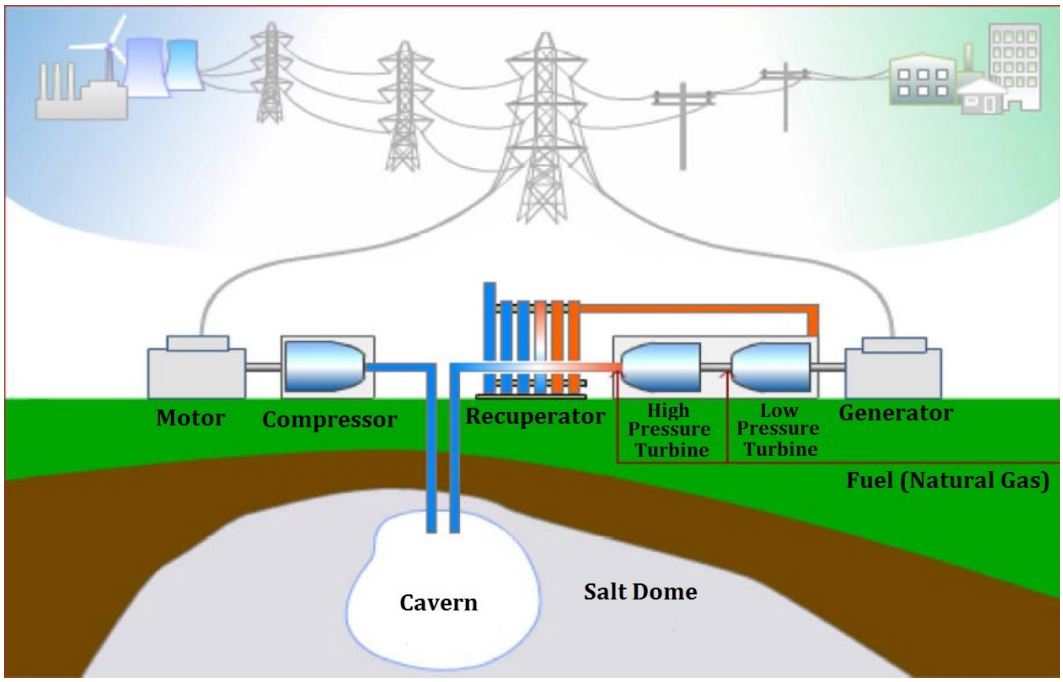

Figure 1.4: A CAES schematic Diagram. Original layout in [2].

- Disadvantages;
  - Certain geological restrictions necessary (pressure-tight cavern)
  - Geographical restriction
  - High investment costs
  - Only two (and old) diabatic pilot plants, no adiabatic power plants available yet
  - Thermal storage for adiabatic CAES not yet demonstrated in full scale
  - High self-discharge of the thermal storage
  - Low efficiency for diabatic CAES (less 55%)
  - Long return of investment (bigger 30 years)
  - Only large units connected to the transmission grid are economical

Table 1.2 describes some important properties of CAES in 2016 and 2030 [21].

1.2.1.3 Flywheel Energy Storage (FES)

FES saves electric energy through the conversion of kinetic energy. This is done by increasing the speed of a rotor and keeping the energy in form of rotational energy. The rotor speed increases when it takes energy and decreases when it gives energy. The

Table 1.2: CAES properties in 2016 and 2030

Parameters for CAES	2016	2030
Energy density (Wh/L)	$2-6$	$2-6$
Energy installation cost (USD/kWh)	$2-84$	$2-71$
Cycle life (equivalent full-cycles)	$10000-100000$	$10000-100000$
Calendar life (years)	$20-100$	$20-100$
Depth of discharge (%)	$35-50$	$35-50$
Round-trip efficiency (%)	60	~ 70

main components of flywheel storage systems are included of motor/generator, flywheel, bearings, vacuum chamber and power electronic control system. Fig. 1.5 shows simple structure of a Flywheel reported in [1]. Although, the starting point of research and proposal of usage of FES coming back to Early twentieth century [57], but the most effective event happened amid the mid 1970's when FES was proposed as an essential target for electric vehicles (EV) and Back up of stationary power [1, 58, 43].

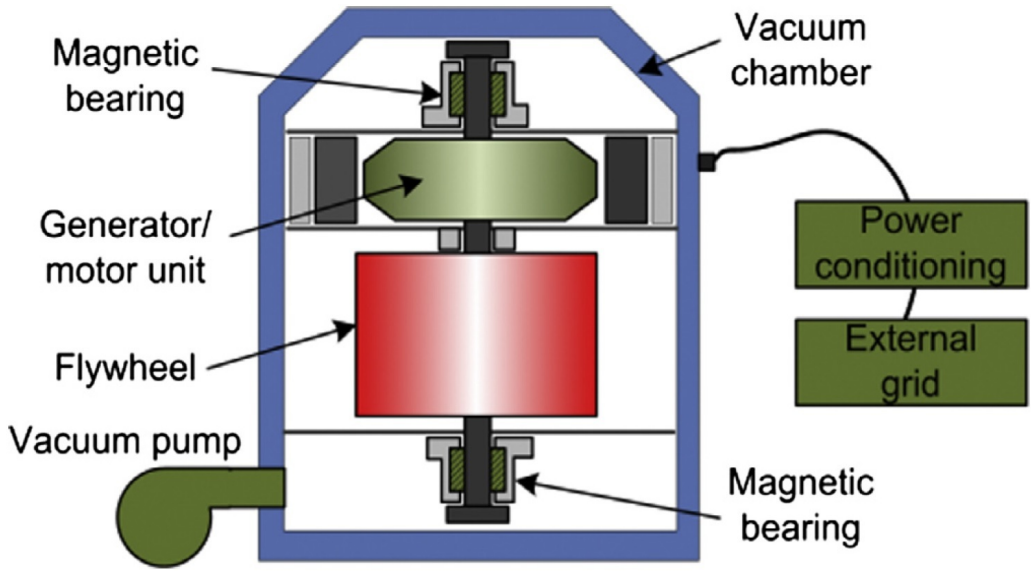

Figure 1.5: A Flywheel Diagram. Original schematic in [1].

The system, in non-peak hours, takes energy from the grid and uses that energy for its own motor to rotate the flywheel and in peak hours, the grid uses this kinetic energy. The kinetic energy stored by the FES is re-transformed and send back to the grid. Since, the stored energy inside flywheel are directly related to its square rotational velocity and this causes an increase for its rotational speed in order to increase the stored energy in the flywheel. The stored energy will then be wasted after some times because of aberration, and after that, the rotor will stop its moving and practically FES can not be

Table 1.3: Flywheel properties in 2016 and 2030

Parameters for Flywheel	2016	2030
Energy density (Wh/L)	$20 - 200$	$20 - 200$
Energy installation cost (USD/kWh)	$1500 - 6000$	$979 - 3917$
Cycle life (equivalent full-cycles)	$10^5 - 10^6$	$151259 - 1.5 \times 10^6$
Calendar life (years)	$15 - 25$	$23 - 38$
Depth of discharge (%)	$75 - 90$	$75 - 90$
Round-trip efficiency (%)	84	87

used. Therefore, flywheels are suitable for short time and high power demands. They are utilized, for instance, for network adjustment purposes for underground trains and trams [1, 43, 59, 44].

The most significant advantages and disadvantages of FES is classified as following [50, 60, 61, 43, 56, 1, 44].

- Advantages;
  - Fast charge capability
  - Low maintenance requirements
  - Long life time
  - Better composite materials may allow higher rotational speed and therefore an increased energy density
- Disadvantages;
  - Low energy density
  - Vacuum chamber needed (complicated and expensive technology)
  - High investment costs
  - Safety reasons; crack occur due to dynamic loads, bearing failure on the supports, external shocks
  - Cooling system for superconducting bearings
  - Very high self-discharge

Table 1.3 describes some important properties of CAES in 2016 and 2030 [21].

1.2.2 Electrical Energy Storage Systems

Electrical energy storage systems store energy in form of electromagnetic energy in the type of an electric field or a magnetic field, the second one commonly created by a current-carrying coil. The common types of electrical energy storage in power system applications are Super-Capacitor Energy Storage and Superconductive Magnetic Energy Storage (SMES) [50, 1].

1.2.2.1 Super-Capacitor Energy Storage

A super-capacitor stores electrical energy in the static electric field among the electrodes (ordinarily made of metal foils) and the ions in the electrolyte (regularly made of glass, ceramic or a plastic film) [1, 4, 2]. The ions go from one electrode to the other amid charging and discharging procedure. The basic super-capacitor is shown in Fig. 1.6 originally reported in [3].

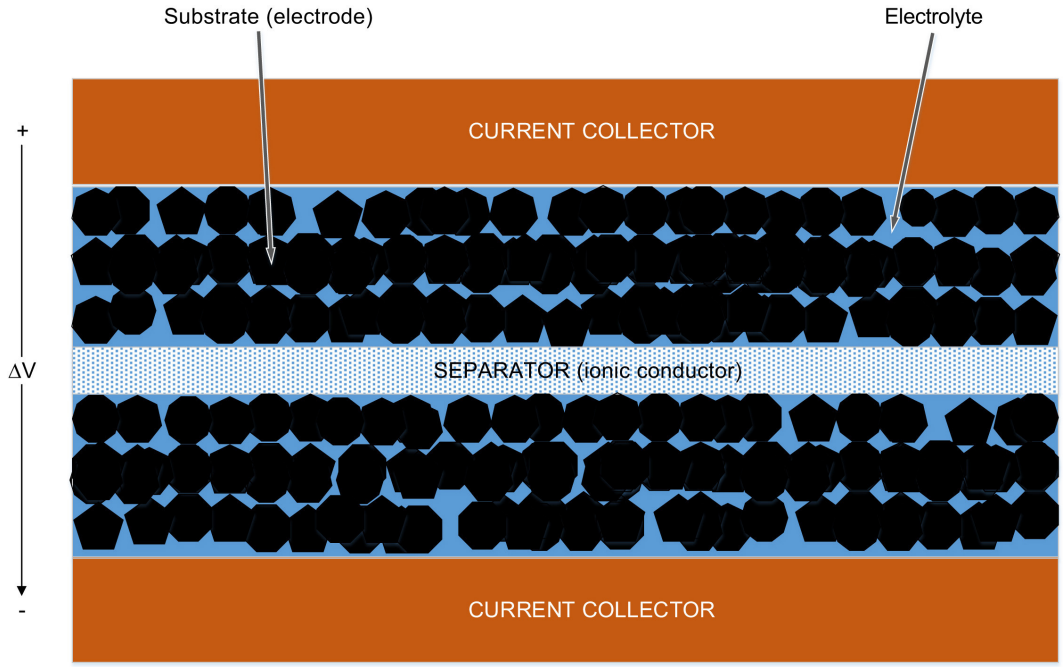

Figure 1.6: Schematic diagram of a super-capacitor. Original schematic is from [3].

Generally, super-capacitors have bigger power density in comparison with classical capacitors, however, energy density of them is less than batteries. Contrasted with batteries, they have a high cycle life and power density but a much lower energy density [1, 62].

One of the most widely utilization of super-capacitors is for applications with high power storage systems in a short timeframe. They are additionally utilized as a part

Table 1.4: Super-Capacitor properties

Parameters for Super-Capacitor	Values
Energy density (Wh/Kg)	$0.5 - 5$
Energy installation cost (Euro/kWh)	$691 - 856$
Cycle life (equivalent full-cycles)	50000
Calendar life (years)	$5 - 8$
Round-trip efficiency (%)	$60 - 65$

of hybrid storage systems with batteries to expand their lifetime. Other application of super-capacitors with regarding of their properties are; improvement of power quality, voltage and frequency regulation in transient mode and correction of power output of generators [63, 4, 43, 44].

The most significant advantages and disadvantages of super-capacitors are classified as following [50, 43, 56, 44].

- Advantages;
  - Very fast charge discharge capability
  - High efficiency
  - Long life time
  - High power capability
- Disadvantages;
  - Low energy density
  - High costs per installed energy
  - High self-discharge
  - Low voltage cells; to get higher voltages, serial connections are required.

1.4 describes some important properties of super-capacitor which is reported in [64].

1.2.2.2 Superconductive Magnetic Energy Storage (SMES)

The main components of SMES consist of a superconducting coil, power conditioning system and cryogenically cooled refrigerator with vacuum subsystem. Amid the charging procedure the superconducting coil is charged with direct current from the power conditioning system. A direct electric current from the power conditioning system makes an invariable inductive magnetic field in superconducting coil part which has the capability to store the energy [1]. The SMES system structure has been described in Fig. 1.7 originally is from [1].

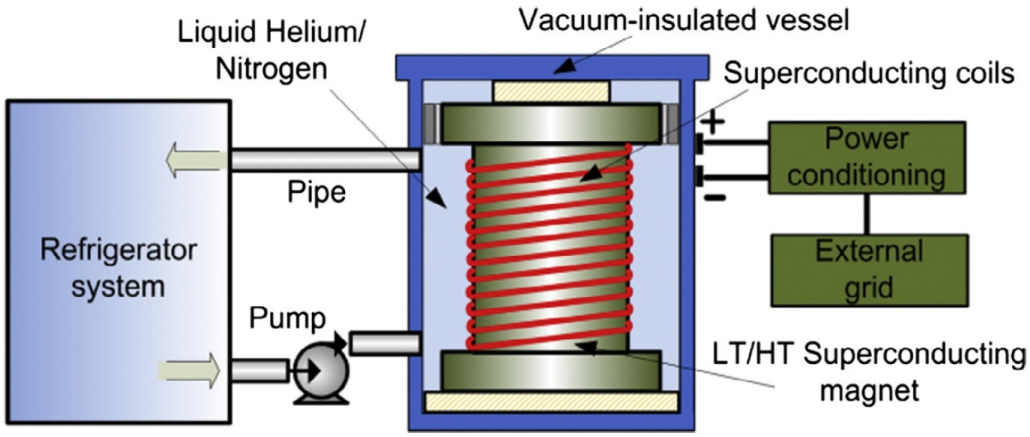

Figure 1.7: Simple layout of a SMES. Original layout is from [1].

In order to have the capacity to utilize the superconducting properties of the coil (make losses zero), it must be put e.g. in fluid helium to ensure temperatures under -260C. The discharging procedure starts with interfacing the coil to an outside load by the power conditioning system. The energy is then provided by the magnetic field which produces a current. The magnetic energy and the current are reduced amid releasing [65, 4, 1, 66, 43, 3].

Energy density of SMES are very low because of this reason they are categorized in short term energy storage and application of them are mostly for supplying of power in short period of time. Since, they need to be maintained in cool condition, their standby losses are very high. However, SMES systems have been in the consideration of both the military and electric utilities because of their quick response and high efficiency (efficiency of charge discharge is above 95%). SMES can be used for voltage and frequency regulation, transient stability, improvement of power quality, load levelling, black-start and etc [67, 68].

The most significant advantages and disadvantages of SMES are classified as following [68, 1, 50, 43, 56].

- Advantages;
  - Very fast charge capability
  - High efficiency
  - High cycle life
  - High power capability
- Disadvantages;
  - Low energy density

Table 1.5: SMES Properties

Parameters for SMES	values
Energy density (Wh/Kg)	$0.5 - 5$
Energy installation cost (Euro/kWh)	$5310 - 6870$
Cycle life (equivalent full-cycles)	~ 100000
Calendar life (years)	$15 - 20$
Round-trip efficiency (%)	$95 - 98$

- High cooling demand
- Expensive raw materials for superconductors
- Complicated inverter design and measurement circuits

Table 1.5 describes some important properties of SMES reported in [69].

1.2.3 Chemical Storage Systems

Chemical energy storage systems store energy in the form of chemical energy and it is converted to electrical and other type of energies. Chemical energy storage can be named as electrochemical energy storage since the wide practical applications of them is in the form of batteries which supply many attitudes of the present and future needs for electrical energy storage. The different type of batteries which are commonly used in power system applications can be mentioned as: Flow Battery, Lead-Acid Battery, NaS Battery and Lithium-ion (Li-ion) Battery [50, 1].

1.2.3.1 Flow Battery

The use of flow batteries is a low-cost and efficient way to save energy produced in sources such as solar and wind power plants. These batteries are structurally similar to acid batteries, with the difference that electrolyte material is stored in an external reservoir. Flow batteries are a kind of rechargeable battery in which two different electrically-charged liquids (called the electrolyte) exchange ions with each other and the ions exchange produce electrical energy. The electrolytes are disposed separately from each other inside the two large compartments. The flow battery schematic has been illustrated in Fig. 1.8 originally is from [4]. The electrolytes is pumped into these compartments according to their needs. In this way, changing the amount of electrolyte can control the produced electrical energy and change the output of these batteries from several kilowatts to several megawatts [70, 71, 1, 4].

The Vanadium Redox-Flow battery (VRFB) is one of the most important commercially available sort of flow batteries. The VRFBs have very fast responses (less than 0.001 s). Their efficiencies is comparatively high, more than 85% . VRFBs can be used in a wide area of applications, above all they can be used for improving power quality, enhancing

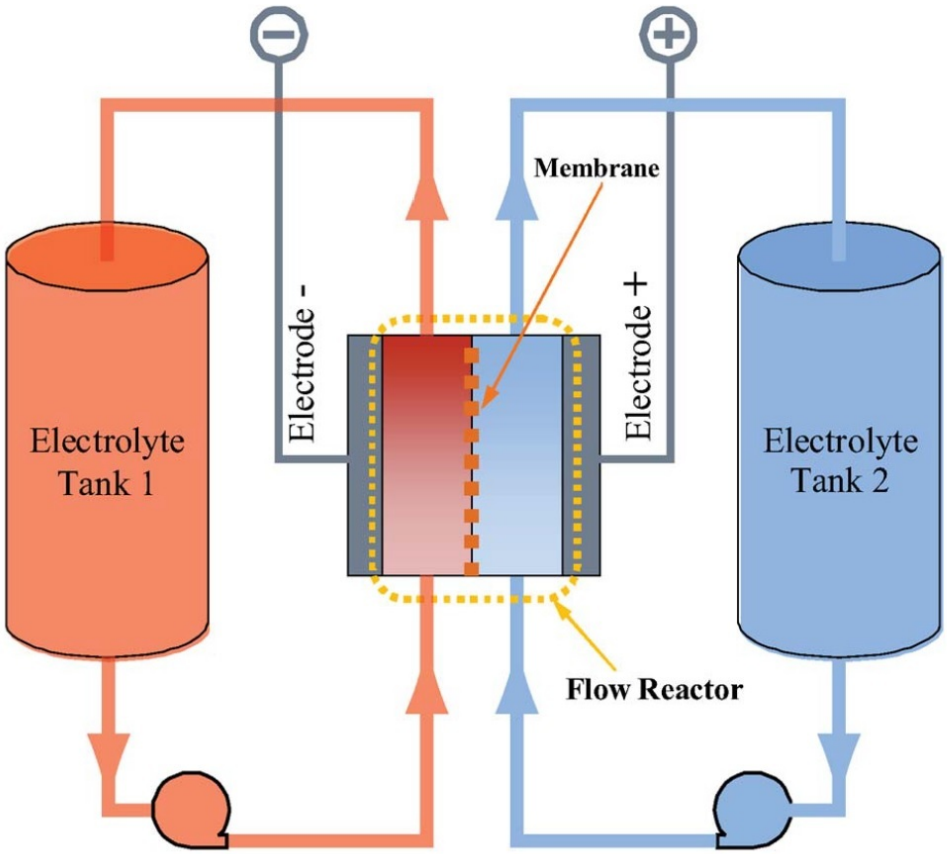

Figure 1.8: Simple schematic of a flow battery. Original layout is from [4].

load levelling, utilized for continuous electricity applications, power transient stability, voltage and frequency regulation [72, 73, 74, 43].

Zinc-Bromine flow batteries (ZnBrFB) are another sort of flow battery. A electrolyte of zinc bromide is stored in two reservoirs. During charge or discharge the electrolytes are pumped through a reactor stack and back into the reservoirs. There are two tanks which one of them reserves the electrolyte for positive electrode another one reserves the electrolyte for negative electrode. The most available application for ZnBr batteries is for load levelling. This battery compose is for instance available from Cellstrom (Austria) and Judicious Energy (USA) with various measured accessible capacities. A various locals with this technology exist, especially, in Japan which are mainly used for load leveling purposes in the scope of a few 100 kW [75, 1, 76, 44].

Table 1.6 describes some important properties of ZnBrFB in 2016 and 2030 [21].

The most significant advantages and disadvantages of flow batteries are classified as following [44, 50, 56, 1, 70, 4, 74].

- Advantages;
  - Energy and power independently scalable

Table 1.6: ZnBrFB properties in 2016 and 2030

Parameters for ZnBrFB	2016	2030
Energy density (Wh/L)	$20 - 70$	$20 - 70$
Energy installation cost (USD/kWh)	$525 - 1680$	$180 - 576$
Cycle life (equivalent full-cycles)	$12000 - 14000$	$12000 - 14000$
Calendar life (years)	$5 - 20$	$8 - 32$
Depth of discharge (%)	100	100
Round-trip efficiency (%)	70	78

Table 1.7: VRFB properties in 2016 and 2030

Parameters for VRFB	2016	2030
Energy density (Wh/L)	$15 - 70$	$15 - 70$
Energy installation cost (USD/kWh)	$315 - 1050$	$108 - 360$
Cycle life (equivalent full-cycles)	$12000 - 14000$	$12000 - 14000$
Calendar life (years)	$5 - 20$	$8 - 32$
Depth of discharge (%)	100	100
Round-trip efficiency (%)	70	78

  - High cycle life
  - Variety of possible redox couples possible
  - Fast response time

- Disadvantages;
  - Leakage caused by acidic fluids
  - Large size applications
  - Costs for vanadium-based redox electrolyte is too high
  - Pumps and valves are prone to errors and costly maintenance
  - Complexity (various components required)

Table 1.7 describes some important properties of VRFB in 2016 and 2030 [21].

1.2.3.2 Lead-Acid Battery

Lead-acid batteries are one of the most developed and oldest battery technologies, which are predominantly utilized as a short-term and medium-term ESSs [1, 50]. If two non-homonym metals (electrodes) are placed in an acidic liquid (electrolyte), there will be a flow between the two electrodes. PbO_2, Pb, H_2SO_4 are the main material of cathode, anode and electrolyte respectively. The positive electrode absorbs the ions and combines

it with the positive electron, which results in the creation of electrical potential in battery negative and positive poles [5, 4]. The structure of lead-acid battery has been shown in Fig. 1.9 originally reported in [5].

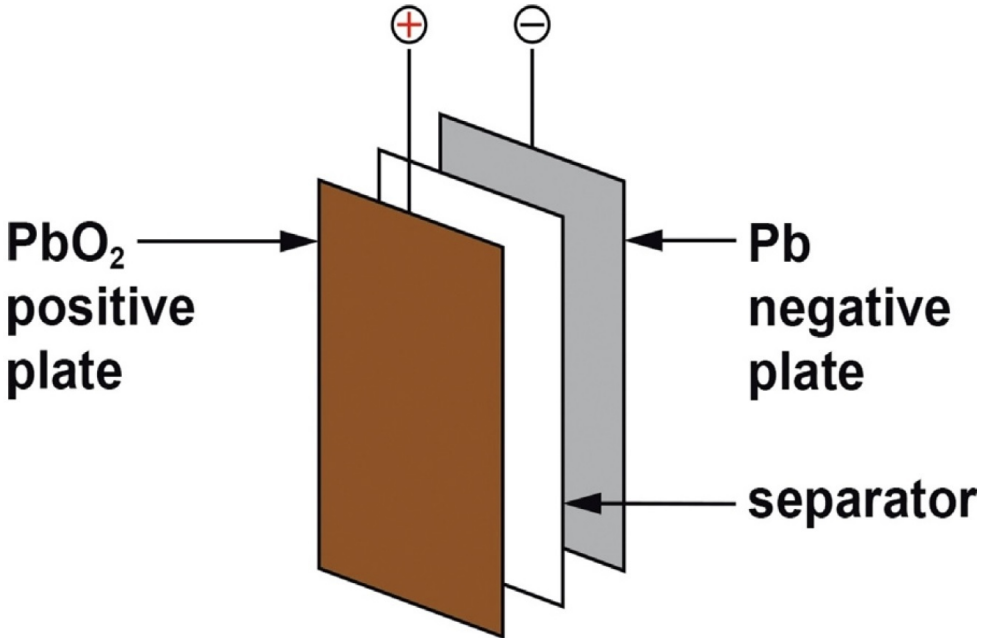

Figure 1.9: Simple layout of a lead-acid battery. Original layout is from [5].

At the time of charging and in the positive pole, lead sulfate $PbSO_4$ combined with water and produces hydrogen ions H^+ and lead oxide PbO_2. The produced hydrogen by the positive electrode reacts with lead sulfate and produces hydrogen sulfate HSO_4 ions which this chemical reaction is exactly the opposite, at the time of discharging [77, 5, 1, 4].

Many manufacturers produce lead-acid batteries. Because of the confinements in the accessibility and the toxicity of lead, reusing of these batteries has important significance for both user and producer. However, Lead-acid batteries are used mostly in automotive industry and UPS systems for telecommunications and they are also widely used for application such as; spinning reserve, frequency control, load leveling, Enhancing stabilization of island grid, power management, load firming, grid integration and Solving intermittency issues of wind energy [1, 78, 4].

The most significant advantages and disadvantages of lead-acid batteries are diveded as following [4, 1, 79, 5, 56, 50].

- Advantages;
  - Acceptable energy and power density for stationary applications
  - Inherent safety by controlled overcharge reaction
  - No complex cell management needed

Table 1.8: Lead-Acid properties in 2016 and 2030

Parameters for Lead-Acid	2016	2030
Energy density (Wh/L)	$50-100$	$50-100$
Energy installation cost (USD/kWh)	$105-473$	$53-237$
Cycle life (equivalent full-cycles)	$250-2500$	$538-5375$
Calendar life (years)	$3-15$	$4-21$
Depth of discharge (%)	$50-60$	$50-60$
Round-trip efficiency (%)	82	85

  - Experience with large storage
  - Short amortization period and relatively low initial investment
  - Today already high number of items (High penetration)

- Disadvantages;
  - Charging and discharging ability are not symmetrical
  - Ventilation requirement
  - Restrictions to the location of the battery system
  - Limited cycle life
  - Industrial batteries are still not built with fully automatic systems

Table 1.8 describes some important properties of Lead-Acid in 2016 and 2030 [21].

1.2.3.3 NaS Battery

A NaS battery utilizes liquid sodium and liquid sulfur as the two terminals, and utilizes beta alumina as the solid electrolyte. The NaS simple layout is shown in Fig. 1.10 originally reported in [6]. The temperature of 574 - 624 K is typically a requirement to guarantee that the electrodes are in fluid states in which prompts a high reactivity. The attractive highlights of NaS batteries incorporate moderately high energy densities (150 to 300Wh/L), daily self-discharge is around zero , higher nominal capacity than different sorts of batteries (up to 244.8 MWh) [66, 80].

These types of batteries, in addition, are able to meet the demand of energy at peak times of consuming and also delivering electricity to areas that have previously been subject to shortcomings due to transmission and distribution constraints. They can be used as a source for protection against electrical disturbances. Their energy density is three times larger than ordinary acid and lead batteries, and energy can be stored in 8 hours and discharge it at the same time. The use of NaS batteries stabilizes the demand for electricity, especially for networks which have significant fluctuations between day

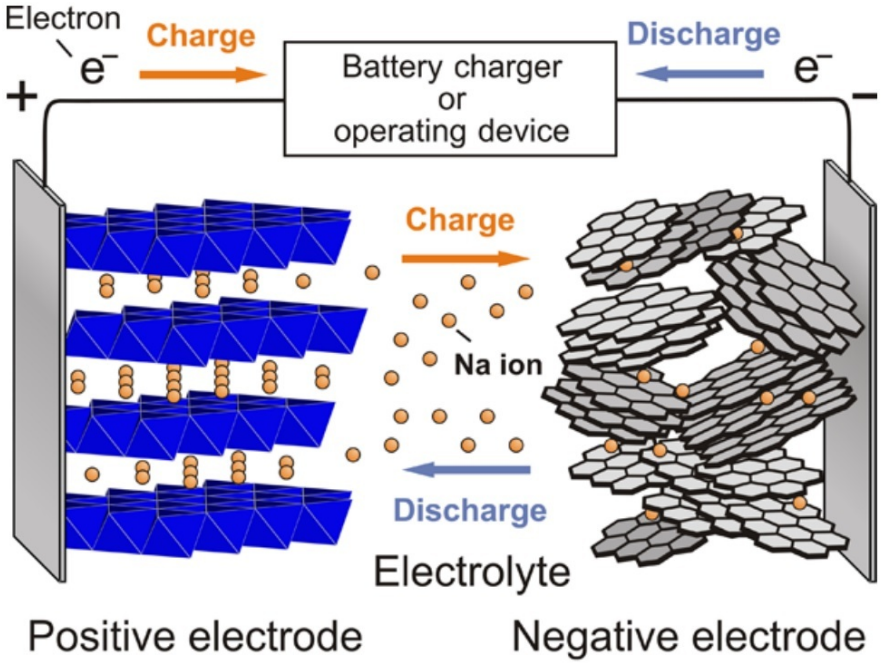

Figure 1.10: Simple layout of a NaS battery. Original layout is from [6].

and night, as result they make energy costs lower for customers. NaS batteries utilizes economical materials which they have a high capability to be recycled [1, 81, 43].

The NaS battery is considered as a standout amongst the most encouraging contender for high power ESS applications. some application of the Nas has been considered such as; Refueling the fixed route vehicles, Wind power fluctuation mitigation, Load levelling and support the autonomous power systems with wind & solar production RESs [1, 4, 44].

The most significant advantages and disadvantages of NaS batteries are considered as following [1, 56, 50, 4, 44].

- Advantages;
  - Acceptable energy and power density for stationary applications
  - High specific energy
  - High cycle and calendar lifetime
  - Cheap raw materials (NaS)
  - Many stationary plants existing (NaS)
- Disadvantages;
  - High thermal standby losses
  - Hazard potential due to high operating temperature

Table 1.9: NaS properties in 2016 and 2030

Parameters for NaS	2016	2030
Energy density (Wh/L)	$140 - 300$	$140 - 300$
Energy installation cost (USD/kWh)	$263 - 735$	$116 - 324$
Cycle life (equivalent full-cycles)	$1000 - 10000$	$1500 - 15000$
Calendar life (years)	$10 - 25$	$14 - 36$
Depth of discharge (%)	100	100
Round-trip efficiency (%)	80	85

– High cost for Nickel-material in Zebra-batteries

Table 1.9 describes some important properties of NaS in 2016 and 2030 [21].

1.2.3.4 Lithium-ion (Li-ion) Battery

Lithium batteries were introduced by British chemist M Stanley Whittingham in 1970. He used titanium sulfide (TiS_2) and l Li as electrodes. But, this rechargeable lithium battery would never be made down in practical. TiS_2 was a poor choice, since it has to be synthesized under completely sealed conditions, also being quite expensive [82]. From innovation date of the lithium butteries till nowadays, they have been undergone changes and they have been considered for researchers as a hot topic.

In 1973, the lithium thionyl chloride battery $Li - Tc$ is proposed by Adam Heller, it is still used in defense industry and embedded medical equipments [83]. Samar Basu developed electrochemical lithium intercalation in graphite in 1973 [84, 85]. In 1979, N.A.Godshall and in 1980 ,John Goodenough and Koichi Mizushima, introduced a rechargeable lithium cell with range of 4 volt using lithium cobalt oxide $LiCoO_2$ as the positive electrode and lithium metal Li as the negative electrode. This advancement gave the positive electrode material that brought possibility to made lithium batteries industrially. $LiCoO_2$ is a steady positive electrode material which reacts as a giver of lithium ions and it can be utilized not only lithium metal but also other material as negative electrode [86, 87]. Alongside with $LiCoO_2$, the other compounds like $LiMn_2O_4$, Li_2MnO_3, $LiMnO_2$, $LiFeO_2$, $LiFe_5O_8$, and $LiFe_5O_4$ were proposed for positive electrode [88].

Rachid Yazami discovered the double-faced electrochemical lithium intercalation in graphite in 1980 [89]. It can be said that current generation of lithium-ion battery tied to the name of Akira Yoshino. In 1985, he used carbonaceous material inside lithium ions as one of the electrodes and $LiCoO_2$ as another one. Since, non metallic lithium had been used the safety of the battery was drastically made strides [90].

Two primary patterns were in the development of electrode materials for Li-ion rechargeable batteries. One was electrochemistry approach related graphite intercalation compounds [91] and the other one was in the field of new nano-carbonaceous materials [92]. The negative electrode of current Li-ion rechargeable batteries identified

by Tokio Yamabe and after that by Shjzukuni Yata which has the originate in polyacenic semiconductive material in the early 1980s [93, 94, 95, 92]. Later, Hideki Shirakawa introduced conductive polymers materials [96] which it can be said the starting point of the polyacetylene lithium ion battery developed by Alan MacDiarmid and Alan J. Heeger et al [97].

In general, each battery consists of three parts: cathode, anode and electrolytes. In rechargeable lithium-ion batteries, a positive electrode is made up of a lithium compound such as $LiCoO_2$, a negative electrode is made up of carbon graphite C and a separating layer is among them [1, 98, 44]. The Li-ion simple layout has been shown in Fig. 1.11 originally reported in [5].

The electrolyte in lithium batteries is also sourced from lithium salts in an organic solvent. The use of organic solvents in the electrolyte due to flammability requires some safety measures. The electrolyte in these batteries is made up of a set of materials that each have their own specific task. Failure in the performance of each electrolyte component causes a malfunction in overall performance of the battery. Lithium-ion batteries are equipped with protective electronic circuits and fuses for protecting of polarization, excessive voltage, overheating and other safety issues [66, 99, 100, 98, 44]. Amid the charging procedure ions of lithium move from the positive to the negative electrode and are accommodate into the carbon layers. Amid discharge the ions of lithium move to the positive electrode, where they are accommodated into the crystal structure [101, 5, 4, 1, 98, 44].

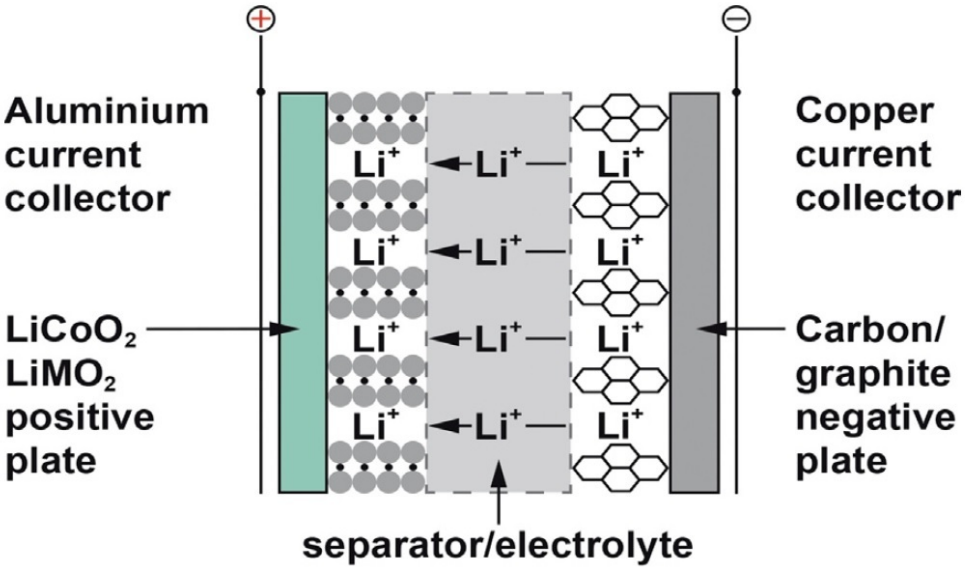

Figure 1.11: Components of a Li-ion battery. Original layout is from [5].

Li-ion batteries are chiefly utilized as medium-term ESSs, however can likewise be utilized as short-term ESSs. Recently, have turned into the most essential storage tech-

nology in the area of portable devices such as laptop, cellphones and etc. Also, in electric vehicles EV, mostly Li-ion batteries are used. In power system applications, they are interested. Several projects with Li-ion batteries already used around the world [43, 102, 1, 2, 66].

The most significant advantages and disadvantages of Li-ion batteries are ordered as following [4, 1, 101, 56, 103, 44, 98, 44].

- Advantages;
  - High energy density
  - High power density
  - Long lifetime
  - High performance
  - Very fast charging and discharging capability
- Disadvantages;
  - Sophisticated battery management system required (single cell monitoring)
  - Packaging and cooling costly depending on the cell shape
  - High cost
  - No inherent security (thermal runaway)

Recently, the key technological improvements and material developments for an expansive scope of Li-ion battery electrodes has been considered as hot topic for researchers and manufacturers. The intercalation materials like lithium nickel cobalt aluminum oxide (NCA), lithium nickel cobalt manganese oxide (NCM or NMC), Lithium Manganese Dioxide (LMO) lithium iron phosphate (LFP) and lithium titanium oxide (LTO), share a broad amount of commercial market of Li-ion batteries [101].

NCA cathode has been shared almost a broad commercial use, for instance, in Panasonic batteries for Tesla Electrical vehicles [101, 104]. The key properties of NCA chemistry Li-ion batteries is long calendar life and higher usable capacity of discharge contrasted with ordinary Co-based oxide cathode [6]. Table 1.10 describes some important properties of NCA chemistry Li-ion Batteries in 2016 and 2030 [21].

LMO can likewise be used since that Mn is considerably less expensive and less toxic contrast with Co or Ni [101, 105]. Energy density of LMO chemistry Li-ion batteries is shorter but these kind of batteries have long life time and less probability of deplorable occasions such as firing, blast and so on. These batteries are broadly utilized for electric devices and medical tools. The properties of NMC chemistry Li-ion batteries is similar with LMO chemistry Li-ion batteries [101, 104]. Table 1.11 describes some important properties of different chemistry Li-ion Batteries (LFP Chemistry) in 2016 and 2030 [21].

LFP chemistry Li-ion is used for electrode material of Li-ion batteries and it is relatively new technology [104]. Since, this kind of Li-ion battery is cheaper with longer

Table 1.10: Li-ion Battery (NCA Chemistry) properties in 2016 and 2030

Parameters for NCA Li-ion	2016	2030
Energy density (Wh/L)	$200 - 620$	$200 - 620$
Energy installation cost (USD/kWh)	$200 - 840$	$82 - 347$
Cycle life (equivalent full-cycles)	$500 - 2000$	$955 - 3819$
Calendar life (years)	$5 - 20$	$8 - 31$
Depth of discharge (%)	$85 - 95$	$85 - 95$
Round-trip efficiency (%)	95	97

Table 1.11: Li-ion Battery (NMC/LMO Chemistry) properties in 2016 and 2030

Parameters for NMC/LMO Li-ion	2016	2030
Energy density (Wh/L)	$200 - 735$	$200 - 735$
Energy installation cost (USD/kWh)	$200 - 840$	$79 - 335$
Cycle life (equivalent full-cycles)	$500 - 4000$	$955 - 7639$
Calendar life (years)	$5 - 20$	$8 - 31$
Depth of discharge (%)	$84 - 100$	$84 - 100$
Round-trip efficiency (%)	95	97

life time and lower toxicity in comparison of ordinary Li-ion batteries and it is found for different application such as EVs and backup power of household [101, 106]. Table 1.12 describes some important properties of chemistry Li-ion Batteries (LFP Chemistry) in 2016 and 2030 [21].

Fast charging, high power thermally stable cells with high cycle life are the most significant properties and it helped these kind of batteries to be commercialized [107, 108]. Due to its high level of safety, LTO chemistery Li-ion battery is now being utilized in mobile medical equipment. Because of their fast charging capability, it is starting to be used in EV especially transportation EVs [109]. Table 1.13 describes some important properties of chemistry Li-ion Batteries (LTO Chemistry) in 2016 and 2030 [21]

Table 1.12: Li-ion Battery (LFP Chemistry) properties in 2016 and 2030

Parameters for LFP Li-ion	2016	2030
Energy density (Wh/L)	$200 - 620$	$200 - 620$
Energy installation cost (USD/kWh)	$200 - 840$	$77 - 326$
Cycle life (equivalent full-cycles)	$1000 - 10000$	$1910 - 19097$
Calendar life (years)	$5 - 20$	$8 - 31$
Depth of discharge (%)	$84 - 100$	$84 - 100$
Round-trip efficiency (%)	92	94

Table 1.13: Li-ion Battery (LTO Chemistry) properties in 2016 and 2030

Parameters for LTO Li-ion	2016	2030
Energy density (Wh/L)	$200 - 620$	$200 - 620$
Energy installation cost (USD/kWh)	$473 - 1260$	$215 - 574$
Cycle life (equivalent full-cycles)	$5000 - 20000$	$9549 - 38194$
Calendar life (years)	$10 - 20$	$15 - 31$
Depth of discharge (%)	$84 - 100$	$84 - 100$
Round-trip efficiency (%)	96	98

Chapter 2

Aging Cost Optimization of Energy Storage Systems in Microgrids

2.1 Introduction

The high penetration of Distributed Generation (DG) is bringing new concept for the control of transmission and distribution systems of power systems [110]. In particular, the discontinuous nature of the power delivered by Renewable Energy Sources (RES) is undermining the steadiness of power systems, expanding the risk of failures and inconsistencies. So as to beat this issue, different studies have projected for the use of ESSs technologies for the management of power systems fluctuations [111, 112, 113, 114, 115, 116]. The suggested solutions include the use of ESSs for the provision of frequency and voltage stability, spinning reserve, load following, and peak shaving. Despite the great advantages related to the wide adoption of ESS technologies, there are still open issues with respect to their modeling in unit commitment problems, particularly while including the ESSs aging costs.

Actually, the ability of ESS to supply services to the power systems is emphatically time subordinated, and cannot be decoupled from their past and future use. Hence, the authoritative single time frame optimization approaches such as Optimal Power Flow (OPF) do not appropriately fit the time-dependence attributes required for the management and control of ESSs in power networks. To beat this limitation, different studies addressed to this issue by proposing Multi-Period Optimal Power Flow (MPOPF) procedures [117, 118, 119, 120, 121, 122]. The current MPOPF solving techniques include robust optimization techniques [120], Semidefinite Programming (SDP) approaches [117, 118, 119], distributed solving algorithms[122] and non-linear programming methods [121]. However, these methodologies fail to address the issue of including the ESSs aging costs in the optimization procedure, particularly in the case of Battery ESSs (BESSs) which are portrayed by significant non-linear aging behavior [42]. The degradation of electrochemical storage can be divided in two aging factors: the calendar aging, strictly relying upon time, and the cycle aging, depending on the usage patterns

of the BESS [42]. Since the utilization of the BESS brings degradation, this results in a devaluation cost of the battery for the end user. This degradation additionally demonstrates a strong non-linear dependence on the SoC of BESS of the performed cycles and temperature [42]. These factors depend on the power profile of the battery amid an expanded timeframe. Subsequently, if the use of the BESS is not regular, as it occurs in presence of discontinuous RES power generation, it is difficult to recognize the BESS aging without considering the time progress of SoC and temperature of the BESS.

Given these necessities, this chapter presents a novel multi-period OPF methodology based on Genetic Algorithms (GA) [123, 124], called GA-MPOPF. The proposed methodology considers complex cost functions characterized over a time period, like the operative costs of BESS, allowing to consider the ESSs degradation as an optimization item, likewise identifying the ideal usage strategy of ESSs in a power system from a cost point of view. Moreover, the particular form of the proposed methodology allows for the verification of the correct operative state of the system during the considered time interval, by taking into account the technical constraints of system.

The GA-MPOPF method is able to enhance both planning and unit-commitment issues in presence of a mix of RES and Fossil-Fuel based generators, loads and ESSs. In order to test these highlights, it has been applied to the standard 69 bus IEEE PG & E network, in attendance of a high penetration of various RESs and Li-ion BESSs. The studied network has been designed as a Virtual Power Plant (VPP) whose goal is to follow a particular power profile amid the day. Any deviation from such profile creates an extra cost for the VPP aggregator under the form of a fine. In this work, the role of the BESS is to counteract the VPP fluctuations with a specific end goal of minimization of the total amount of the fines in a timeframe of one month. To legitimately assess the amortization costs of the Li-ion BESS, a novel time-dependent cost function based on the Battery Degradation Model (BDM) presented in [42] is proposed. The proposed method is applied to the test network from both a management and planning viewpoint. The management or operative analysis consists of the identification of the optimized management of the BESS during the tested monthly time frame. The planning process consists of the identification of the optimal position of the BESS from electric perspective. This allows for the identification of the correct location of the BESS on the base of the evaluation of the system electrical parameters amid a broadened time frame.

Furthermore, in order to test the response of system to various types of fines, the outcomes are assessed with linear, quadratic, and cubic cost functions [125]. Also, an exponential cost function is presented and examined as a limit case of high degree cost functions. Results demonstrate excellent convergence features for all the mentioned cost functions, and highlight the important role of ESS aging costs in both economically optimized and system limits unit commitment issues. Moreover, results additionally recommend to use of the GA-MPOPF technique for optimization problems at time scales bigger than the ones found in the present writing (1 day - multi week), pushing as far as possible to the month time scale.

This chapter is organized as follows: In section 2.2 the GA-MPOPF is depicted, together with the proposed Li-ion time-dependent cost function. Section 2.3 depicts the

case study and the fine systems related to the power fluctuations of the studied VPP. In section 2.4 the results of the optimization technique are presented. In section 2.5 a particularized discussion is accorded and also the outcomes of this study is compared with the other works. At the end, in section 2.5 conclusions and future work are discussed.

2.2 Methods

The point of the proposed approach is the optimization of the usage profiles of ESSs and Controllable Generators (CG) in a power system. The optimization is asked for meeting the equality and inequality operative imperatives depicted by a multi-period model of the system. Equality constraints describe the settled parameters of the model. They portray the power network topology and the power profiles of DGs and loads amid time. On the other hand, the optimization imperatives are given according to inequality relations. These include the static and dynamic power imperatives of CGs and ESSs, together with the voltage phasors, and in addition thermal limits of transmission lines. A detailed definition of the inputs of the proposed methodology is given in subsec. 2.2.1. In addition, the optimization technique itself, together with its output is depicted in detail in subsec. 2.2.2. At long last, subsec. 2.2.3 characterizes the Li-ion Battery Degradation Costs Model (BDCM) used in this chapter for the meaning of the cost profile of the BESS.

2.2.1 Inputs and constraints of the model

The optimization procedure depends on a time-dependent model of the power system, which is given as far as equality and inequality limitations. The equality constraints characterize: the power of the loads $L_n(t)$ for each bus n of the grid and per each time t of the considered time interim; the DG generation $DG_n(t)$, on each considered node n and for each considered time t; the resistance R_{ij} and reactance X_{ij} of the electrical lines between buses i and j. On the other hand, the inequality constraints set the optimization limits. This includes voltage phasors imperatives, including their magnitudes V_n^{min}, V_n^{max} and, if needed in the particular application, their phases φ_n^{min} and φ_n^{max}, as detailed in (2.1) and (2.2), for each node n and each time t.

$$V_n^{min} \leq V_n(t) \leq V_n^{max} \tag{2.1}$$

$$\varphi_n^{min} \leq \varphi_n(t) \leq \varphi_n^{max} \tag{2.2}$$

Additionally, transmission lines thermal limits S_{ij}^T are considered, as characterized in (2.3), where $S_{ij}(t)$ is the apparent power flowing through buses i and j at time t. These limits must be satisfied per each time t. In the general design of the proposed model, the quantities $V_n(t)$, $\varphi_n(t)$ and $S_{ij}(t)$ can in principle be evaluated per each time t by means of any current (or future technique) able to perform their estimation, without losing the viability of the optimization. In this work, backward/forward sweep AC Power Flow (ACPF) solver has been used, and the set of input data required for the proper

performance of this calculation has been considered [125, 126]. This specific solver has been picked in view of its performance for radial networks with high R/X ratio.

$$| S_{ij}(t) | \leq S_{ij}^{T} \tag{2.3}$$

Ordering each CG as g, their static and dynamic operative inequality imperatives are characterized as follows: the generator's minimum and maximum power output limitations are given by (2.4). The ramping limits of the generators P_{ramp}^{down} and P_{ramp}^{up} (setting the maximum variety of power that every generator g can achieve amid an interim of time Δt) are described by (2.5) and (2.6). The inequalities ought to be satisfied per each time t, and S_g^{min} and S_g^{max} are the CGs minimum and maximum power power outputs, accordingly. $S_g(t)$ is the power output profile of the generator g amid time t, which is the optimization variable. In addition, each generator g is portrayed by a cost function C_g. In general, if the value S_g^{min} is not zero, the generator can be turned off with a specific end goal to give an null power yield. In general, if the value S_g^{min} is not zero, the generator can be turned off with a specific end goal of providing a null power output. For this situation, on/off switching of the generator g must be considered as an operative cost that ought to be included into the cost function C_g.

$$S_g^{min} \leq S_g(t) \leq S_g^{max} \tag{2.4}$$

$$S_g(t+1) \leq S_g(t) + P_{ramp}^{up} \tag{2.5}$$

$$S_g(t+1) \geq S_g(t) - P_{ramp}^{down} \tag{2.6}$$

The constraints of ESS are described in (2.7) and (2.8). Each ESS, characterized by index e, is depicted by its energy capacity E_e^{Nom}, and by its rating power S_e^{max} and S_e^{min}. The energy stored in the ESS at time t is $E_e(t)$, and is updated according to (2.9). η_e^c and η_e^d are the ESS charging and discharging efficiencies, and $P_e(t)$ is the active power provided by the ESS e at time t. In general, a cost function C_e is related to each ESS e of the system, depending both on its aging and operative costs:

$$0.1 \times E_e^{Nom} \leq E_e(t) \leq 0.9 \times E_e^{Nom} \tag{2.7}$$

$$S_e^{min} \leq S_e(t) \leq S_e^{max} \tag{2.8}$$

$$E_e(t) = \begin{cases} E_e(t-1) + \eta_c \int P_e(t)dt, & \text{if charging} \\ E_e(t-1) + \frac{1}{\eta_d} \int P_e(t)dt, & \text{if discharging} \end{cases} \tag{2.9}$$

2.2.2 Optimization procedure and outputs

GA-MPOPF is based on the GA-based heuristic optimization of the global system cost function

$$C_f = \sum_g C_g + \sum_e C_e. \tag{2.10}$$

The Genetic Algorithm (GA) approach has been presented by Holland [123] as a part of the computational methods created in the field of Artificial Life and complex systems[127]. The idea behind the GA is to produce excellent answers for optimization and search problems by applying bio-inspired operators, like *mutation*, *crossover*, and *selection* to a population of randomly created solutions object to the evolutionary pressure represented by a fitness function, i.e. a functional measuring the ability of each component of the population to solve the problem. The optimal solution is figured by iterating the calculation until the value of fitness function converges to a equilibrium value (usually 30-100 iterations). GAs have been effectively applied to a scope of various fields, the most important of which are: neural networks, control engineering, bioinformatics, and medicine [124]. GAs additionally discovered applications in power systems such as: network reconfiguration to minimize losses [128], network reconfiguration in case of failures [129] and optimal DG placement [130].

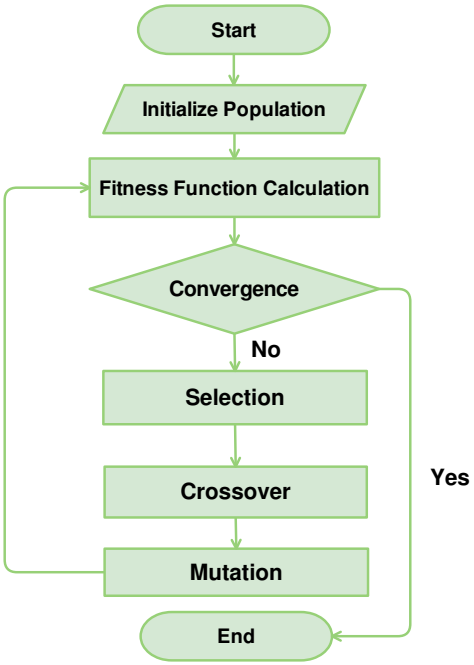

Figure 2.1: The flowchart of the genetic algorithm

The proposed optimization method is presented in the flowchart in Fig. 2.1. The optimization technique starts with the generation of a number N_{pop} of initial matrices $\mathbf{M}$. $\mathbf{M}$ is a $T \times G$ matrix, where T is the number of considered time interims, and G is the number of generators including both ESSs and CGs. Each line of the matrix is indicated by the $CG_g(t)$ and $ESS_e(t)$, the power profiles of the considered CGs and ESSs amid time, developed by following the constraints given in subsec. 2.2.1. Starting from this initial population, the GA is then applied to the initial population after satisfying a convergence criteria. Each GA iteration is sorted out as follows: the cost function C_f is figured

per every component of the populace. At that point, selection, crossover, and mutation operators [123] are applied. In this work, the convergence is accomplished when a variability edge of 1% or a maximum number of iterations $I_{max} = 100$ is considered. The crossover has been set to $C = 0.8$, while mutation has been set to $M = 0.2$. At long last, when the convergence criteria are satisfied, the optimized $CG_g(t)$ and $ESS_e(t)$ are extracted from the obtained $\mathbf{M}$, and are selected as result of the optimization procedure.

2.2.3 Battery cost model

The estimation of battery operative costs depends on the Battery Degradation Model (BDM) proposed by *Xu et al.* in [42]. The BDM depends on (2.11), relating the battery life L with a battery degradation function f_d. The battery life is described as $L = 1 - D$, where D is the remaining of the capacity of the BESS, normalized to 1. The relation among L and f_d is non-linear, and consists impacts proper of the Li-ion BESSs, like the initial Solid Electrolyte Inter-phase (SEI) film formation by means of parameters α_{sei} and β_{sei}, as given in equation (2.11).

$$L = 1 - \alpha_{sei} e^{-\beta_{sei} f_d} - (1 - \alpha_{sei}) e^{-f_d} \tag{2.11}$$

The battery degradation function f_d relies upon the sum of a cycle aging function f_c and calendar aging function f_t, as given in (2.12). The number of performed cycles is N.

$$f_d(t, \delta, \sigma, T_C) = f_t(t_{use}, \bar{\sigma}, \bar{T_c}) + \sum_{n}^{N} f_c(\delta, \sigma, T_c) \tag{2.12}$$

Both calendar and cycling aging functions demonstrate a reliance on the time evolution of the operative parameters of the BESS. These are the BESS utilization time t_{use}, its SoC σ, the Depth of Discharge (DoD) of its performed cycles δ, and its temperature T_c. Specifically, the δ parameter can be gotten from the time development of the battery SoC by by means the rainflow algorithm[42].

The calendar aging function $f_t(t_{use}, \bar{\sigma}, \bar{T_c})$ depends on the utilization time t_{use} and on average SoC $\bar{\sigma}$ and temperature $\bar{T_c}$ amid the considered time interim. Equation (2.13) shows the dependence from these parameters. S_t, S_σ and S_{T_C} are depicted in (2.14), (2.15) and (2.16) separately. T_{ref}, k_T, k_σ, and σ_{ref} indicate the aging parameters of Li-ion BESS tested and investigated in [42].

$$f_t(t, \sigma, T_C) = S_t(t) \cdot S_\sigma(\sigma) \cdot S_{T_C}(T_C) \tag{2.13}$$

$$S_t(t) = k_t t \tag{2.14}$$

$$S_\sigma(\sigma) = e^{k_\sigma(\sigma - \sigma_{ref})} \tag{2.15}$$

$$S_{T_C}(T_C) = e^{-k_T(T_C - T_{ref})\frac{T_c}{T_{ref}}} \tag{2.16}$$

In addition, cycle aging function $f_c(\delta, \sigma, T_c)$ demonstrates a direct reliance on the battery cycling: It relies upon δ, average σ, and average temperature T_c of the considered

cycle. The expressions of $f_c(\delta, \sigma, T_c)$ is given in (2.17). The expressions of S_δ, S_σ and S_{T_C} are given in (2.18), (2.15) and (2.16), respectively. The parameters $k_{\delta 1}$, $k_{\delta 2}$ and $k_{\delta 3}$ are gotten from [42].

$$f_c(\delta, \sigma, T_C) = S_\delta(\delta) \cdot S_\sigma(\sigma) \cdot S_{T_C}(T_C) \tag{2.17}$$

$$S_\delta(\delta) = (k_{\delta 1}\delta^{k_{\delta 2}} + k_{\delta 3})^{-1} \tag{2.18}$$

The definition of calendar and cycle aging functions takes into consideration the separate assessment of the two battery amortization phenomena. Since the calendar aging function embeds the averaging of σ and T_C, the exactness of the estimation of this phenomenon is improved by computing the f_t over ν sub-interims of time length Δt, each called $f_{\Delta t}^{\nu}$. Then, the aggregate calendar aging for a time interim $\Delta\tau$ has been calculated as $f_t^{\Delta\tau} = \sum_{\nu \in \Delta\tau} f_{\Delta t}^{\nu}$. With regards to the cycle aging, the effect of each cycle cyc has been independently computed as f_c^{cyc}. To calculate the cycling pattern amid the same timeframe of the calendar one, it is important to run the rainflow calculation on the same considered time interim $\Delta\tau$. However, given the specific type of the rainflow algorithm [42], the computed cycling patterns of at least two continuous time interims can differ if considered separated or as a whole, since the cycles spanning in excess of one interval can be truncated and not appropriately calculated if the interims are considered separately. Thus, it is advisable to consider a large enough time interval $\Delta\tau$ amid this calculation, in order to decrease the truncation error in the cycle evaluation. According to this assumption, the resulting effect of the cycles performed amid the time interim $\Delta\tau$ can be gotten as $f_c^{\Delta\tau} = \sum_{cyc \in \Delta\tau} f_c^{cyc}$. Thusly, the aging experienced by the BESS amid a time interim $\Delta\tau$ is computed as (2.19).

$$f_d^{\Delta\tau} = f_t^{\Delta\tau} + f_c^{\Delta\tau} \tag{2.19}$$

The BDM detailing in [42] has been extended in this work with the description of a Battery Degradation Cost Model (BDCM). The goal has been to interface the battery degradation properties with its amortization costs. Since the battery is considered as degraded when it reaches a capacity D equivalent to 80% of its nominal capacity, it is conceivable to identify $f_d^* = f_d^{-1}(0.2)$, i.e. the value of the degradation function at which the battery is accounted as degraded. The novel concept introduced in this work is to consider f_d as a linear indication of the condition of degradation of the BESS, which can be directly lined to a cost function. Considering that f_d the range of values extend between 0 for a brand new battery and f_d^* for a degraded battery, it is possible to identify the BESS degradation amid a time interim $\Delta\tau$ in means of fractions of f_d^* as described in (2.20).

$$d^{\Delta\tau} = \frac{f_d^{\Delta\tau}}{f_d^*} = \frac{\sum_{\nu}^{\tau} f_{\Delta t}^{\nu} + \sum_{cyc \in \Delta\tau} f_c^{cyc}}{f_d^*} \tag{2.20}$$

Given this amount, the BESS degradation amid each considered time interim $\Delta\tau$ can be related to a degradation cost $C_d^{\Delta\tau}$. This is carried out by linking the amortization

costs amid the considered time interim with its associated degradation function $f_d^{\Delta\tau}$. Describing the total life costs identified with the BESS as C_B^*, it is possible to assume the full amortization of this expenses for a value of $f_d = f_d^*$. Given the linear connection between $f_d^{\Delta\tau}$ and f_d^*, it is then possible to interface $f_d^{\Delta\tau}$ and $C_d^{\Delta\tau}$ by means of (2.21):

$$C_d^{\Delta\tau} = \frac{f_d^{\Delta\tau}}{f_d^*} \cdot C_B^* = d^{\Delta\tau} \cdot C_B^* \tag{2.21}$$

Interfacing the aging of a Li-ion BESS amid a time interim with its amortization costs.

2.3 Case study

The GA-MPOPF optimization method has been designed to achieve high adaptability, and can be applied to a wide range of applications. In this chapter, it has been applied to the planning and management strategy of a Li-ion BESS in a VPP environment. As case study the IEEE PG & E Medium Voltage (MV) grid, portrayed in detail in subsec. 2.3.1, has been chosen. The motivation behind the VPP aggregator is to deal with the power output at the Point of Common Coupling (PCC) of the network. This is performed by utilizing the support of the BESS providing a daily active power profile $P^*(t)$. if this is not obtained, the VPP aggregator is asked for to pay a fine based on the difference from the expected profile. To do this, the PCC of the tested network has been considered as a infinite generator. Along these lines, the values S_g^{min} and S_g^{max} have been set to $-\infty$ and $+\infty$ respectively, and because of this reason no on and off switching expenses of the generator have been considered. Its cost function is as a steady part, contingent upon the profile $P^*(t)$, and a fine part depending on the fluctuations around this value as following equation:

$$C_f(P) = F(P^*(t)) + R(|P(t) - P^*(t)|). \tag{2.22}$$

The fix cost function $F(P^*(t))$ follows the day-ahead market prices, and the fines cost functions $R(|P(t) - P^*(t)|)$ are selected between the ones demonstrated in subsec. 2.3.2.

2.3.1 The test grid

The standard PG & E 69-bus radial distribution network utilized in [131] is chosen and shown in Fig. 2.2. The data with respect to DG has been taken from [132, 133], where the authors optimized DG position and nominal power stabilizing the system by using a heuristic, Tabu-Search based method. The load data has been gotten by using the approach depicted in [134], where the consumption profiles of Medium Voltage (MV) buses are aggregated randomly, beginning from a set of consumption time series of single households obtained from [134]. Following this method, the load profile of each bus of the system has been assessed, with a hourly sampling and for a timeframe of a month. The profiles of the DG production in this work have been gathered from the site of IESO,

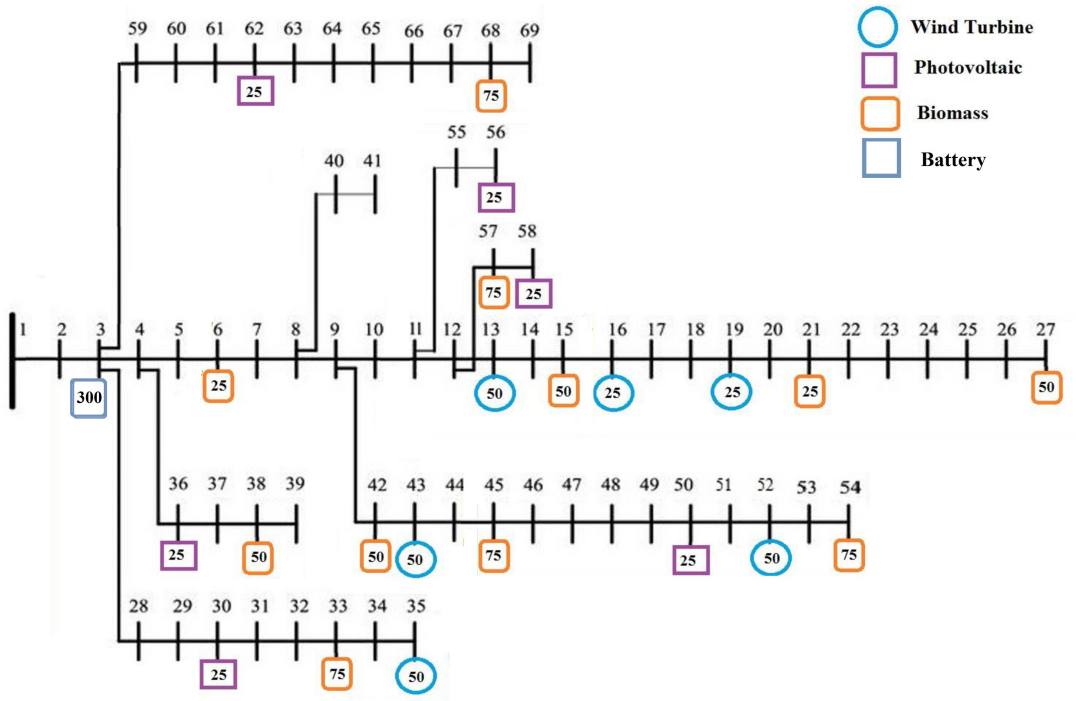

Figure 2.2: The used IEEE PG& E 69 bus network.

the Power System Operator located in Ontario (Canada) [135]. The studied Li-ion BESS has a capacity of 300 kWh and a rated power of 300 kW. All the datasets used in this study cover the period from April to May 2016.

2.3.2 Cost functions

The optimization methodology proposed in sec. 2.2 has been tested by four unique kinds of fines cost functions $R(P)$: linear, quadratic, cubic, and exponential, portrayed separately in (2.23), (2.24), (2.25), and (2.26). The first three of them have been selected as representative cost functions in power generation [125].The exponential one has been proposed in this chapter as a limit case for testing the method reaction for cost functions of higher grade. The strength of the fines is tuned by the parameter β, which is different per each cost function, and characterized in order to get an average fine of $P_{av} = 150 Euro/MWh$.

$$R_l(P(t)) = \beta_l |P(t) - P^*(t)| \tag{2.23}$$

$$R_q(P(t)) = \beta_q (P(t) - P^*(t))^2 \tag{2.24}$$

$$R_c(P(t)) = \beta_c (|P(t) - P^*(t)|)^3 \tag{2.25}$$

$$R_e(P(t)) = \beta_e e^{|P(t)-P^*(t)|} \tag{2.26}$$

Fig. 2.3 shows the shape of the studied cost functions. Besides, the proposed cost functions are compared with the histogram of the power fluctuations measured in the PCC with regards to the power profile $P^*(t)$. Fluctuations are distributed around the interim $(-200, 200)$ kW, with some outrageous values among 200 and 300 kW.

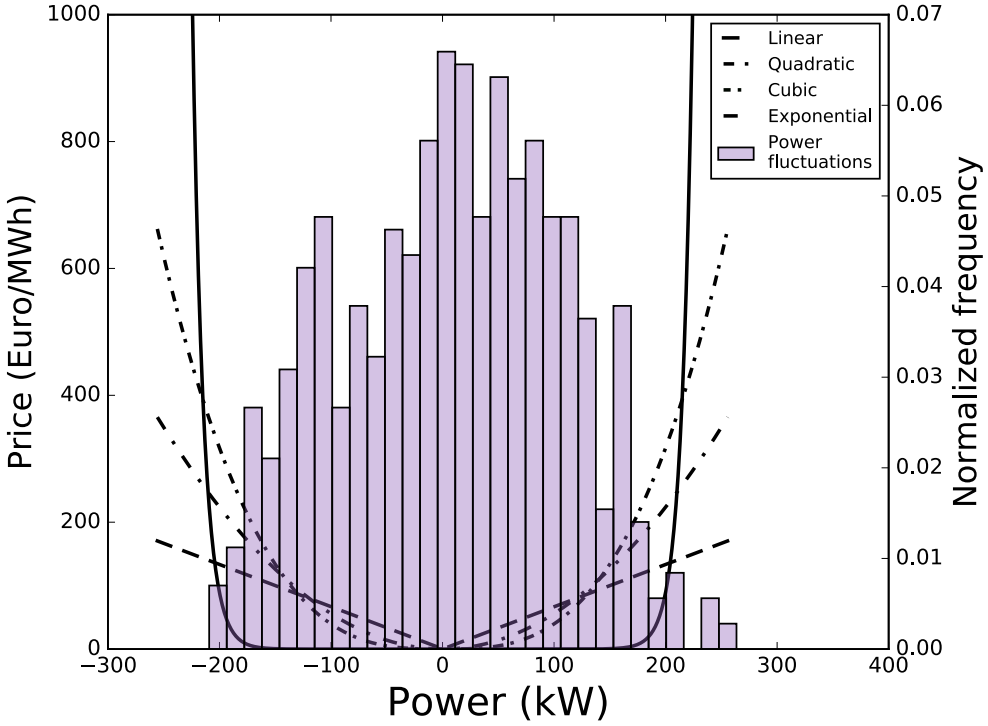

Figure 2.3: The used cost functions, and the histogram of the power fluctuations at the network PCC.

2.4 Results

The GA-MPOPF method is used to optimize the usage of a BESS in a VPP, as defined in detail in subsec. 2.3.

Aim of the optimization is to choose the best choice between the usage (and causing degradation) of the BESS and the installment of the fines because of the VPP power fluctuations around the selected equilibrium value $P^*(t)$. The proposed method will select the best combinations of these two components from an economic perspective and amid a broadened timeframe, guaranteeing that the electrical constraints of the grid are satisfied amid the full time interim. In the tested case, $P^*(t)$ has been selected as

a daily flat value, equivalent to the average balance of the system amid the day. The results have been gotten by setting the total life costs identified with the BESS as $C_B^* = E_e^{Nom} \cdot C^{inst}$, where E_e^{Nom} is the nominal size of the BESS, and $C^{inst} = 1000 Eur/kWh$ are the BESS overnight costs per unit of capacity. The average fines costs has been set to $P_{av} = 150 Eur/MWh$.

The proposed technique has been applied for the planning step including the correct positioning of the BESS. Then, the impacts of the tested BESS have been assessed by simulating the presence of the optimized BESS in one node of the network. The methodology has been replicated per each bus of the grid, comparing the effect of the BESS position on the operating parameters. As first outcome, it has been discovered that all the network constraints given in sec. 2.2 are met for each considered time interim and for each position of the BESS. This high stability of the system is because of two factors: the nearness of household users, and the optimal location of DGs performed in [132]. Thus, no considerations with respect to the system voltage phasors and thermal limits ought to be taken for characterizing the correct position of the BESS. However, the proposed technique would be able to include these parameters in the planning step in case of potentially unstable grids.

Besides, the GA-MPOPF took into account the estimation of the network losses for the different positioning of the BESS. The outcomes of this technique are given in Fig. 2.4 and Fig. 2.5. The values related to each bus n demonstrate the monthly losses of the system when the BESS is located on the bus itself. Values are given in kWh. The best position of the BESS has been observed to be at hub 11.

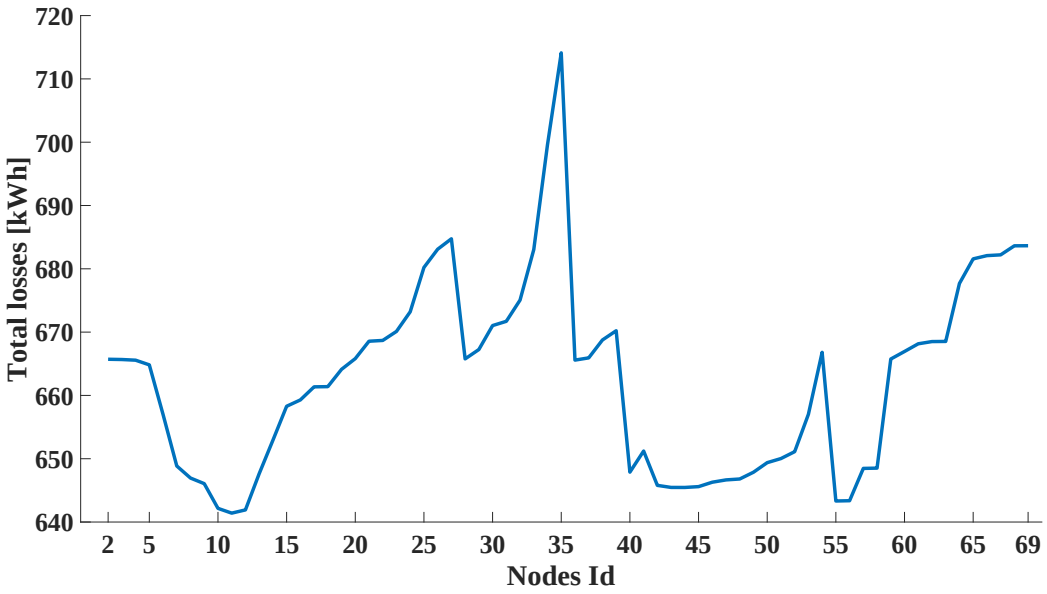

Figure 2.4: Monthly energy losses for different positioning of the BESS.

Once identified the best position of the BESS, it is possible to assess the economic effect of the BESS on the network. Fig. 2.6 and Fig. 2.7 demonstrate the optimization

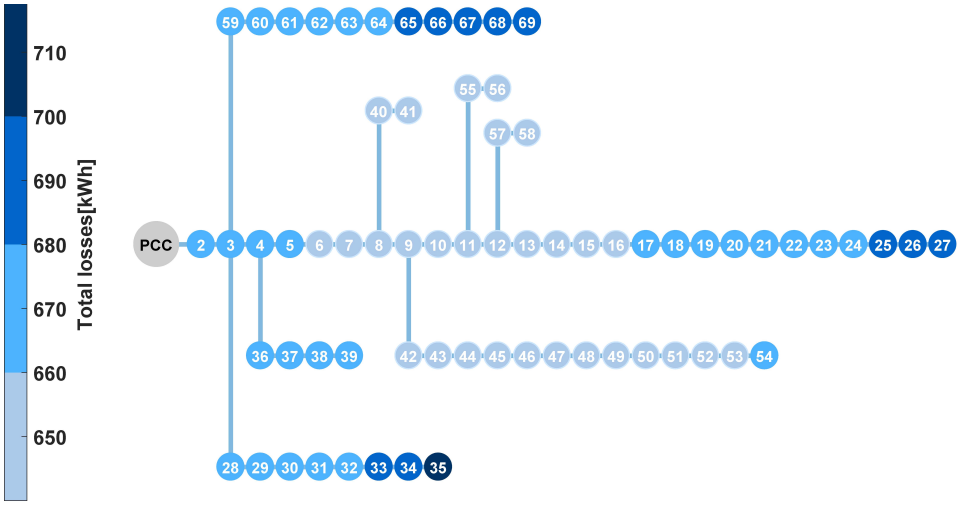

Figure 2.5: Monthly energy losses associated to each different location of BESS. The losses are given by means of a color code, described in the legend.

results for the considered month, considering quadratic cost fines, and for the position of the BESS on bus 11. Additionally, Fig. 2.6 demonstrates the power output at the PCC of the VPP. This result is demonstrated both with and without the BESS for the quadratic cost function. Fig. 2.7 demonstrates the SoC profile of the BESS amid the studied month. Figures indicate how, depending on the specific shape of the system power fluctuations, the optimized number of daily full cycles is somewhere in the range of zero and two, with the general BESS micro cycles. Furthermore, Fig. 2.8 demonstrates the daily costs for the studied moth. More in detail, the black line demonstrates the reference fines cost value of the system without the BESS, the green line demonstrates the system fines in nearness of the BESS, and the orange and red lines demonstrate the cumulative cost of fines and calendar aging, and the cumulative cost of fines, calendar and cycle aging respectively. The last one shows the aggregated cost of the considered system in nearness of the BESS. These costs have been computed over the monthly optimization by following the technique given in Sec. 2.2. The calendar aging impact has been calculated by setting a time window $\Delta\tau$ per each day, while the daily cycling aging impact has been computed by considering all the cycles performed in the day.In the case in which one or more considered cycles crossed over one day, the amortization cost of the cycle has been divided among the days accordingly, to the proportion between the time that the cycle spanned amid the days and the aggregate cycle length. Also, the result with regards to the system costs accumulated on a monthly base is given in table 2.1, while the aggregated monthly fluctuations $\int |P(t) - P^*(t)|dt$ at PCC are given in table 2.2.

Thus, the optimized utilization of the BESS demonstrates a decrease in the fines cost between 30 and 60% on a daily basis, if compared with the fines cost without the BESS. A similar results calculated on a monthly basis leads a fines cost decrease of 50%. Since both the BESS calendar and cycle aging demonstrated daily amortization cost ranging

between 10% and 15% of the daily fines without the BESS, this interpreted in a reduction of the system amortization costs in the range of 10 and 25%. A same quantity computed on a monthly basis demonstrated a decrease in the system total costs of 18%.

Table 2.1: Comparison of monthly costs with and without BESS

Monthly considered costs	Costs (Euro)	Cumulative Costs (Euro)
Fines with BESS	5'200	5'200
Calendar aging	1'800	7'000
Cycling aging	1'700	8'700
Fines w/o BESS	10'500	10'500

Table 2.2: Comparison of monthly energy fluctuations $\int |P(t) - P^*(t)|dt$ at PCC level with and without BESS

Type	Energy (MWh)
With BESS	49.7
Without BESS	70.2

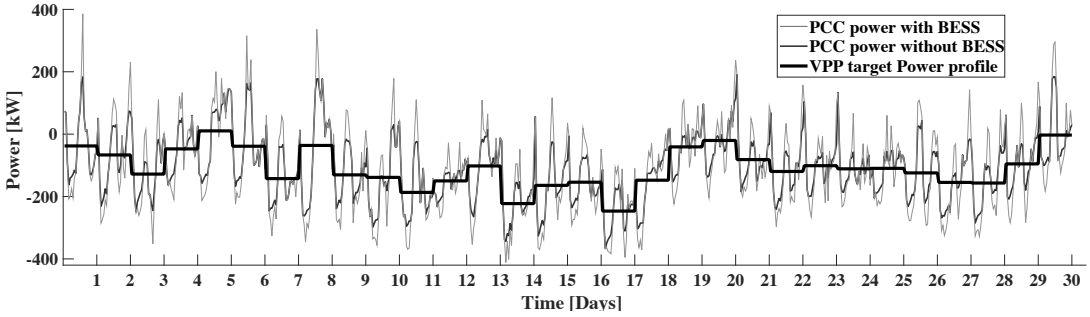

Figure 2.6: The power profile at the PCC of the considered VPP, in both presence and absence of the BESS.

In particular, the results shown in fig. 2.9 highlight that all the cost functions show a relative convergence error under 1.5%. Cubic and exponential cost functions show even better convergence properties, of the order of 0.2% and 0.1%, respectively. This is due to the particular shape of the cost functions, depicted in fig. 2.3. In fact, both the cubic and the exponential cost functions show a flat cost for small power fluctuations. For this reason, the usage of the battery in the flat area is not economically advantageous. Since the usage of the BESS is economically forbidden in this areas for cubic and exponential cost functions, the optimization easier to achieve.

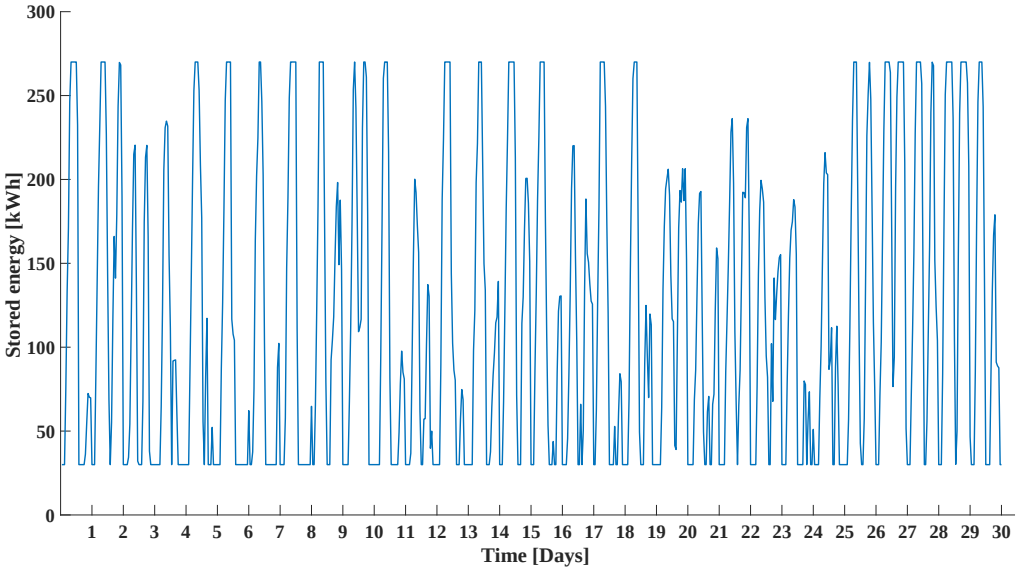

Figure 2.7: The time evolution of the energy stored in the considered BESS.

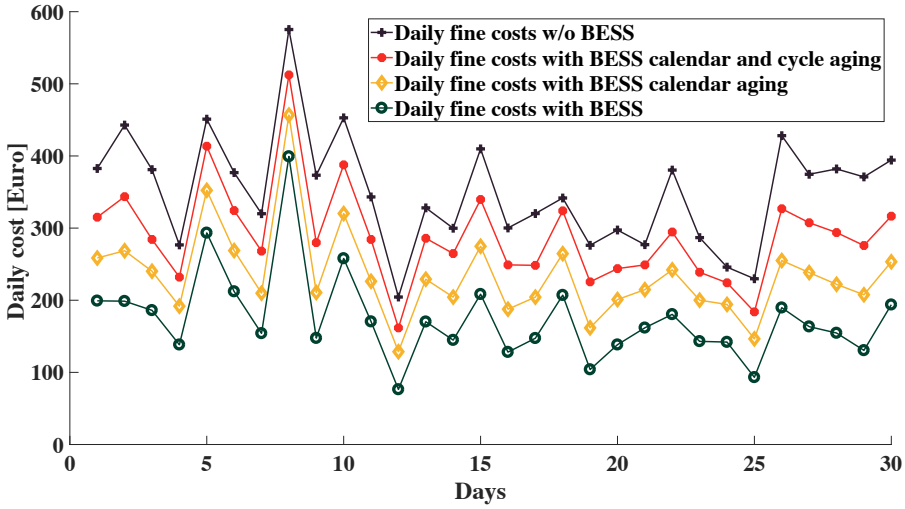

Figure 2.8: The daily cost of the system. The fines cost and the BESS calendar and cycling aging amortization costs are given as a sum. Also, the daily fines cost of the system without the BESS is given as a reference.

Regarding the algorithm's performance, figures 2.9 and 2.10 demonstrate the convergence properties of the proposed GA-MPOPF. Since the GA method includes random sampling of the given space, the results of various optimization runs performed on a same system configuration can differ, providing different results in regards to the final optimized fitness function and the running time. To distinguish the effect of this random sampling and estimate the convergence properties of this stochastic procedure, the optimization method has been repeated for 1000 times in a same time interim. At that point, the achieved daily optimal costs and running times are shown as histograms. Fig. 2.9 demonstrates the histograms of the optimal costs and Fig. 2.10 demonstrates the histograms of the running time. In order to examine the different convergence properties of the method for various sorts of cost functions, a similar strategy has been applied for the cost functions depicted in sec. 2.3. The outcomes shown in Fig. 2.9 feature that all the cost functions demonstrate a relative convergence error under 1.5%. Cubic and exponential cost capacities demonstrate far better convergence properties around 0.2 and 0.1 %, respectively. This is because of the specific shape of the cost functions, portrayed in Fig. 2.3. Indeed, both the cubic and the exponential cost functions demonstrate a flat cost for little power fluctuations. Thus, the use of the BESS in the flat area isn't financially valuable. Since the use of the BESS is economically forbidden around there for cubic and exponential cost functions, the optimization easier to obtain.

As results, the algorithm shows excellent convergence properties for all types of cost functions.

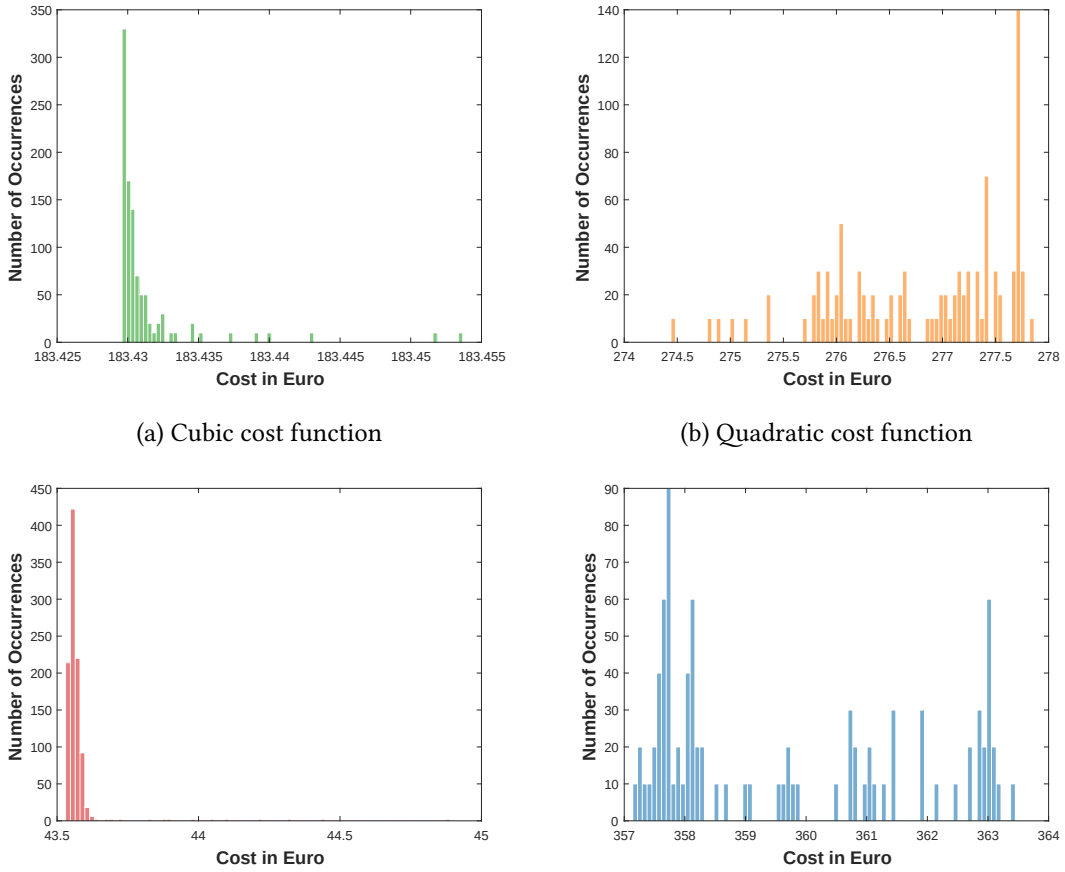

(a) Cubic cost function

(b) Quadratic cost function

(c) Exponential cost function

(d) Linear cost function

Figure 2.9: Histograms of the convergence of the total cost considering the four different tested cost functions.

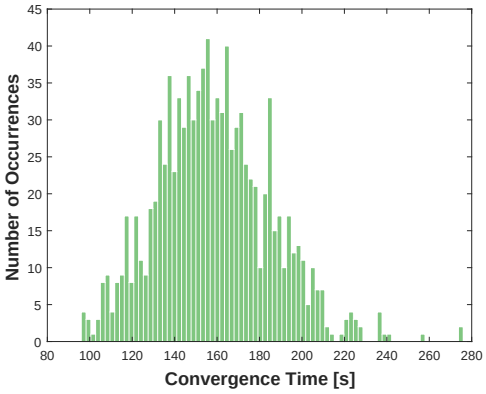

(a) Cubic cost function

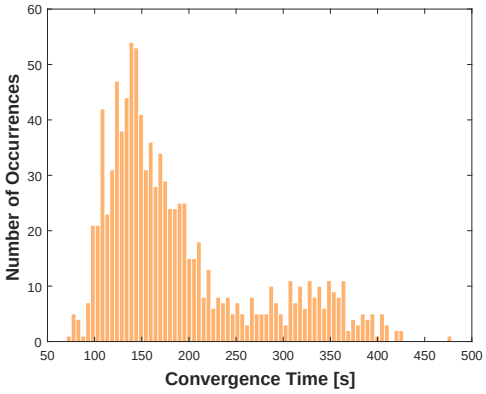

(b) Quadratic cost function

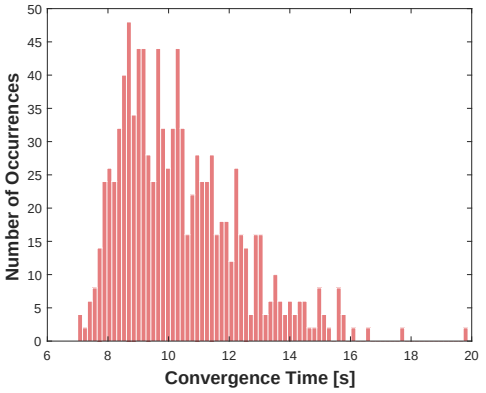

(c) Exponential cost function

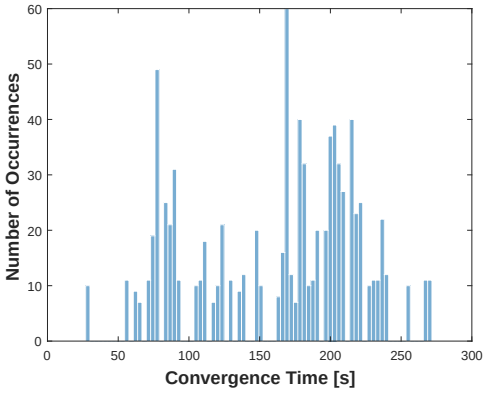

(d) Linear cost function

Figure 2.10: Histograms of the running time for different cost functions.

2.5 Discussion & Conclusions

The results regarding the BESS positioning are given in Fig. 2.4 and Fig. 2.5. The figures show how the correct positioning of the BESS in this framework can set aside to 10% losses. From a systemic point of view, the best location of the BESS with respect to system loss minimization, has been observed to be in the topological center of the network, in node 11. As demonstrated in Fig. 2.5, the location of the BESS on the encompassing buses has been turned out to be a decent decision.

About the results of the optimization given in Figs. 2.6, 2.7 and 2.8, the algorithm has been observed to be solid in restricting high power fluctuations, demonstrating non-trivial management choices in the case of fluctuations over timeframes of different hours, potentially prompting a high fine for the aggregator. In order to lessen these fines, the algorithm chose to aplit the accessible energy capacity of the BESS amid the full interim. In addition, it is imperative to see how small fluctuations are not compensated by the utilization of the BESS, since the fines related to them are lower than the cycling aging expenses of the BESS. This impact is clear when Figs. 2.6, 2.7 and 2.8 are compared: the days described by small power fluctuations indicate wasted BESS capacity and low cycling costs, because of the restricted usage of the BESS.

At long last, taking into account the behavior of the system in nearness of relevant power peaks, it is possible to see how the BESS energy is almost used for diminishing the high peaks of fluctuation. This is because of the quadratic shape of the fine cost function, which forces the algorithm to give priority to high fluctuations. The power requested at PCC level in presence of the highest peaks is decreased in the range of 30 and 50%. The impact of this decrease clearly impacts on the daily system costs. This is obvious when comparing Figs. 2.6 and 2.8 in the days in which the highest fluctuations are happened around the mean value. In particular, these are the days 2, 5, 8, 10, 15, 22 and 26. Particularly on days 2, 8 and 26, it is clearly obvious how the fine cost is decreased by around 60% by using the BESS. By comparing this values in details, such a major reduction in fines costs is legitimate of the days in which it is possible to see steady fluctuations in power, which does not keep going for more than two-three hours. If they last longer, considering the day 8, the reduction in the fines costs because of the presence of the BESS is decreased to a value around 30%.

The cost results of the optimization are compared with the available literature, and especially with papers which evaluate the cost effect of ESSs using MPOPF strategies and quadratic cost functions for the balancing generation [120, 117]. The subsequent cost reduction achieved in [120] in the range of 40 and 50%, regarding the cost of the system without ESS. In the study performed in [117], the authors identified an improvement around 10% in the cost with respect to the case without ESS. The two papers did not determine the type of considered ESS, and did not consider any aging cost for them. In any case, it is possible to compare their outcomes and the ones displayed here, without considering the BESS aging costs. In this specific case, the findings of this work concur with the ones in [120], and in addition indicating better cost improvements over the ones

found in [117].

This chapter also introduced a Multi-Period Optimal Power Flow technique based on Genetic Algorithms. The proposed method is intended for the optimization of both planning and unit-commitment issues in presence of ESSs and fluctuations actuated by distributed RESs, and can consider the costs identified with the aging of the ESSs. As a test case, it has been applied to an IEEE prototypical test network aiming to work as a VPP by means of the application of a Li-ion battery. The proposed methodology has been utilized for two different applications: a first, planning one, including the meaning of the correct positioning of the BESS in the grid; and a second, operative one, including the meaning of the correct management strategy of ESS. In addition, a convergence analysis of the proposed technique is introduced. Four cost function models (linear, exponential, quadratic, and cubic) have been considered for this analysis.

Results confirm the significance of the GA-based multi-period optimization method when dealing with ESSs. The proposed methodology has been observed to be able to manage complex choice decision criteria with respect to the optimal management of both the cycle aging costs and the SoC profile of the BESS. Additionally, the proposed method is able to manage longer time ranges regarding the methodologies proposed in literature, going beyond the common time scales between one day and on week, proving to be able to optimize dataset even monthly time scales. This allowed its application for planning strategies. Also, a comparison of the results of the proposed approach with similar ones present in literature, highlights the significance in considering the ESS aging costs amid the economic optimization. In particular, results demonstrate that including aging expenses can fundamentally change the quantitative results of the economic evaluation. Since the amortization costs because of BESS aging indicate a portion somewhere in the range of 40 and 60% of the total system costs, neglecting to consider them can prompt a critical underestimation of the costs. On the other hand, the analysis performed in this work affirmed the economic advantages related to the installation of a BESS, for the investigated purposes.

Additionally, a convergence analysis of the proposed GA-MPOPF indicated excellent convergence properties when converging to the optimal cost, even in the extraordinary instance of the exponential cost function (i.e. when using ESS is not ideal due to the lower cost of the fine). This allowed the identification of the different response of BESS for various fine systems.

In general, the use of genetic algorithms provides the user with the advantage of an adaptable and completely configurable device both under the technical and economic perspective. This is featured by the results with respect to the algorithm convergence properties, which have indicated incredible and quick convergence even on account of nonlinear limitations and nonlinear objective functions.

Chapter 3

Real-Time Planning and Management of Storage Systems Considering Cycle and Calender Aging Costs

3.1 Introduction

Many studies have been performed for the management and planning of ESSs [111, 112, 113, 114, 115, 116]. Although the usage of ESSs bring many advantages for the power systems but modeling of them still have own issues, particularly when including the amortization costs in the model. Actually, the performance of ESSs are highly depended on a period of time, and can not be separated from their past, present and future utilization. Therefore, for the optimization of ESSs multi-period optimization techniques [117, 118, 119, 120, 121, 122] should be considered and single period optimization techniques do not meet the realities of the management and control of ESSs. Moreover, the multi-period optimization techniques must model the ESS aging costs in the optimization procedure, exclusively for electrochemical ESSs such as battery. The BESSs aging models have considerable non-linear behaviour and can be characterized by the calendar aging which depends on time and cycle aging which depends on the usage way of the BESS [42].

On the other hand, another major problem for managing and controlling of the ESSs is the Real-Time control and management of them. In real cases, the model of the usage of ESSs must be addressed in the Real-Time applications, otherwise the planning and management of them fail to be applicable. As mentioned above, for optimal management and control of ESSs two factors must be considered: (1) Multi-Period optimization; (2) Including the aging costs during the optimization procedure. These factors should be considered in the Real-Time optimization techniques. There are some studies about Real-Time optimization of ESSs in the power systems [136, 137, 138, 139, 140]. However, they are failed to address the multi-period optimization and including the aging costs in the real-time optimization procedure.

By considering the real-time optimization requirements, this study proposes a novel multi-period OPF method real timely, called Real-Time GA-MPOPF. The GA-MPOPF has been described in details in[141]. The Real-Time GA-MPOPF allows an optimization of complex cost functions during a lengthened time period considering BESS degradation costs and optimize the usage of it in the power system taking into account energy market costs. Additionally, the system constraints and technical parameters has been considered in the optimization procedure by using the power flows calculation for each time step.

The origin of real-time optimization requires the optimization for each real-time step. However, as previously mentioned, the BESS aging costs optimization must be done for an extended time period. For this reason, in the proposed methodology the data has been characterized as historical power and predicted power. In fact, by passing the time, the name of actual data can be turned to historical data. The historical (actual) power which is known from the name of it, the power from past to present and the predicted power is the power from present to future. Knowing that the real-time optimization must be done for the present time, the novelty of this work is that the present time optimization is performed by considering both historical(actual) and predicted power (Multi-Period) to have more reliable calculation for including of the BESS aging costs.

The Real-Time GA-MPOPF method is able to optimize both Multi-Period and including aging costs of BESS real-timely. In order to test these highlights, it has been employed into the standard 69 bus IEEE PG & E grid, in attendance of a high penetration of RES DGs and Li-ion BESS. For testing the proposed approach the grid has been designed as a Virtual Power Plant (VPP) whose goal for each real-time interval is to follow a particular power profile amid the day. Any deviation from such profile produces an extra cost for the VPP aggregator under the type of a fine. In this work, the BESS is used to balance the VPP fluctuations with a specific end goal to reduce the aggregate sum of the fines in a period of one year. To appropriately assess the amortization expenses of the Li-ion BESS, a novel time subordinate cost function is proposed in view of the Battery Degradation Model (BDM) presented in [42]. The used power profile in this study is for one year, sampled at one hour time intervals for a total of 8761 time steps. The power profile of first week (168 time sample) has been used for producing the predicted power for each time sample. The predicted power profile is estimated for 6 hours in forward for each time sample. Then, the total predicted power which is processed for the entire year is included $(8761 - 168) \times 6 = 51558$ time samples. The Real-Time GAMPOPF method is used for each time interval, the 18 hours historical power profile and 6 hours predicted power profile.

The proposed procedure is applied to the test grid from both a planning and a management perspective. The planning procedure consists in the identification of the optimal size of the BESS. The operative analysis consists in the identification of the optimized management of the BESS for each time step and fulfilling the optimization procedure for the entire year.

3.2 Methods

The objective of the proposed Real-Time method is the optimization of ESSs and Controllable Generators (CG) in a power system in the form of real time. First of all, the feasible area for optimization process must be described for the method. For this reason, the optimization has to satisfy the system constraints. This constraints can be described in means of equality and inequality constraints. A detail of the inputs of the proposed procedure is described in subsec. 2.2.1. Additionally, the real-Time optimization procedure with its outputs is defined in detail in subsec. 3.2.2. The analysis of data for providing the predicted or estimated data, aiming the usage of them for real-time applications has been defined in subsec. 3.2.1. Furthermore, the cost function C_f has been described in subsec. 2.3.2. At long last, subsec. 2.2.3 characterizes the Li-ion Battery Degradation Costs Model (BDCM) utilized as a part of this study for the meaning of the cost profile of the BESS.

3.2.1 Exponential smoothing and ARMA model

The time series associated to the fluctuations are indicated with y. Each time series is composed by 8761 samples (hourly sample for the studied year). Referring to the literature [142], two time scales can be identified: a slow one, corresponding to scales over the daily oscillations, and a faster one, corresponding to the hourly fluctuations. To separate the two time scales a baseline y_{bl} is estimated by means of an exponential smoothing method described in [143].

Figure 3.1 shows an example of baseline estimation from the fluctuation of microgrid.

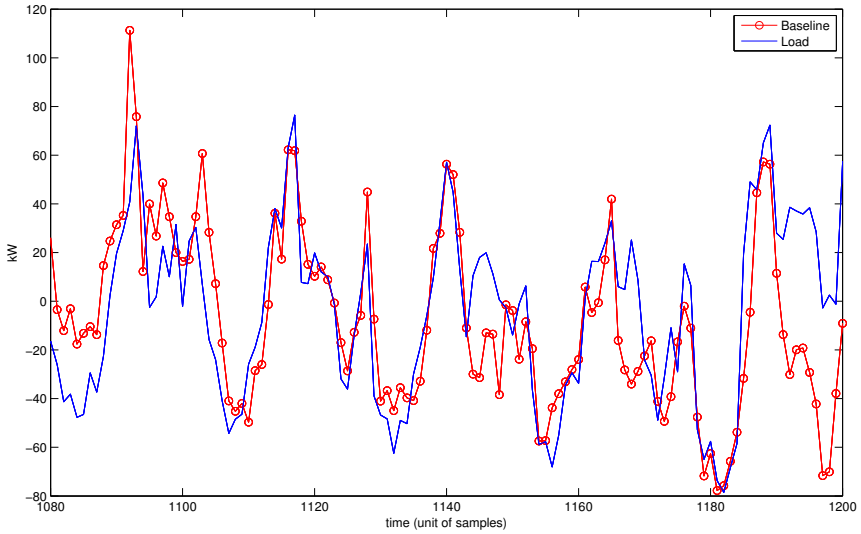

Figure 3.1: Exponential smoothing used to estimate the baseline

Given a time series $y = [y_1, y_2, \ldots, y_N]$, the baseline at each time step k is estimated by referring to the same time of the week before, assuming that load profiles are strongly conditioned by the specific day of the week (i.e. Mondays are similar to successive Mondays, and different from Sundays), [142]:

$$y^i_{bl}(k) = \beta y^i(k - \Delta) + (1 - \beta) y^i_{bl}(k - \Delta), \tag{3.1}$$

where k is the current time step and Δ is a delay of 168 time steps, corresponding to exactly seven days, while the smoothing parameter β is selected in order to minimize the root mean squared error of the residuals r:

$$r^i(k) = y^i(k) - y^i_{bl}(k) \tag{3.2}$$

The residuals r^i can be further modeled by means of a ARMA model of the type:

$$r^i(k) = \frac{C(q)}{A(q)} e(k) \tag{3.3}$$

where $e(k)$ is a zero-mean white stochastic process and $C(q), A(q)$ are polynomials in q^{-1}:

$$A(q) = 1 + c_1 q^{-1} + c_2 q^{-2} + \cdots + c_N q^{-N} \tag{3.4}$$
$$C(q) = 1 + a_1 q^{-1} + a_2 q^{-2} + \cdots + a_N q^{-N} \tag{3.5}$$

3.2.2 Optimization Procedure and Outputs

The details of GA-MPOPF based optimization procedure has been described in subsec. 2.2.2. The GA-MPOPF is used for the proposed real-time method optimization procedure.

Fig. 3.2 shows the time-line (the way data are used) for the Real-Time GA-MPOPF method. The predicted power profile $P_p(t)$ is obtained by the method mentioned in subsec. 3.2.1. $P^h_r(t)$ indicates the historical first week data which the reason of usage of them has been described in subsec. 3.2.1. The historical (actual) power $P_r(t)$ is a power profile which is considered as real-time power profile obtaining from online data center at PCC. This real-time power is also can be said the actual power of the system. The corresponding of this data for optimization procedure as real-time is necessarily important. The Real-Time method uses historical power profile from $P^h_r(t_{k-m})$ to $P^h_r(t_{k-1})$ in order to estimate the power level at PCC for each time $t_{k+1} \ldots t_{k+n}$. Making it more clear, again from Fig. 3.2 can be seen, when the real-time is at t_k, the real-time power level is updated by its actual value (from online data center) and the model estimates the power profile for next i time intervals in forward till t_{k+i}, and then when the real-time is at t_{k+1}, the power estimator predicts the power for next i time intervals in forward till t_{k+1+i}, and this mode will continue for the all real-time intervals $t_{k+2}, t_{k+3}, \ldots$.

As it is mentioned in subsec. 2.2.2 the cost function $C_f = C_f^{\Delta\tau} + C_f(P)$ has two parts: $C_f^{\Delta\tau}$ is the aging cost function of BESS, and $C_f(P)$ is fine cost function. The calendar

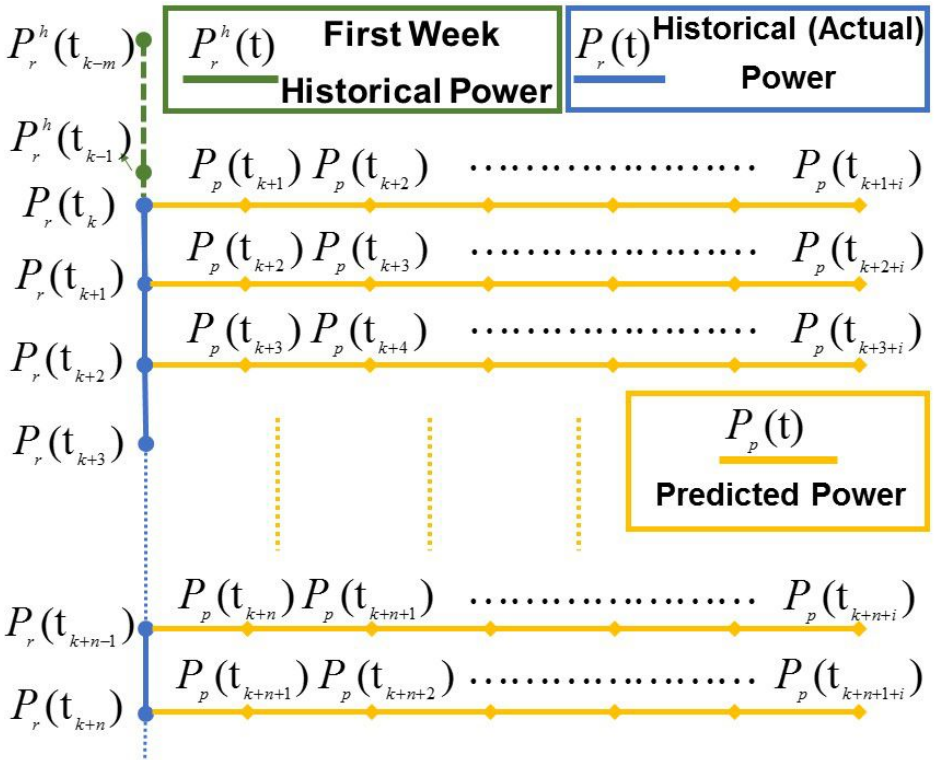

Figure 3.2: Data-set used as Real-Time

and cycle aging is belong to $C_f^{\Delta\tau}$. So, in optimization procedure of $C_f^{\Delta\tau}$, it should be considered as multi-period optimization. In particular, when the multi-period optimization has been considered with prediction of some times in forward, Battery Management Systems BMS can decide whether to charge or discharge or neither charge or discharge of BESS based on aging costs optimization. In details, SoC of BESS for the some next times can be estimated, by knowing the level of requested energy for those times. In this way the aging costs of BESS are included in the calculations considering multi-period optimization. Simultaneously, $C_f(P)$ should also be optimized in the procedure of BESS costs optimization. The BESS cost model has been described in subsec. 2.2.3. For providing the data in multi-period way and using that data for real-time purposes, the data are used as they are shown in Fig. 3.2.

Fig. 3.3 shows how the historical and predicted power profiles contribute in the Real-Time multi-period optimization of BESS. To obtain optimized power of BESS P_{BESS} at time t_{k+1} the historical power profile $P_r(t_{k-m}), \ldots, P_r(t_k)$ has been used for 2 goals; first of all, to use them for generation of predicted (estimated) powers (subsec. 3.2.1). Secondly, to use them for multi-period optimization purposes. Once the estimator forecasts predicted power profile $P_p(t_{k+1}), \ldots, P_p(t_{k+1+i})$, the BESS power profile can be obtained by using Real-Time GA-MPOPF method shown in Fig. 3.4 for the period of time $t_{k-m}, \ldots, t_{k+1+i}$, which from time t_{k-m} to time t_k, the $P_{BESS}(t_{k-m}), \ldots, P_{BESS}(t_k)$ are historical optimized power profile of BESS and from time t_{k+1} to time t_{k+1+i}, $P_{BESS}(t_{k+1}), \ldots, P_{BESS}(t_{k+1+i})$ are predicted optimized power profile of BESS. When

the online time step will be updated to t_{k+1}, the real power of PCC will be updated by its actual value $P_r(t_{k+1})$ (real-time data is coming from online data center), and this value will be used for the estimation of predicted power for next time step, $P_p(t_{k+2}), \ldots, P_p(t_{k+2+i})$. So, Real-Time GA-MPOPF method can optimize the power profile of the BESS $P_{BESS}(t_{k+2}), \ldots, P_{BESS}(t_{k+2+i})$ for the next time steps from t_{k+2} to t_{k+2+i}. This procedure will continue for the next time intervals in this way. It should be noted that the calculation of cost function $C_f(P)$ for time t_{k+1} will be $P_r(t_{k+1}) + P_{BESS}(t_{k+1})$ and for t_{k+2} will be $P_r(t_{k+2}) + P_{BESS}(t_{k+2})$ and so on.

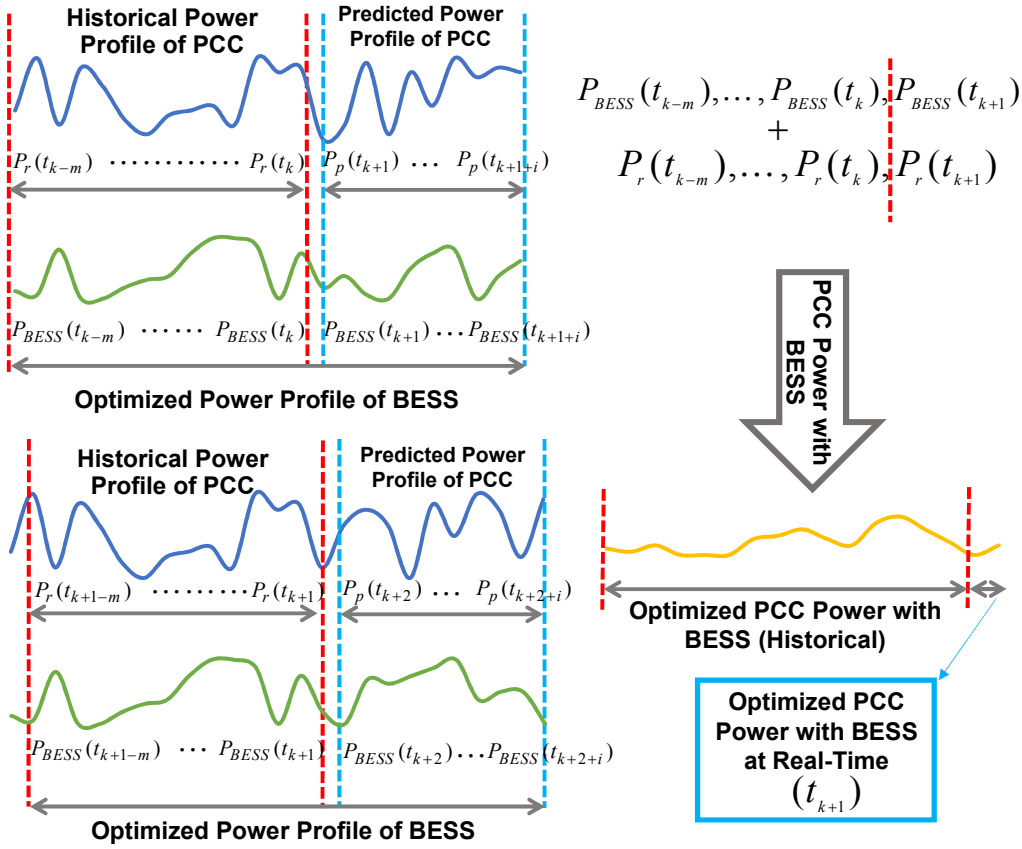

Figure 3.3: The procedure of analysis of the historical and predicted power in ordered to obtain optimized BESS power profile $P_{BESS}(t_{k+1})$ at real-time interval t_{k+1}

Although, power profile of BESS is optimized for historical and predicted powers $P_{BESS}(t_{k-m}), \ldots, P_{BESS}(t_k), P_{BESS}(t_{k+1}), \ldots, P_{BESS}(t_{k+1+i})$, but for the calculation of $C_f^{\Delta\tau}$ for each real-time step, the real-time value of $P_{BESS}(t)$ must be used. For example when the real-time is at t_{k+1}, the optimization of BESS power is performed for $P_{BESS}(t_{k-m}), \ldots, P_{BESS}(t_{k+1}), P_{BESS}(t_{k+2}), \ldots, P_{BESS}(t_{k+2+i})$, but for calculation of $C_f^{\Delta\tau}$ must be used just $P_{BESS}(t_{k+1})$. This procedures are clearly described in Fig. 3.3, illustrating the procedure just for 2 time intervals and the procedure for the next time steps is the same.

The proposed Real-Time GA-MPOPF optimization method which is shown in the

flowchart in Fig. 3.4 describes the real-time optimization procedure. The online data is sent from online measurement center (SCADA), the real-time power is updated for each time interval which can be named historical(actual) power profile and these historical (actual) power profiles are simultaneously used for generating of predicted power profiles. Both of them are sent to GA-MPOPF (well described in subsec. 2.2.2) to analysis and provides the optimal power profile of BESS $P_{BESS}(t)$ for each time interval, and it is considered for getting optimal power profile of BESS $P_{BESS}(t)$, the cost function C_f must be optimized.

It should be noted that the process time of GA-MPOPF $t_{GA-MPOPF}$ for finding the best solution must be well below the real time steps because to have ability of providing the $P_{BESS}(t)$ for the next real-time step, for example the real-time step is passing from t_k+1 to t_k+2, the time of analysis of GA-MPOPF must be $t_{GA-MPOPF} <<< |t_{k+2}-t_{k+1}|$.

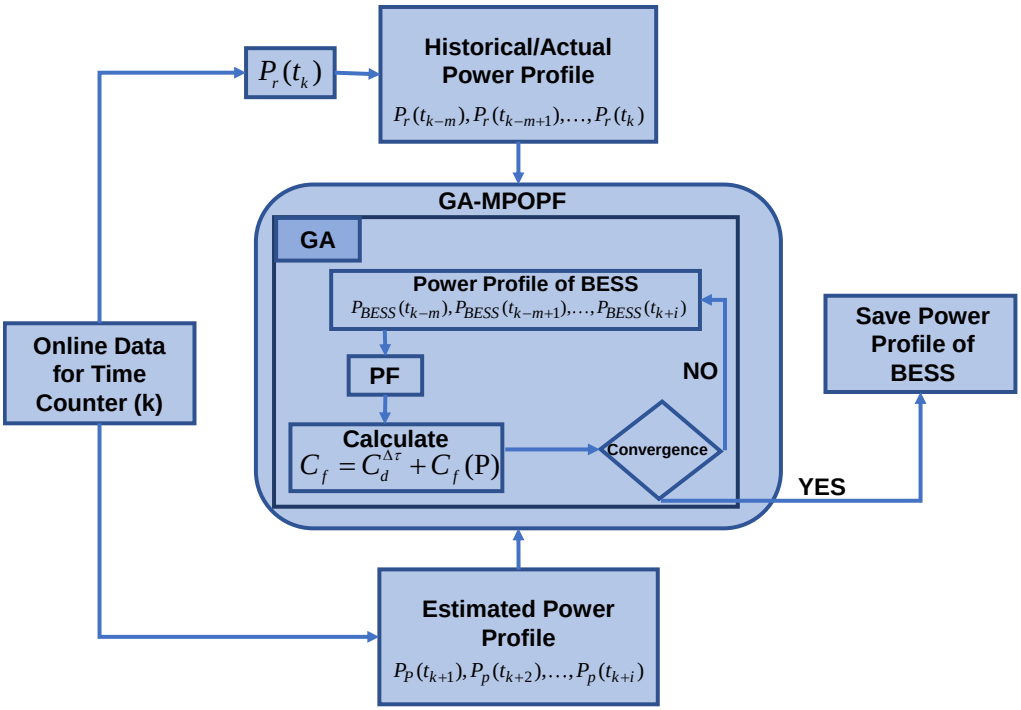

Figure 3.4: Real-Time GA-MPOPF flowchart

In this study, as first step, historical data of one year has been used to provide the predicted data using the method in subsection 3.2.1 and those predicted data has been used in the Real-Time GA-MPOPF optimization procedure, secondly, for evaluation of the proposed method, the historical power profile are used as actual data. For this reason, actual data are arranged in the same way that the predicted data profile are used (perfect knowledge of future).

3.3 Case Study

The Real-Time GA-MPOPF optimization method in this study has been applied to the real-time controlling and planning and sizing of a Li-ion BESS in a VPP. The Real-Time GA-MPOPF method goal is to provide a condition for VPP to manage the power output of it at PCC for each real time step. To obtain this goal, the VPP aggregator, has been supported by using of BESS. The details of the operation of the VPP and the cost function $C_f(P)$ has been described in sec. 2.3.

Moreover, for the Real-Time GA-MPOPF optimization method, the cost function is described in 3.6:

$$C_f(P) = F(P^*(t)) + R(|P(t) - P^*(t)|) \tag{3.6}$$

As it is mentioned in sec. 2.3, the constant cost function $F(P^*(t))$ follows the day-ahead market prices, and the fines cost function $\beta(P(t) - P^*(t))^2$ has been selected for $R(|P(t) - P^*(t)|)$. For the proposed method, $P^*(t)$ or target power profile has been chosen as a daily flat value, equal to the average predicted baseline power of network during the day. The coefficient β is defined in order to get an average fine of $P_{av} = 150 Euro/MWh$. To obtain this, the average predicted baseline power of the network for the studied year has been applied. $P(t)$ is the power of PCC with BESS $P_{pcc}(t) + P_{BESS}(t)$. In subsec. 3.2.2 is hinted that the proposed Real-Time method output is the optimized of $P(t)$ which it should make the cost function C_f minimum.

The IEEE 69 node PG & E Medium Voltage (MV) radial network has been chosen as case study, and the details of the network has been described in subsec. 2.3.1. However, in the subsec. 2.3.1 one size of BESS with 300 kWh is tested. In this chapter, different sizes of BESS 200, 300, 400, 500, 600 and 700 kWh has been also considered.

The analyzed timeline power data which is explained in subsec. 3.2.2. The data is sampled hourly for one year and totally 8761 hours of data has been analyzed in this work. The analyzed power profile of PCC P_pcc, is included of two parts; actual $P_r(t)$ power (by passing the time is changing the status to historical power) and predicted $P_p(t)$ power. In this case study, the historical (actual) power profile $P_r(t)$ and predicted power profile $P_p(t)$ for each day in the optimization procedure has been considered 18 hours and 6 hours, respectively. In this regard, from Fig. 3.2 and Fig. 3.3 for analysis of the real-time t_0, the historical power profile can be written as $P_r(t_{-17}), P_r(t_{-16}), \ldots, P_r(t_{-1}), P_r(t_0)$. Consequently, for the predicted power profile for the real-time t_0, $P_p(t_1), P_p(t_2), \ldots, P_p(t_5), P_p(t_6)$. For the next time steps by moving window of one hour (duration of each time step) and total cots of system is minimized for the whole year.

3.4 Results

The Real-Time GA-MPOPF method is used to optimize the usage of a BESS in a VPP, as described in detail in sec. 3.3.

The goal of the optimization is to choose the best choice between the use of the BESS (with consequent of degradation) and the installment of the fines because of the VPP power oscillation around the selected balance value $P^*(t)$ with a Real-Time approach. In the best possible way, the proposed technique will select the best combinations of these two aspects from an economic perspective and amid a broadened timeframes, guaranteeing that the electrical requirements of the network described in sec.2.2 are satisfied amid the whole time interim. In this study, $P^*(t)$ has been selected as a daily value, equivalent to the average of predicted baseline power value of the network amid the day. The following results have been obtained by setting the total life costs identified with the BESS as $C_B^* = E_e^{Nom} \cdot C^{inst}$, where E_e^{Nom} is the nominal capacity of the BESS, and C^{inst} considered 1000 €/kWh, 800€/kWh and 600€/kWh, is the BESS installation costs per kWh. The average fines costs has been set to $P_{av} = 150Eur/MWh$.

The proposed approach has been applied for the Real-time planning procedure including the sizing of the BESS. The procedure has been performed for different size of BESS, in order to obtain the best size of BESS on the operating parameters and minimizing the cost function C_f. As first outcome, it has been discovered that all the system constraints given in sec.2.2 are met for each considered time interim and for each size of the BESS. This high stability of the system is due to two factors: first, the demands of the tested network are household users only which the industrial loads of the network have been eliminated in [132], and second, the the optimal positioning of DG performed in [132]. In this regard, the tested network parameters allows for employing of different size of BESS. However, the system constraints have been considered as limits in power flow calculations. Hence, the proposed methodology can also be used in the planning procedure in case of potentially unstable grids.

The sec. 3.3 reminds that the predicted power for each time interval has been provided 6 hours in forward as an estimation of power profile at PCC. Whereas the historical power are considered as 18 hours in the past (each time step is one hour). In this way, historical and predicted power both used in means of Real-Time optimization approach considering a multi-period optimization of SoC of BESS taking into account BESS aging cots and market energy prices. The used power profile in this study is for one year, sampled at one hour time intervals for a total of 8761 time steps. It is also hinted in the subsec. 3.2.2 that the historical power profile are used as actual power to examine the predicted power exactness. For this reason, actual power are arranged in the same way that the predicted power profile are used (perfect knowledge of 6 hours in forward).

Fig. 3.5 shows the optimization results for the entire year, in the case of quadratic cost fines, and for both historical (actual) and predicted power for different BESS sizes and installation costs. In details, from Fig. 3.5 the green line is the reagent of total yearly cost of system in presence of BESS with 600 €/kWh installation cost and it shows when the BESS size is between 500 kWh and 700 kWh, the system cost is least. For 800 €/kWh installation cost of BESS which is indicated by orange line, when the BESS size is between 300 kWh and 500 kWh, the yearly fine cost of the system with BESS aging is minimum. Moreover, the red line is the green line is the reagent of total yearly cost of system in presence of BESS with 1000 €/kWh installation cost when the BESS

size is between 200 kWh and 300 kWh the system total cost is minimum. The dot lines are indicators of the yearly cost of the system with BESS 600, 800 and 1000 €/kWh installation cost considering the historical (actual) power profile. As it can be seen from Fig. 3.5, the results of historical (actual) and predicted power are almost similar for the BESS with same installation costs. It should be noted that the error of the estimation of the predicted power leads the differences between them and this difference is acceptable.

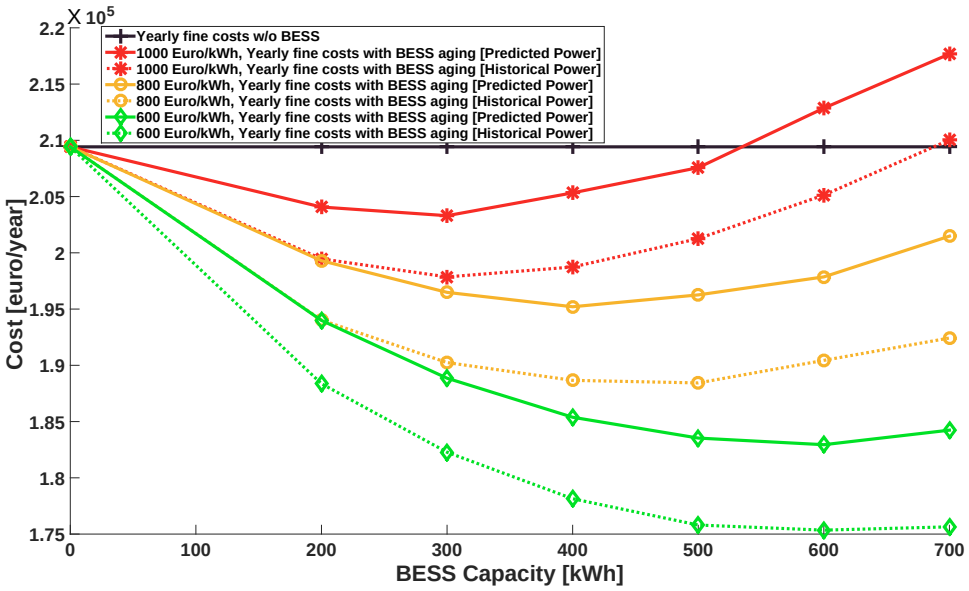

Figure 3.5: The Yearly cost of the system with different size of BESS and 600, 800 and 1000 €/kWh installation cost considering both historical and predicted power. The fine cost and the total BESS aging costs are given as a sum for the year. Also, the sum of yearly fine cost of the system without the BESS is given as a reference.

Fig. 3.6 shows separately the yearly costs of BESS for historical (actual) and predicted power for different BESS size and installation costs. In particular, the black line demonstrates the yearly reference fines cost value of the system without the BESS, the green lines demonstrate the system yearly sum fines with the BESSs, the orange lines illustrate the cumulative cost of yearly sum fines and calendar aging, and red lines show the cumulative cost of yearly sum fines, calendar and cycle aging. The last one describes the aggregate cost of the contemplated system in presence of the BESS. The red line in Fig. 3.6e is crossed the black line when the BESS size is around 700 kWh and as well as in Fig. 3.6f, the red line is passed the black line when the BESS size is around 500 kwh. Those characteristics show that the system with BESS 1000 €/kWh installation cost and those nominal capacities can not make economic profits and even it makes economic losses.

Also, the results regarding the system yearly profit with different installation costs and capacities of BESS are given in the tables 3.1, 3.2 and 3.3 for both historical and

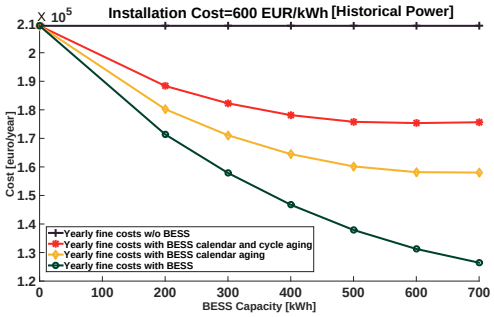

(a) Historical power, Installation cost 600 €/kWh

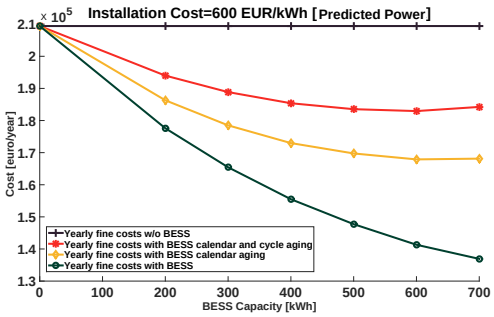

(b) Predicted power, Installation cost 600 €/kWh

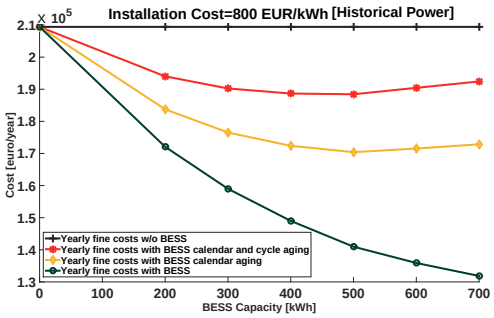

(c) Historical power, Installation cost 800 €/kWh

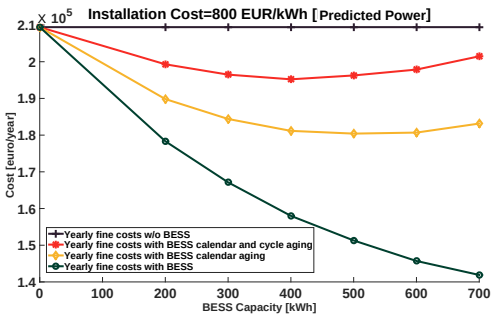

(d) Predicted power, Installation cost 800 €/kWh

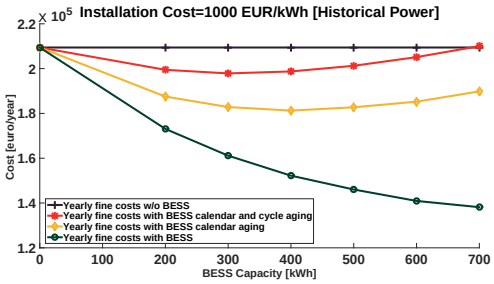

(e) Historical power, Installation cost 1000 €/kWh

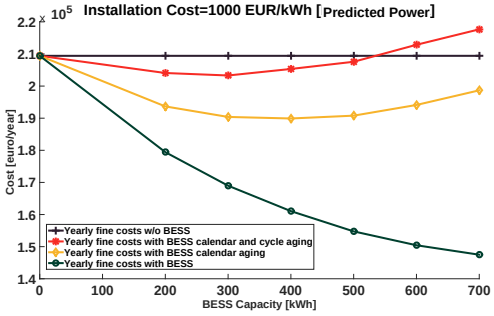

(f) Predicted power, Installation cost 1000 €/kWh

Figure 3.6: The Yearly cost of the system with different size of BESS and 600, 800 and 1000 €/kWh installation costs considering both historical and predicted power. The total fine cost and the BESS calendar and cycling aging amortization costs are given as a sum for the year. Also, the sum of yearly fine cost of the system without the BESS is given as a reference.

Table 3.1: Profit with 1000 €/kWh Installation Cost of BESS

1000 €/kWh Installation Cost of BESS		
BESS Size [kWh]	Yearly Profit [Historical power]	Yearly Profit [Predicted power]
700	€-628.26 [-0.30%]	€-8251.2 [-3.94%]
600	€4293.11 [2.05%]	€-3434.5 [-1.64%]
500	€8167.38 [3.9%]	€1863.8 [0.89%]
400	€10680.42 [5.1%]	€4104.6 [1.96%]
300	€11560 [5.52%]	€6115.1 [2.92%]
200	€9968.39 [4.76%]	€5361.2 [2.56%]

predicted power. From table 3.1, it can be seen, the yearly profit of the BESS 700 kWh capacity analysis with historical (actual) power is €-628.26 which means the system has an economic losses, and the system biggest gain is 5.5% with 300 kWh BESS size. Where, with predicted power the system with BESS size 600 kWh suffers economic losses more than 1.6%, and biggest profit is €6115 in presence of BESS size 300 kWh. As it is previously mentioned, the differences between historical (actual, best knowledge of future power) and predicted power are because of the error of estimation of the predicted power.

Table 3.2 shows that the system with 800 €/kWh installation cost considering both historical (actual) and predicted power does not make any economic losses for the various BESS capacities and the system biggest profit 10% with historical power is with BESS size 500 kWh. While, for the predicted power, 6.79% is the biggest profit of the system with the 400 kWh BESS nominal capacity but the system profit with 500 kWh is 6.28% which is close to 500 kWh BESS size profit.

Table 3.3 illustrates the system profit considering 600 €/kWh installation cost of BESS for historical (actual) and predicted power. In regards to predicted power the system makes yearly profit around €26470 (12.64%) and €25884 (12.36%) with BESS size 600 kWh and 500 kWh, respectively. While, considering the results with historical (actual) power, the system profit with BESS 500 kWh and 600 kWh are around €34554 (16.50%) and €34072 (16.27%) respectively. Furthermore, the tables 3.1, 3.2 and 3.3 show the system behaviour in presence of the BESS different capacities for the same installation costs for historical (actual) and predicted power is almost same. It means that the proposed Real-Time method which should work with predictive data has acceptable performance in comparison with its proficiency by using actual data. Also, it can be seen from those tables if the appropriate battery size is chosen, the system would have acceptable profit for the different BESS installation costs.

Moreover, Fig. 3.7 shows the monthly fine cost of the system in presence and absence of BESS, cumulative cost of fines and calendar aging and cumulative cost of fines and calendar and cycle aging for 600 €/kWh installation costs of BESS with 500 kWh size, 800 €/kWh installation costs of BESS with 500 kWh size and 1000 €/kWh installation costs of BESS with 300 kWh size. In particular, the black signs show the sum fine costs of system for each month in absence of BESS, the green signs show the system fines

Table 3.2: Profit with 800 €/kWh Installation Cost of BESS

800 €/kWh Installation Cost of BESS		
BESS Size [kWh]	Yearly Profit [Historical power]	Yearly Profit [Predicted power]
700	€17004.904 [8.12%]	€7937.018 [3.79%]
600	€18973.452 [9.06%]	€11559.984 [5.52%]
500	€20983.884 [10.02%]	€13151.576 [6.28%]
400	€20753.522 [9.91%]	€14219.618 [6.79%]
300	€19182.872 [9.16%]	€12942.156 [6.18%]
200	€15392.37 [7.35%]	€10114.986 [4.83%]

Table 3.3: Profit with 600 €/kWh Installation Cost of BESS

600 €/kWh Installation Cost of BESS		
BESS Size [kWh]	Yearly Profit [Historical power]	Yearly Profit [Predicted power]
700	€33779.446 [16.13%]	€25193.226 [12.03%]
600	€34072.634 [16.27%]	€26470.688 [12.64%]
500	€34554.3 [16.50%]	€25884.312 [12.36%]
400	€31287.348 [14.94%]	€24041.416 [11.48%]
300	€27140.832 [12.96%]	€20565.044 [9.82%]
200	€21046.71 [10.05%]	€15434.254 [7.37%]

in presence of the BESS for each month, the orange signs show the cumulative cost of fines and calendar aging for each month and red signs show the cumulative cost of fines, calendar and cycle aging for each month. The red signs represent the total cost of the system in the presence of the BESS for each month.

The quadratic fine cost function which is described in subsec. 2.3.2 has been calculated based on yearly average of baseline of power $P_b(t)$ fluctuation and the parameter β defined in order to obtain an average fine of $P_{av} = 150 Euro/MWh$. It can clearly be seen from Fig. 3.7a and Fig. 3.7b, for the months 1, 11 and 12 the fine cost of system without BESS and the fine cost of system with total cost of BESS are too close. Since, in those months the power magnitude $|P(t)|$ is too small, therefore, 500 kWh BESS usage provides cycle and calendar costs. It should be noted that by decreasing the size of BESS, the system total fine cost with BESS can be improved for those months while it causes the less improvement for the other months especially months 9 and 10. Since, the calculation of the fine cost function is yearly, so that, the effect of those months on order to minimize the total costs of system, is more than the months 1, 11 and 12. More in details, tables 3.4 and 3.5 which describe the total cost of the system with BESS for each month and 200, 300, 400, 500, 600 and 700 kWh BESS sizes for historical and predicted power, respectively, can prove the above mentioned fact. According to the predicted power analysis in table 3.5, for example, for month 11, with 200, 300 and 400 kWh BESS capacities the total costs are €10445, €10334 and €10350, respectively, and those costs are

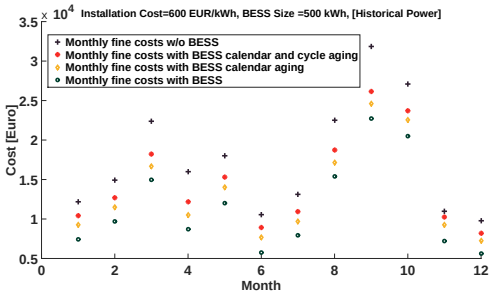

(a) Historical power, Installation cost 600 €/kWh

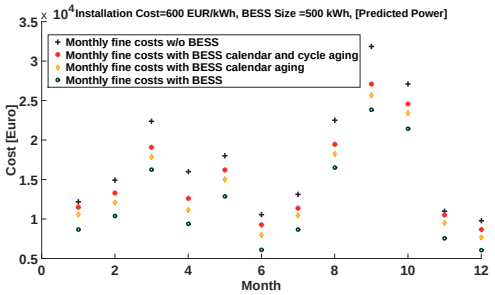

(b) Predicted power, Installation cost 600 €/kWh

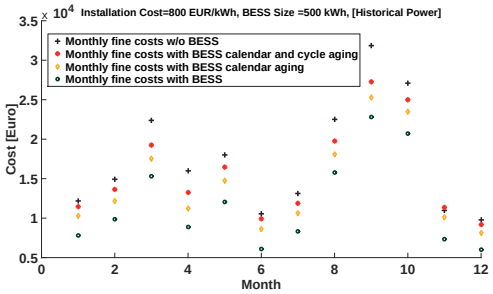

(c) Historical power, Installation cost 800 €/kWh

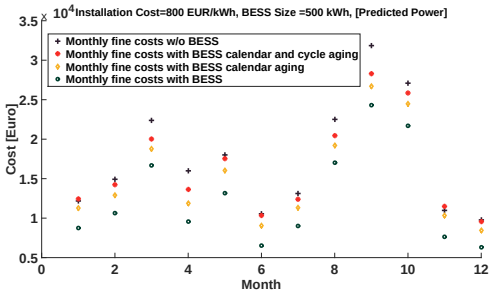

(d) Predicted power, Installation cost 800 €/kWh

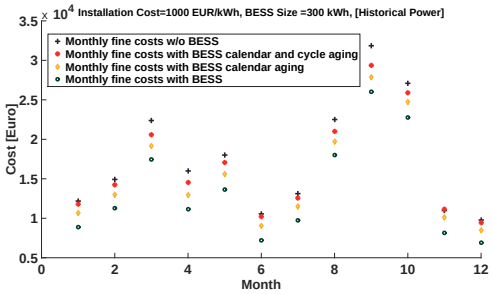

(e) Historical power, Installation cost 1000 €/kWh

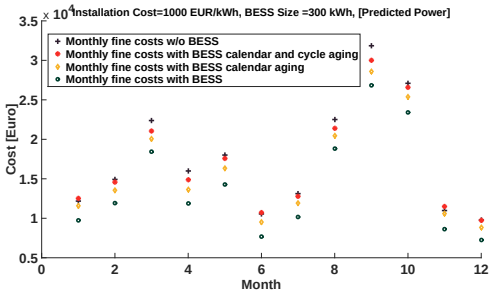

(f) Predicted power, Installation cost 1000 €/kWh

Figure 3.7: The monthly cost of the system with BESS 500 kWh and 600 €/kWh installation cost, 500 kWh and 800 €/kWh installation cost and 300 kWh and 1000 €/kWh installation cost for both historical and predicted power. The total fine cost with and without BESS and also the BESS calendar and cycle aging amortization costs are given as a sum for each month.

Table 3.4: Total cost of system in the presence of the BESSs with 600 €/kWh installation cost for each month [Historical power]

600 €/kWh Installation Cost of BESS [Historical power]							
BESS [kWh] / Month	0	200	300	400	500	600	700
1	12186	10791	10532	10406	10417	10664	10890
2	14921	13388	13008	12776	12707	12829	12754
3	22369	19963	19209	18624	18221	17919	17556
4	16010	13807	13087	12533	12173	11887	11690
5	18002	16194	15745	15386	15304	15605	16039
6	10565	9277	9039	8906	8939	9118	9351
7	13124	11749	11334	11078	10956	10932	11137
8	22510	20497	19796	19256	18734	18265	17976
9	31854	29051	27960	26997	26153	25479	24870
10	27105	25181	24513	23990	23723	23718	23702
11	10998	9924	9742	9992	10269	10560	11106
12	9779	8546	8312	8196	8206	8375	8574

less than the cost with 500 kWh BESS size which is €10499. Whereas, for the month 9, the costs with 200, 300 and 400 kWh BESS capacities are €29582, €28649 and €27788, respectively, which those costs are greater than the cost with 500 kWh BESS size which is €27078. Table 3.5 proves that the yearly Real-Time optimization of system with 500, 600 and 700 kWh BESS sizes for each month are more and less similar with historical (actual) power. It is clear from Fig.3.5 and table 3.3 the best size is 600 kWh which makes more profit for the system but because of the historical (actual) power optimized BESS size is 500 kWh for comparison 500 kWh BESS size has been selected for predicted power as well. On the other hand the differences between them is not too much. This predicted power has been provided for the real application of proposed Real-Time method, and historical (actual) power is only used to realize the method performance.

Fig. 3.7c and Fig. 3.7d belong to monthly costs for 500 kWh BESS with 800 €/kWh installation cost for historical (actual) and predicted power, respectively. The total fine costs with BESS for months 1, 6, 11 and 12 are too close to the fine cost without BESS even for month 11 the BESS usage caused an economic losses. Fig. 3.7d shows monthly real-time optimization results for the predicted power analysis, and it can be seen in the months 1 and 11, the usage of BESS causes economic losses. Table 3.7 shows that these costs are €12441 and €11479 for month 1 and 11, respectively. While, the costs without BESS for month 1 is €12186 and for month 11 is €10998 which are less than the costs in presence of 500 kWh BESS size. However, as above mentioned the optimization is done for the entire year and the BESS 500 kWh size is selected as almost the best size for 800 €/kWh installation cost for comparison with the historical (actual) power output BESS best size. It is clear from table 3.7 that by decreasing the size of BESS, the total

Table 3.5: Total cost of system in the presence of the BESSs with 600 €/kWh installation cost for each month [Predicted power]

600 €/kWh Installation Cost of BESS [Predictio Data]							
BESS [kWh] / Month	0	200	300	400	500	600	700
1	12186	11362	11190	11219	11490	11449	11882
2	14921	13763	13475	13286	13288	13335	13506
3	22369	20561	19870	19379	19061	18882	18719
4	16010	14301	13650	13111	12614	12321	12041
5	18002	16627	16242	16164	16198	16472	16859
6	10565	9705	9454	9297	9254	9429	9828
7	13124	12051	11722	11498	11381	11452	11576
8	22510	20834	20241	19808	19457	19119	19164
9	31854	29582	28649	27788	27078	26438	25998
10	27105	25803	25288	24917	24564	24451	24273
11	10998	10445	10334	10350	10499	10797	11260
12	9779	8957	8738	8567	8649	8798	9131

fine cost with BESS is improved for those months while the costs improved less for the other months. It can be seen from table 3.2 and Fig. 3.5 the system cost is decreased with 400 kWh BESS size more than other sizes of BESS for the optimization with predicted power.

Fig. 3.7e and Fig. 3.7f belong to monthly costs for 300 kWh BESS with 1000 €/kWh installation cost for historical and predicted power, respectively. Particularly, from 3.7f the months 1, 6 and 11 the costs with BESS is more than the costs without BESS. In more details, from table 3.9 the costs for months 1, 6 and 11 are €12522, €10713 and €11506, respectively. While the cots for those months without BESS are €12186, €10565 and €10998, respectively. However, as it is mentioned before the aim of the proposed Real-Time method is yearly optimization and the 300 kWh BESS size all in all for the entire year is improved more than other BESS sizes (table 3.1). If the proposed Real-Time method performs for the monthly optimization purposes the system performance with regards of the fine costs should be improved for each month not yearly and it is not applicable in the real cases whereas distribution operators consider for the planning and its energy markets yearly or seasonally. On the other hands, the BESS installation goal is not only making profit but also tolerate the system demand and response sufficiently. For example, if the planning be applied monthly, the months which consumption is less, BESS size should be smaller than the months with higher consumption which BESS size should be bigger, and this approach causes the BESS unuseful in some months and in this way the system can not make an economic profit for long term planning approaches.

Fig. 3.8 and Fig. 3.9 show the optimization results for each month, in the case of quadratic cost fines, and for historical (actual) and predicted power with 500 kWh BESS

Table 3.6: Total cost of system in the presence of the BESSs with 800 €/kWh installation cost for each month [Historical power]

800 €/kWh Installation Cost of BESS [Historical power]							
BESS [kWh] / Month	0	200	300	400	500	600	700
1	12186	11270	11128	11172	11452	11864	12085
2	14921	13862	13634	13571	13629	13848	13916
3	22369	20470	19942	19552	19239	18952	18925
4	16010	14314	13862	13531	13259	13193	13047
5	18002	16644	16395	16312	16482	17046	17046
6	10565	9785	9687	9854	9922	10261	11028
7	13124	12185	11971	11969	11896	12105	12310
8	22510	20997	20463	20029	19752	19328	19365
9	31854	29553	28669	27932	27278	26885	26455
10	27105	25661	25124	24986	24992	25264	25332
11	10998	10323	10423	10856	11346	12200	13018
12	9779	8956	8949	8901	9189	9493	9900

Table 3.7: Total cost of system in the presence of the BESSs with 800 €/kWh installation cost for each month [Predicted power]

800 €/kWh Installation Cost of BESS [Predicted power]							
BESS [kWh] / Month	0	200	300	400	500	600	700
1	12186	11764	11803	12006	12441	12799	13170
2	14921	14206	14126	14081	14248	14173	14543
3	22369	20990	20542	20158	20031	20037	20001
4	16010	14773	14326	13947	13629	13510	13524
5	18002	17092	16944	17122	17540	17927	18699
6	10565	10167	10125	10115	10340	10648	11089
7	13124	12445	12230	12188	12386	12622	13118
8	22510	21316	20939	20631	20461	20417	20600
9	31854	30068	29363	28653	28275	27900	27504
10	27105	26253	25906	25779	25852	25844	25907
11	10998	10902	10936	11122	11479	12149	12923
12	9779	9322	9246	9403	9580	9834	10402

Table 3.8: Total cost of system in the presence of the BESSs with 1000 €/kWh installation cost for each month [Historical power]

1000 €/kWh Installation Cost of BESS [Historical power]							
BESS [kWh] / Month	0	200	300	400	500	600	700
1	12186	11717	11782	12002	12451	12977	13524
2	14921	14278	14218	14382	14670	14976	14936
3	22369	20951	20565	20373	20125	20135	20251
4	16010	14821	14539	14428	14210	14206	14252
5	18002	17123	17081	17192	17788	18559	19405
6	10565	10323	10227	10563	11090	11681	12372
7	13124	12612	12548	12682	12776	13211	13595
8	22510	21388	20987	20716	20502	20572	20871
9	31854	30031	29380	28855	28458	28111	28000
10	27105	26154	25910	25865	26309	26614	27169
11	10998	10746	11171	11956	12829	13551	14655
12	9779	9318	9451	9731	10055	10540	11001

Table 3.9: Total cost of system in the presence of the BESSs with 1000 €/kWh installation cost for each month [predicted power]

1000 €/kWh Installation Cost of BESS [predicted power]							
BESS [kWh] / Month	0	200	300	400	500	600	700
1	12186	12189	12522	13051	13477	14145	14857
2	14921	14618	14596	14801	14908	15217	15482
3	22369	21421	21048	20937	20970	21126	21370
4	16010	15185	14884	14769	14582	14669	14590
5	18002	17487	17585	18134	18659	19497	20276
6	10565	10572	10713	10902	11207	11870	12467
7	13124	12822	12781	12990	13296	13806	14422
8	22510	21731	21396	21443	21370	21622	21697
9	31854	30448	29989	29513	29192	29057	29060
10	27105	26614	26565	26759	26682	27168	27631
11	10998	11277	11506	11919	12808	13680	14259
12	9779	9702	9718	10109	10414	11002	11560

size and 600 €/kWh installation cost. The figures show the power output at the PCC of the tested VPP. This result is shown both in presence and in absence of the BESS for the quadratic cost function. Also, Fig. 3.10 shows the SOC profile of the BESS for each month with historical and predicted power. In a glance, it can be understood the full cycles for 24 hours is between zero and two with some smaller cycles provided with BESS and also clearly can be seen from the figures the dependency of stored energy with power fluctuation. In particular, Real-Time method makes decisions smartly between the usage of BESS which provides cycle and calendar aging costs and not using the BESS which the system has to pay the fines. In the other word, the optimization process includes two kind of decisions; or to pay the fine or to use the BESS, decision about both cases should be in a smart way. It should be noted that if the usage of BESS not be in a smart way, it will be degraded faster and it means the investment cost for BESS does not bring the profit for the systems. So, the charge and discharge of BESS should be control in a smart way and at the same time for having reasonable profit for the system above mentioned decision criteria should be considered for all systems include BESS.

The total yearly energy fluctuations $\int |P(t) - P^*(t)|dt$ at PCC level are given in tables 3.10, 3.11 and 3.10 in means of historical (actual) and predicted power with 200, 300, 400, 500, 600 and 700 kWh BESS sizes and 1000, 800 and 600 €/kWh installation costs, respectively. As a result, the reduction of total yearly energy $\int |P(t) - P^*(t)|dt$ in presence of BESS with greater capacity for all installation costs for both historical (actual) and predicted power is higher. In details, from table 3.10 the saved yearly energy $\int |P(t) - P^*(t)|dt$ with 300 kWh BESS size which is the most profitable size for the 1000 €/kWh installation cost, is more than 130 MWh for the processed predicted power optimization. For 800 €/kWh installation cost and with 400 kWh BESS size in table 3.11, the reduction of total yearly energy is more than 171 MWh for the processed predicted power optimization. Finally, 600 €/kWh installation cost and with 600 kWh BESS size (most profitable size) in table 3.11, the saved total yearly energy is more than 240 MWh for the processed predicted power optimization. Tables 3.10, 3.11 and 3.10 show that the both historical and predicted power have a same behaviour (the energy consumption reduced more with the bigger BESS size for both historical (actual) and predicted power) and also the optimization results show that the gap between processed historical (actual) and predicted power for each size of BESS is acceptable.

Figs. 3.11, 3.12 and 3.13, shows the histogram of power $|P(t) - P^*(t)|$ for the tested year with historical (actual) and predicted power for 200, 300, 400, 500, 600 and 700 kWh BESS sizes and 600, 800 and 1000 €/kWh installation costs. It can be seen the usage of BESS how reduced the power $|P(t) - P^*(t)|$, especially, the shaved peaks bigger than 200 kW are more in presence of BESS. Also, it is clear that the bigger size of BESS causes more peaks to be shaved. Here again, it can be seen the optimization results for historical and predicted power are similar which this proves the strength of proposed Real-Time method.

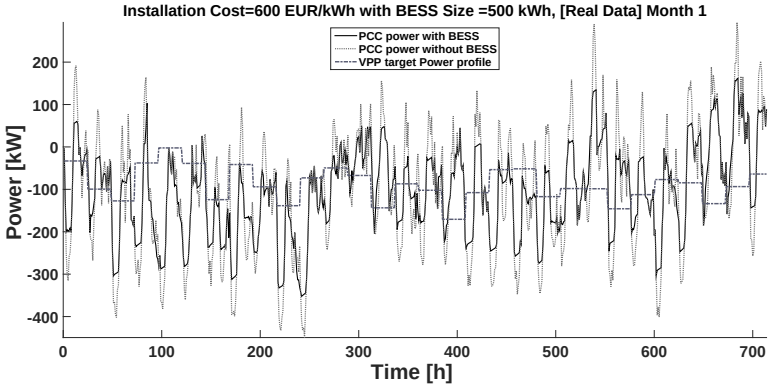

Month (1)

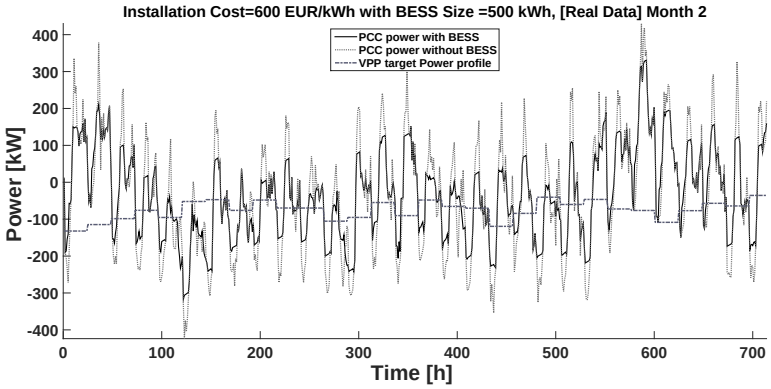

Month (2)

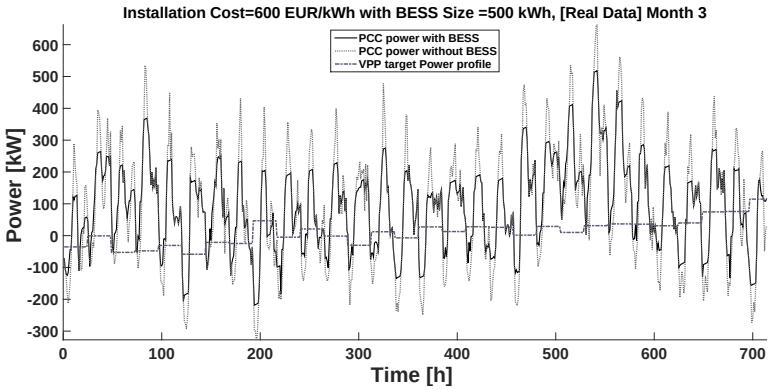

Month (3)

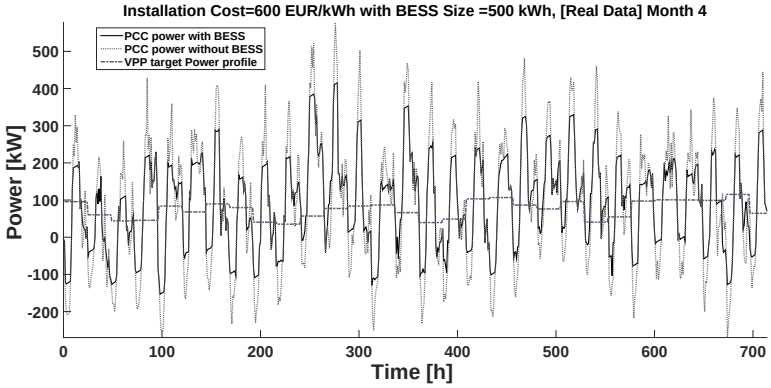

Month (4)

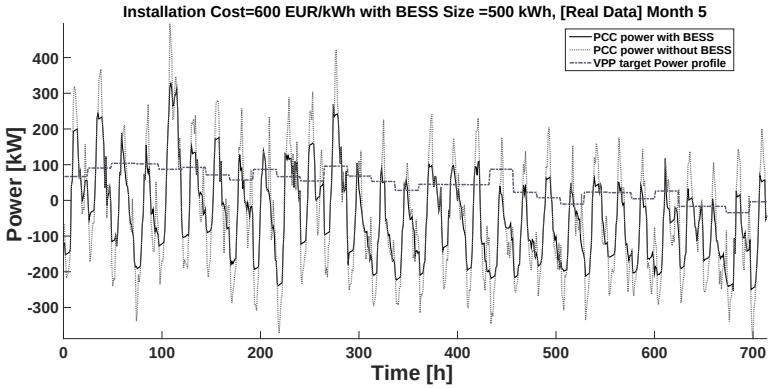

Month (5)

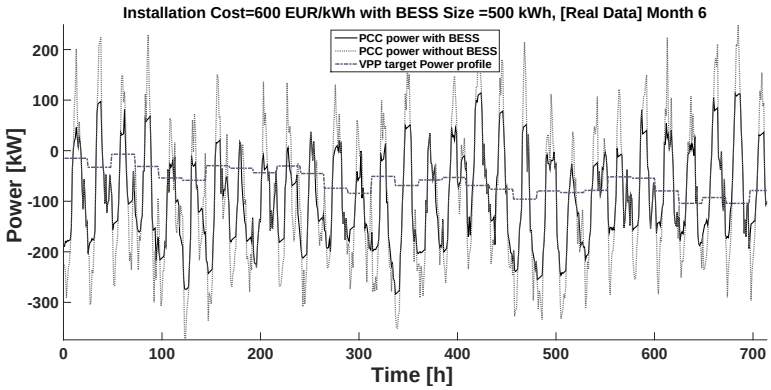

Month (6)

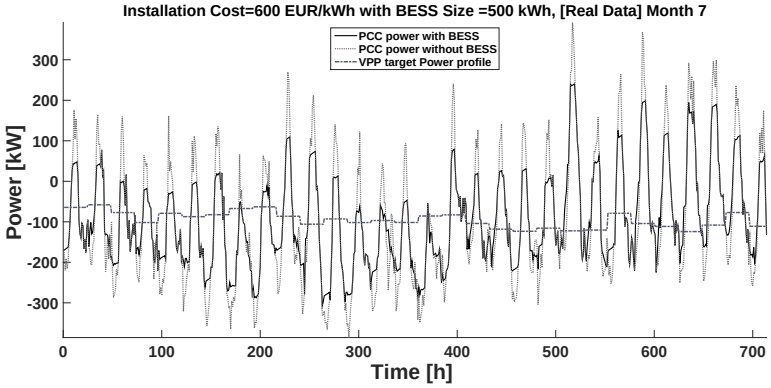

Month (7)

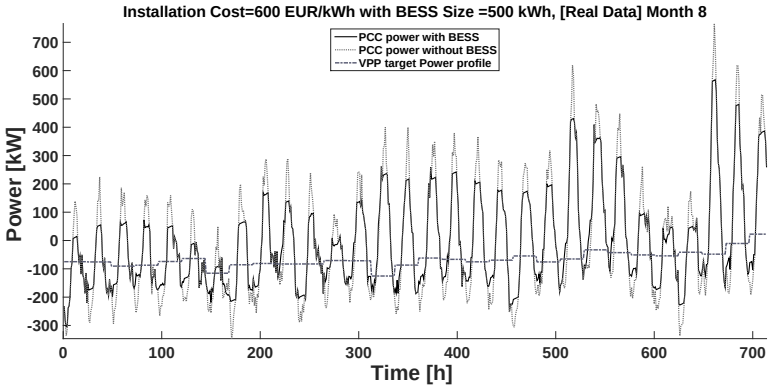

Month (8)

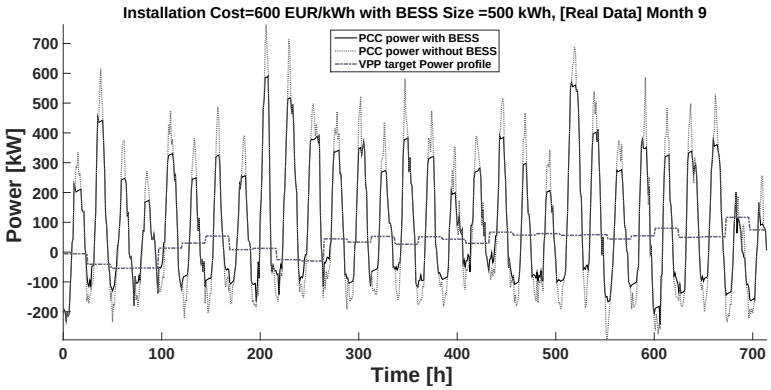

Month (9)

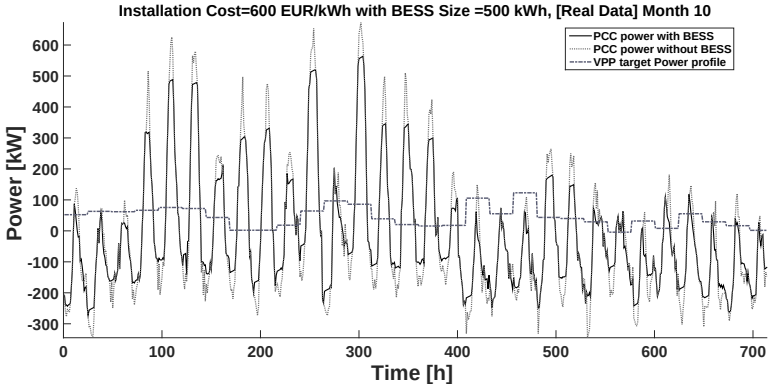

Month (10)

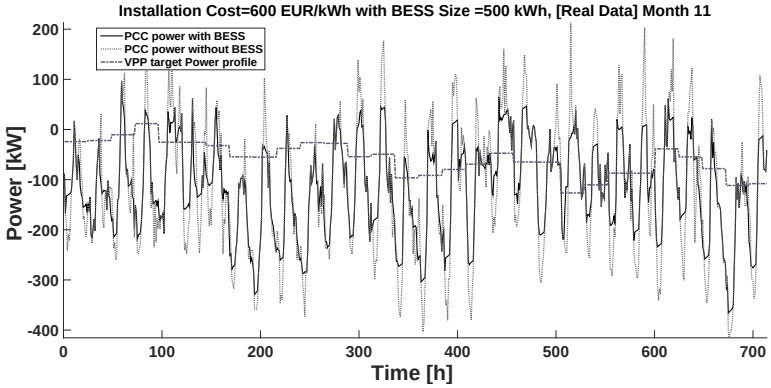

Month (11)

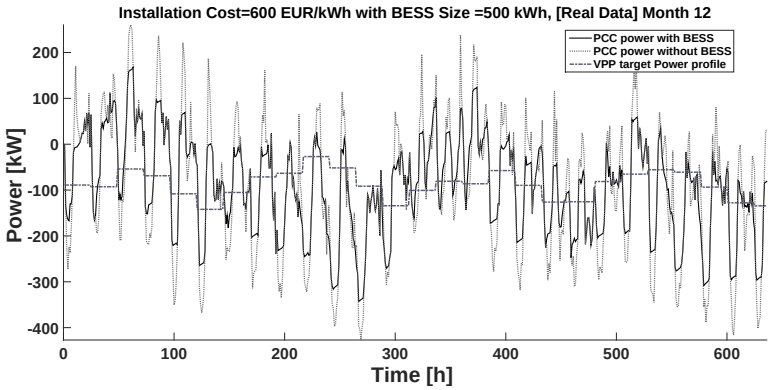

Month (12)

Figure 3.8: The power profile at the PCC with and without BESS from month 1 to 12 with Installation Cost=600 €/kWh and BESS Size=500 kWh with Historical power

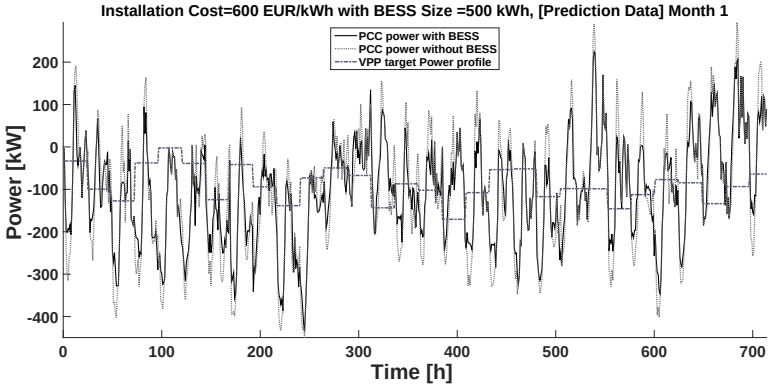

Month (1)

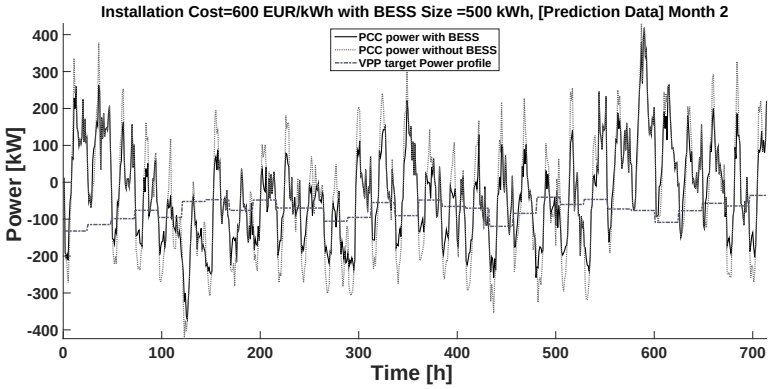

Month (2)

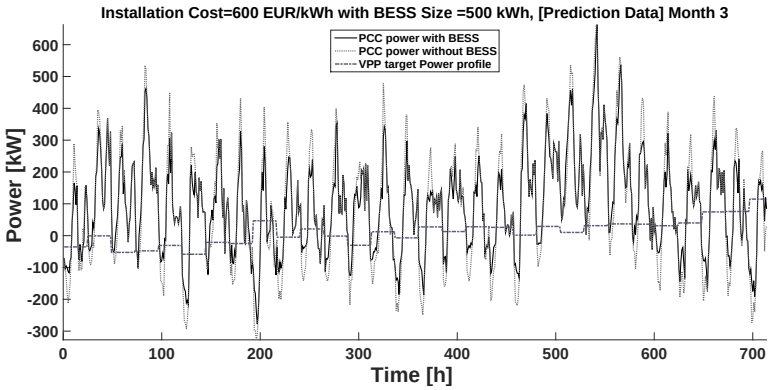

Month (3)

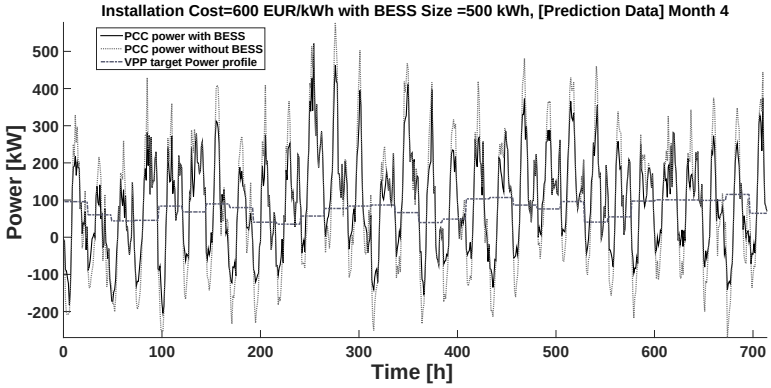

Month (4)

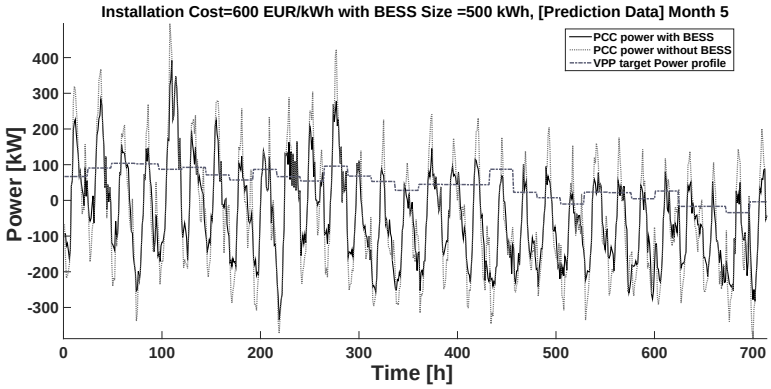

Month (5)

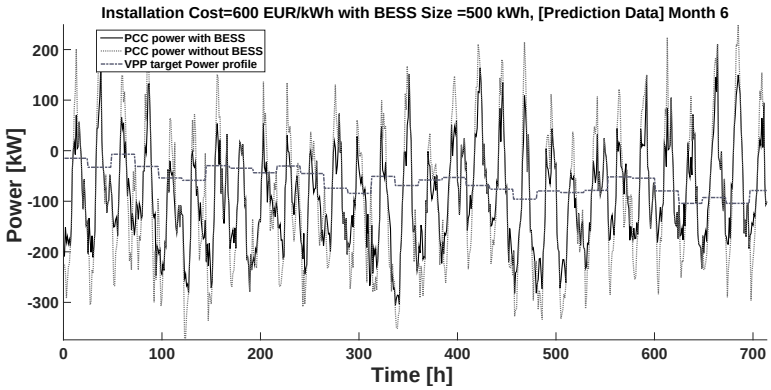

Month (6)

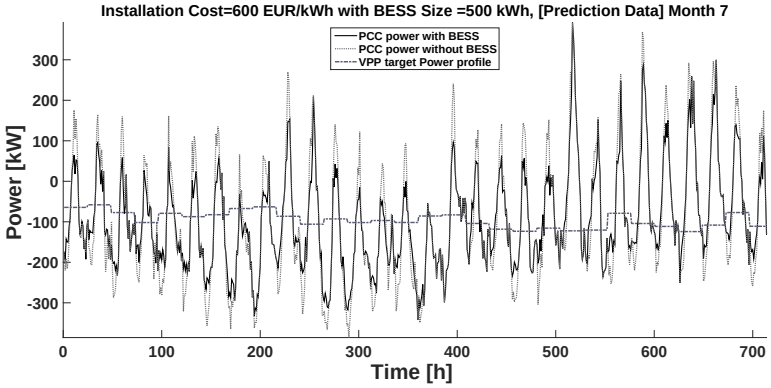

Month (7)

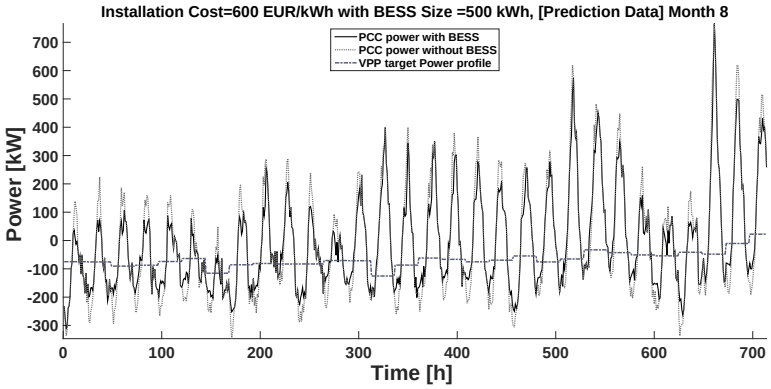

Month (8)

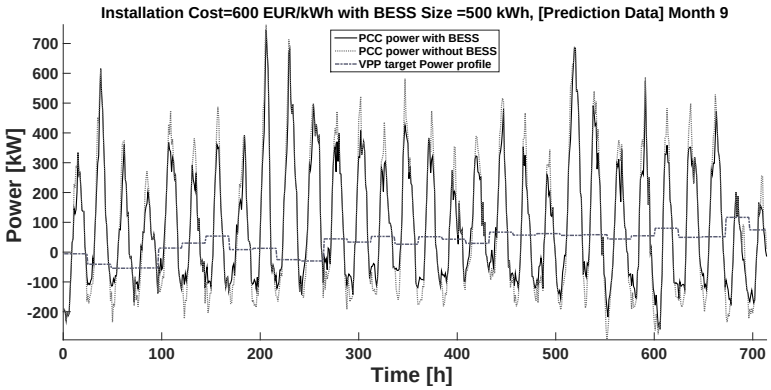

Month (9)

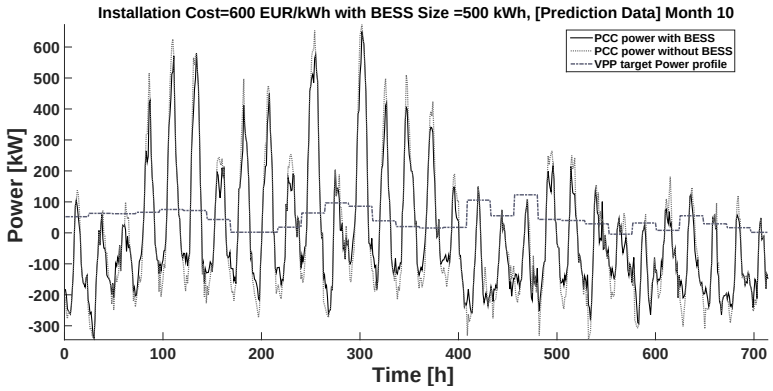

Month (10)

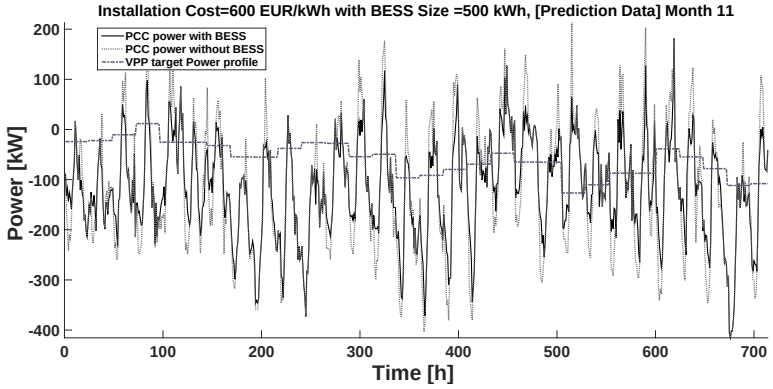

Month (11)

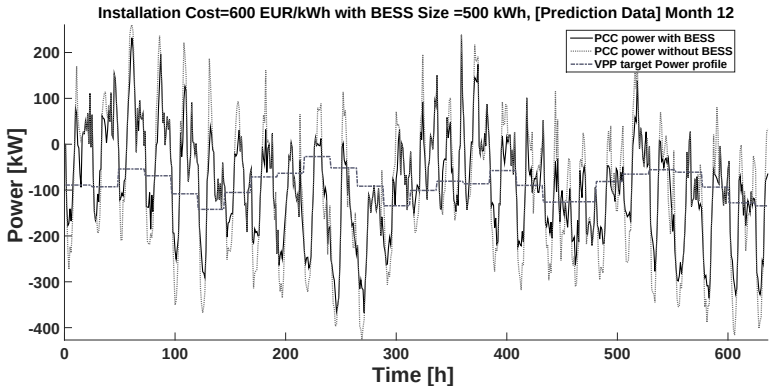

Month (12)

Figure 3.9: The power profile at the PCC with and without BESS from month 1 to 12 with Installation Cost=600 €/kWh and BESS Size=500 kWh with predicted power

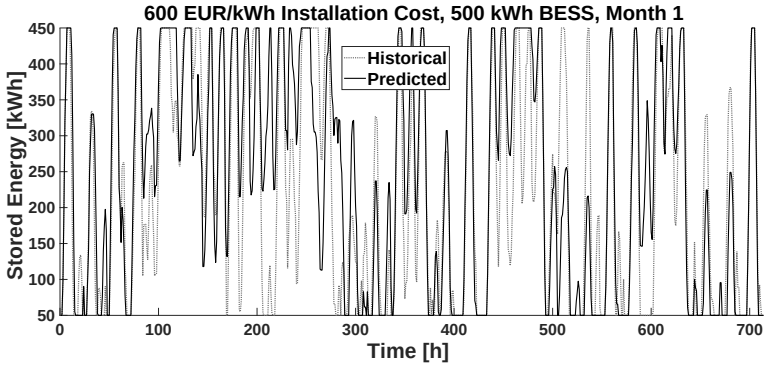

Month (1)

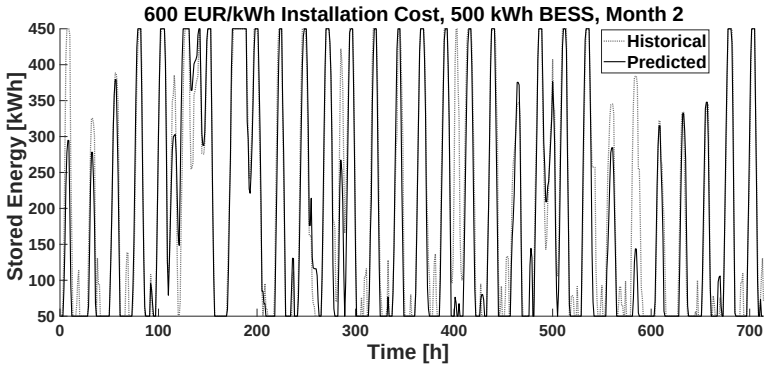

Month (2)

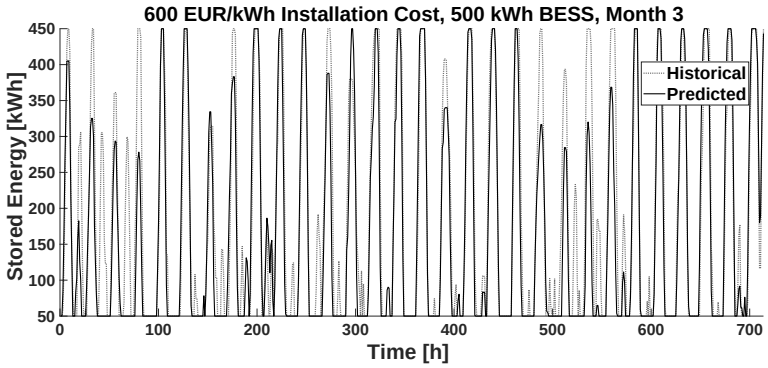

Month (3)

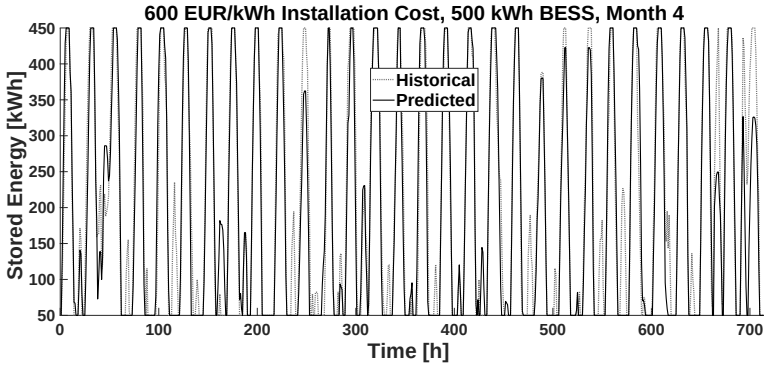

Month (4)

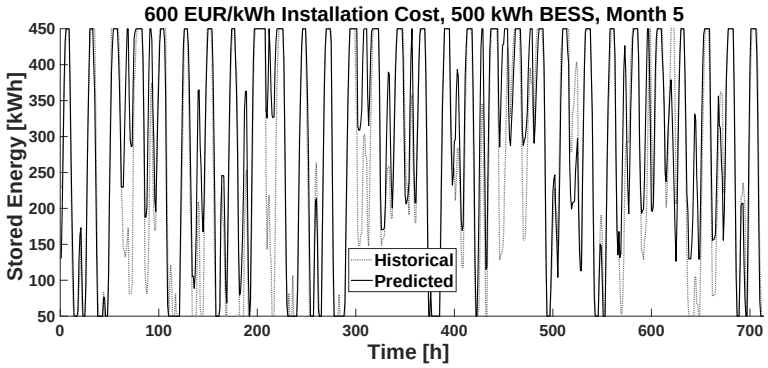

Month (5)

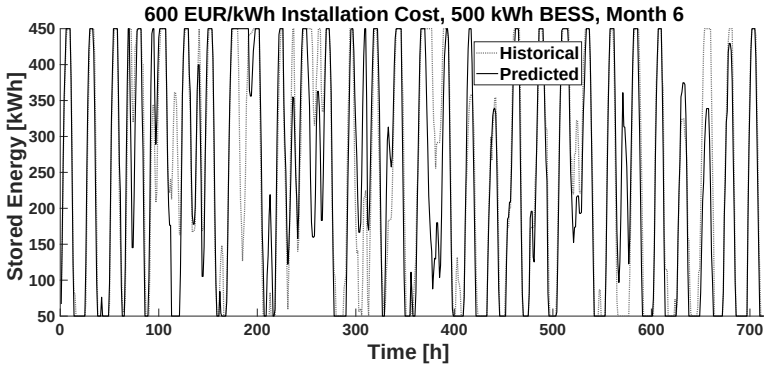

Month (6)

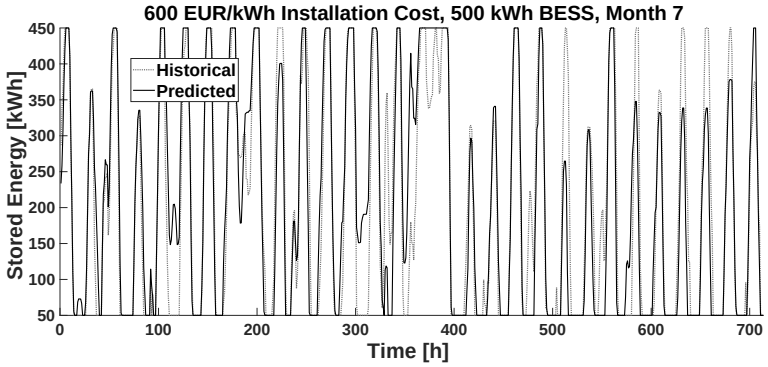

Month (7)

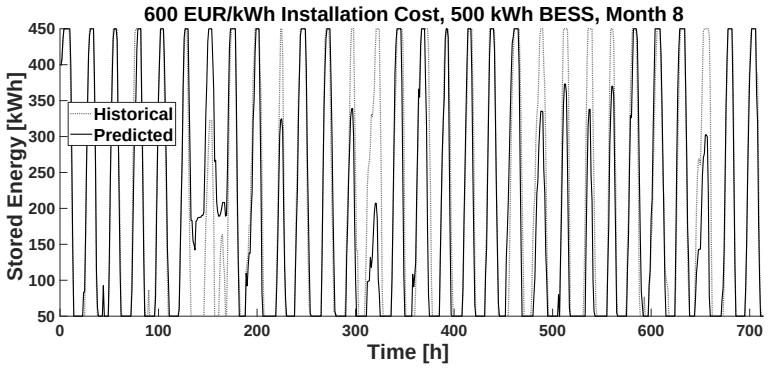

Month (8)

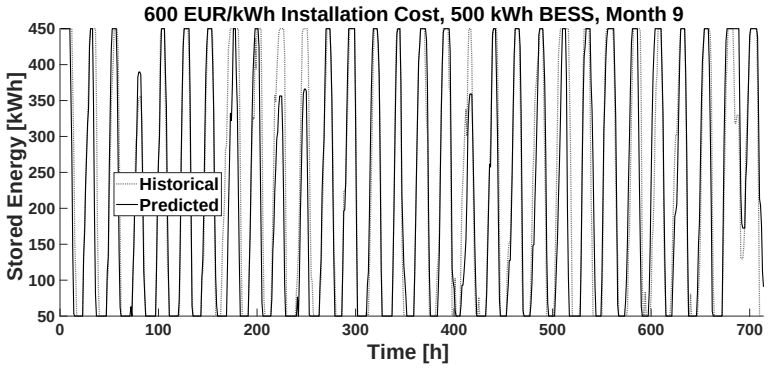

Month (9)

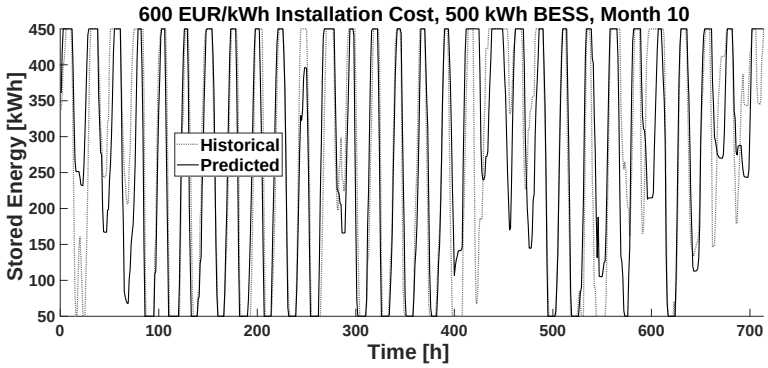

Month (10)

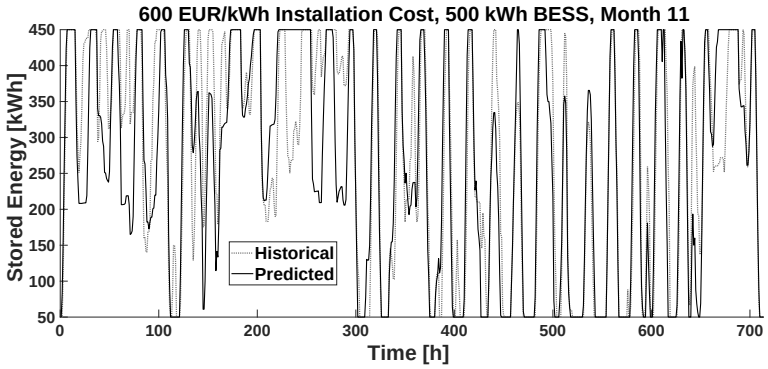

Month (11)

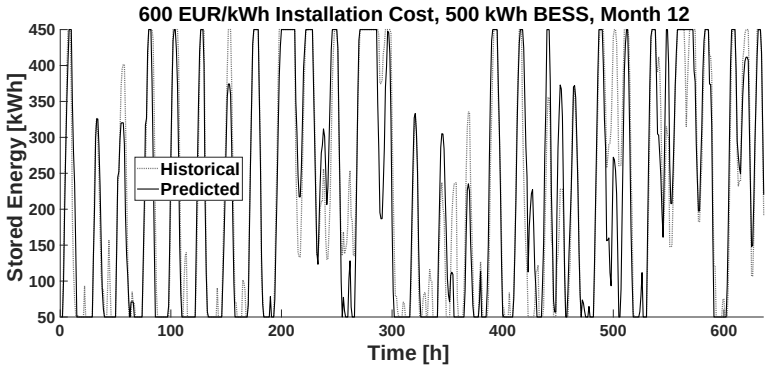

Month (12)

Figure 3.10: The time evolution of the energy stored in the BESS from month 1 to 12 with Installation Cost=600 €/kWh and BESS Size=500 kWh with historical and predicted power

Table 3.10: Comparison of yearly energy fluctuations $\int |P(t) - P^*(t)|dt$ at PCC level in presence of different sizes of BESS and 1000 €/kWh installation cost with historical and predicted power

1000 [€/kWh] Installation Cost of BESS		
BESS Size [kWh]	Yearly energy [GWh] [Historical power]	Yearly energy [GWh] [Predicted power]
0	1.203026	1.203026
200	1.092586	1.106842
300	1.055141	1.070124
400	1.025270	1.039989
500	1.004100	1.015750
600	0.985346	0.998989
700	0.976871	0.985569

Table 3.11: Comparison of yearly energy fluctuations $\int |P(t) - P^*(t)|dt$ at PCC level in presence of different sizes of BESS and 800 €/kWh installation cost with historical and predicted power

800 [€/kWh] Installation Cost of BESS		
BESS Size [kWh]	Yearly energy [GWh] [Historical power]	Yearly energy [GWh] [Predicted power]
0	1.203026	1.203026
200	1.088876	1.103080
300	1.045974	1.063954
400	1.013052	1.028799
500	0.983644	1.001962
600	0.963696	0.978161
700	0.949247	0.961812

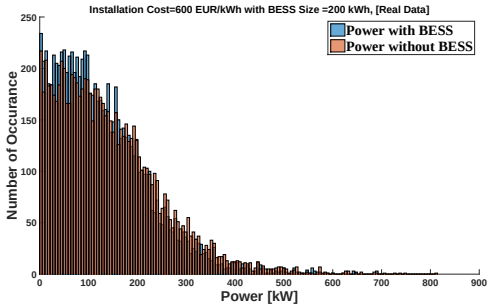

(a) Historical power, BESS Size 200 kWh

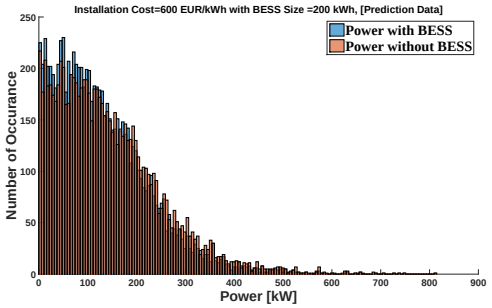

(b) Predicted power, BESS Size 200 kWh

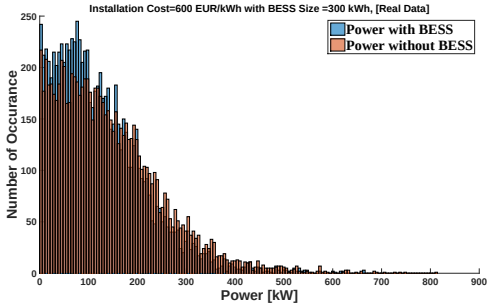

(c) Historical power, BESS Size 300 kWh

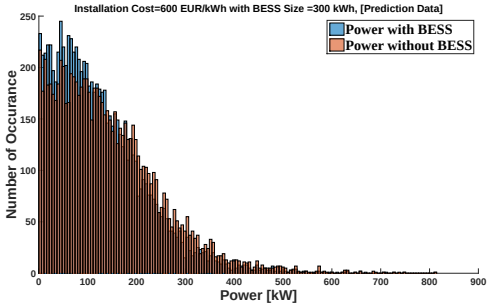

(d) Predicted power, BESS Size 300 kWh

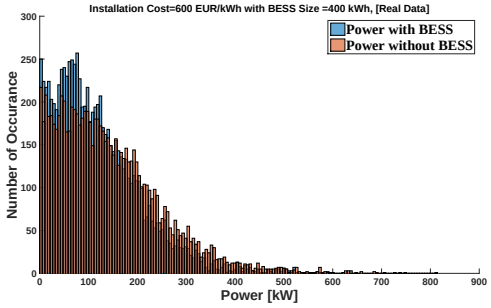

(e) Historical power, BESS Size 400 kWh

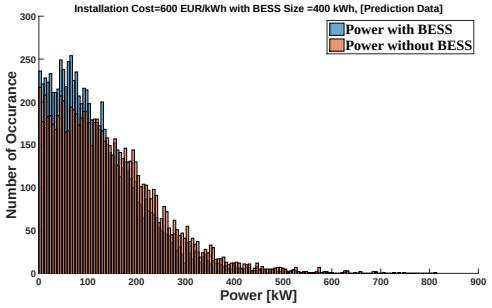

(f) Predicted power, BESS Size 400 kWh

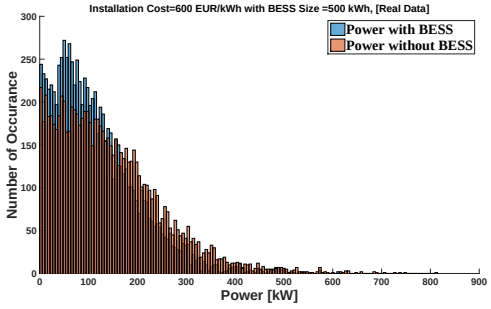

(g) Historical power, BESS Size 500 kWh

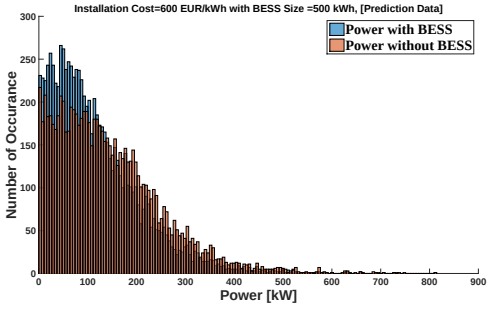

(h) Predicted power, BESS Size 500 kWh

Table 3.12: Comparison of yearly energy fluctuations $\int |P(t) - P^*(t)|dt$ at PCC level in presence of different sizes of BESS and 600 €/kWh installation cost with historical and predicted power

600 [€/kWh] Installation Cost of BESS		
BESS Size [kWh]	Yearly energy [GWh] [Historical power]	Yearly energy [GWh] [Predicted power]
0	1.203026	1.203026
200	1.085537	1.100168
300	1.040785	1.057152
400	1.001683	1.018352
500	0.968927	0.985831
600	0.944830	0.957995
700	0.924741	0.936956

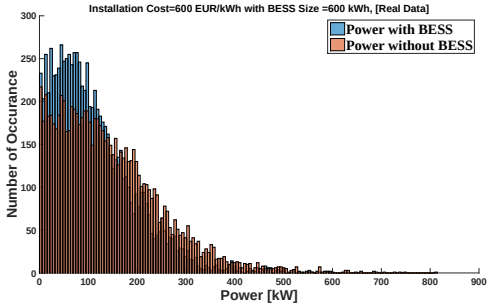

(i) Historical power, BESS Size 600 kWh

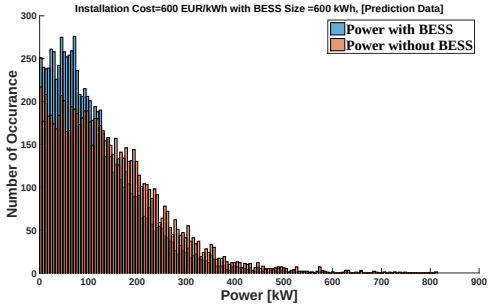

(j) Predicted power, BESS Size 600 kWh

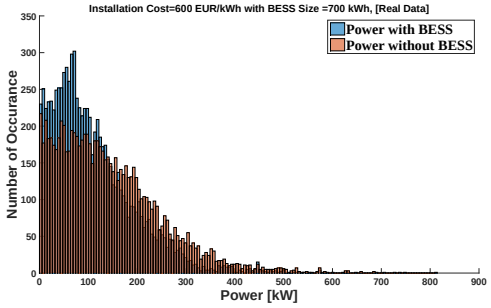

(k) Historical power, BESS Size 700 kWh

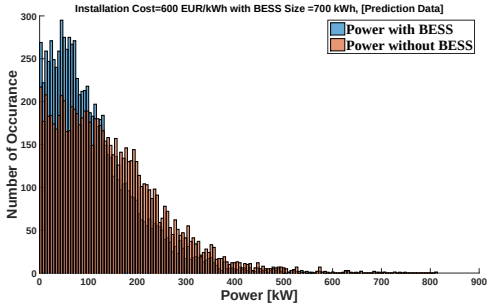

(l) Predicted power, BESS Size 700 kWh

Figure 3.11: Histograms of the absolute value of all powers from target power with and without BESS [historical and predicted power] with 600€/kWh installation cost

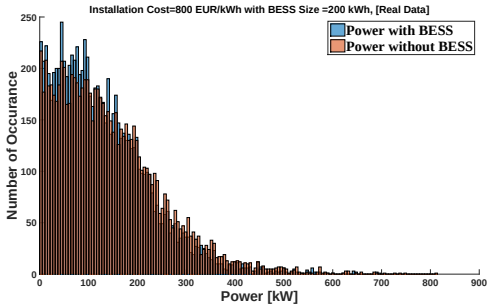

(a) Historical power, BESS Size 200 kWh

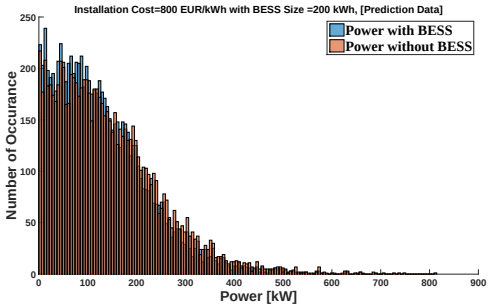

(b) Predicted power, BESS Size 200 kWh

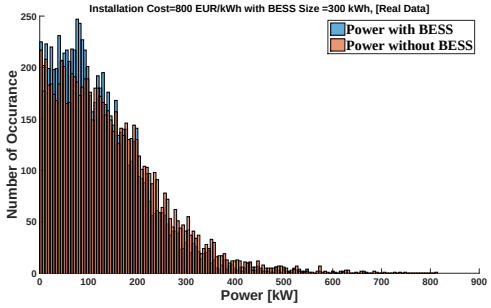

(c) Historical power, BESS Size 300 kWh

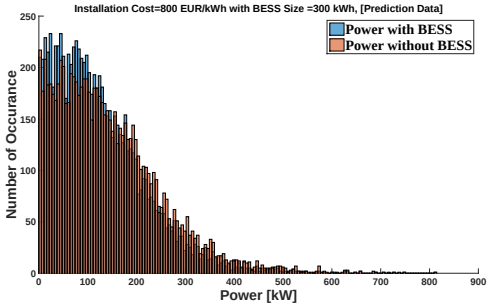

(d) Predicted power, BESS Size 300 kWh

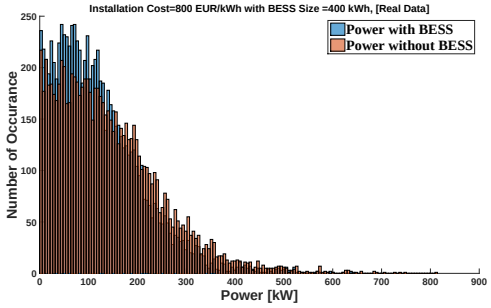

(e) Historical power, BESS Size 400 kWh

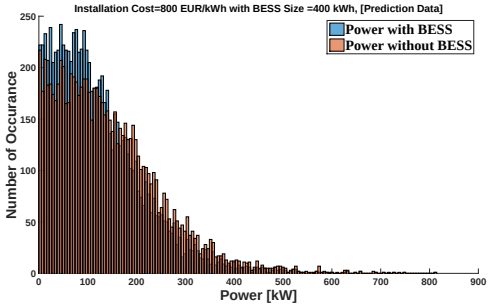

(f) Predicted power, BESS Size 400 kWh

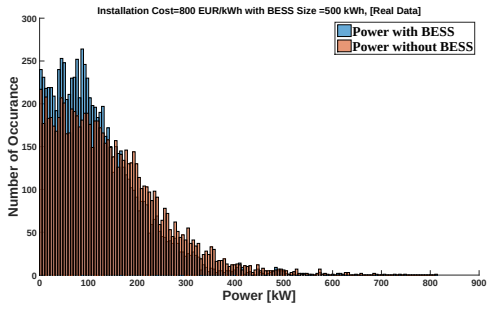

(g) Historical power, BESS Size 500 kWh

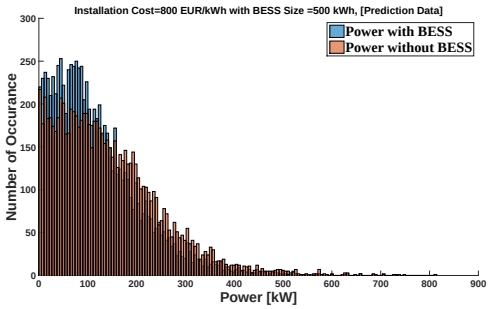

(h) Predicted power, BESS Size 500 kWh

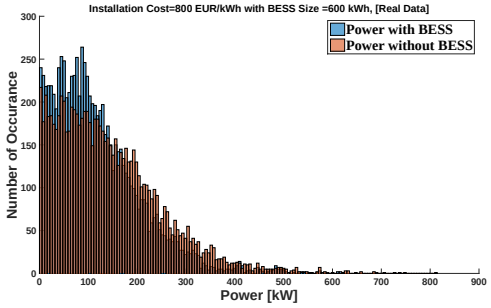

(i) Historical power, BESS Size 600 kWh

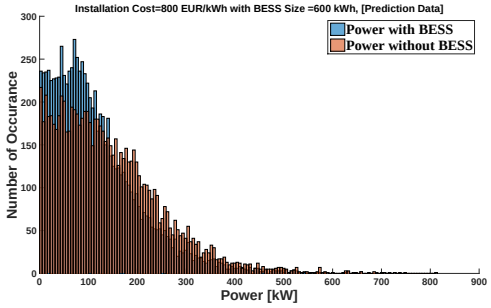

(j) Predicted power, BESS Size 600 kWh

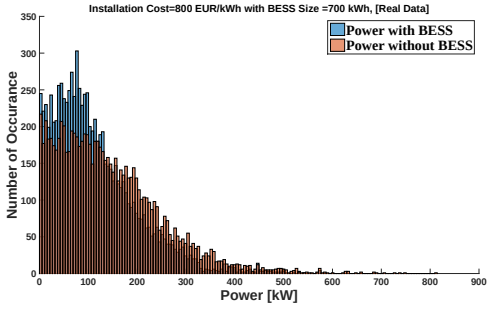

(k) Historical power, BESS Size 700 kWh

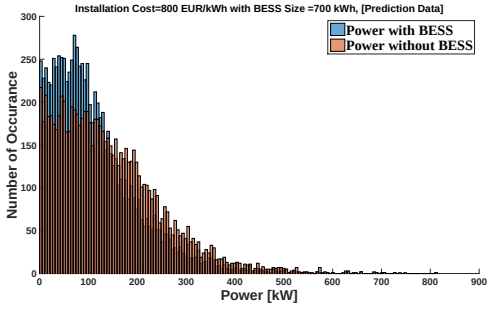

(l) Predicted power, BESS Size 700 kWh

Figure 3.12: Histograms of the absolute value of all powers from target power with and without BESS [historical and predicted power] with 800€/kWh installation cost

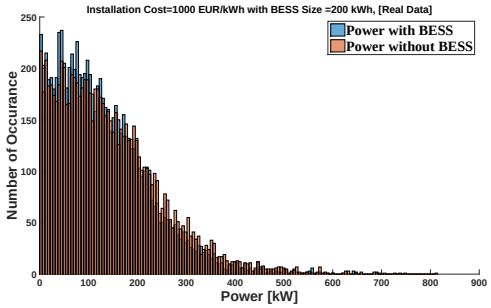

(a) Historical power, BESS Size 200 kWh

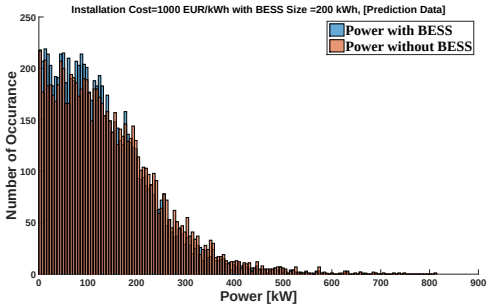

(b) Predicted power, BESS Size 200 kWh

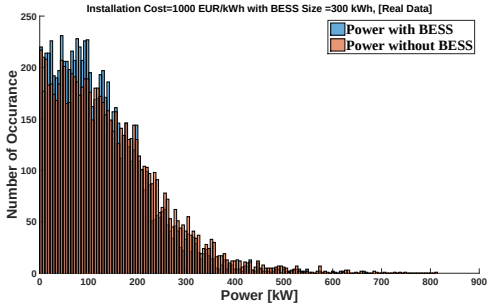

(c) Historical power, BESS Size 300 kWh

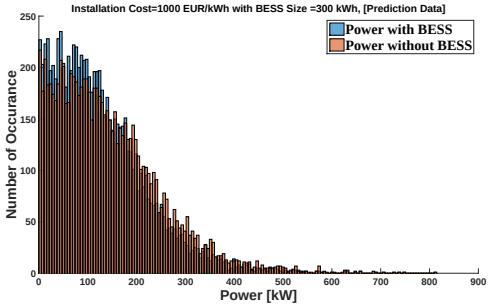

(d) Predicted power, BESS Size 300 kWh

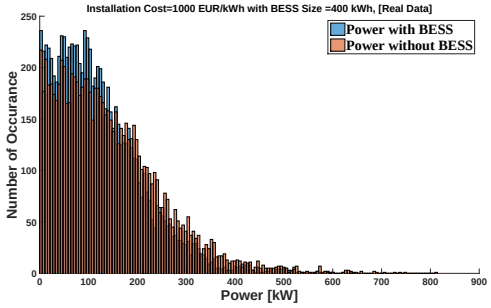

(e) Historical power, BESS Size 400 kWh

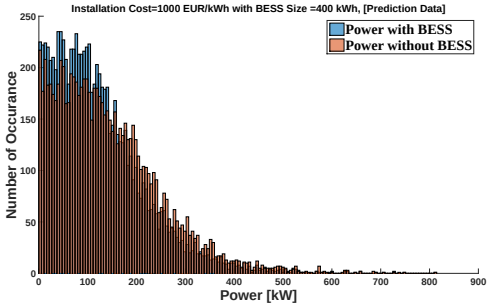

(f) Predicted power, BESS Size 400 kWh

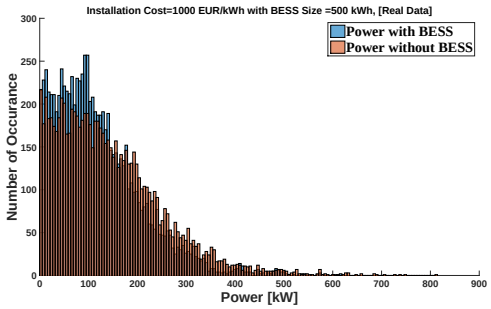

(g) Historical power, BESS Size 500 kWh

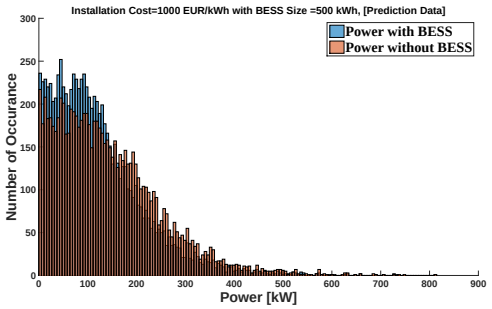

(h) Predicted power, BESS Size 500 kWh

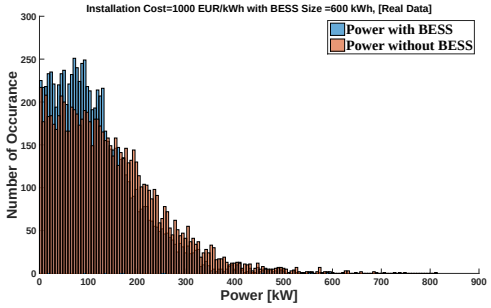

(i) Historical power, BESS Size 600 kWh

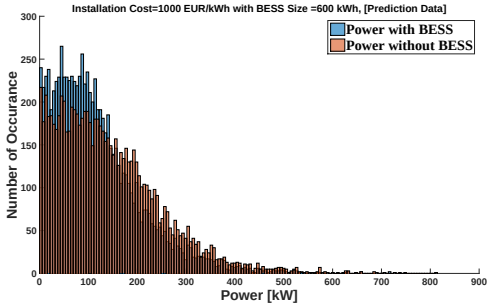

(j) Predicted power, BESS Size 600 kWh

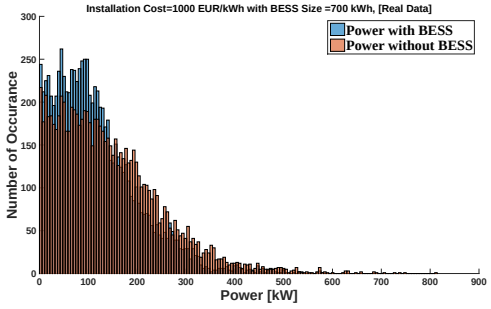

(k) Historical power, BESS Size 700 kWh

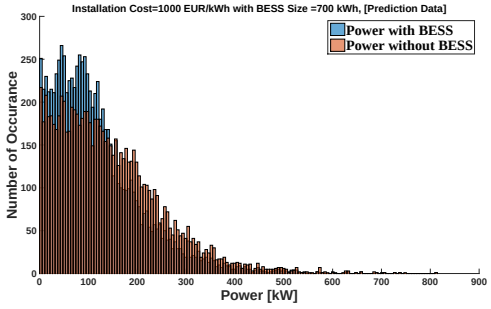

(l) Predicted power, BESS Size 700 kWh

Figure 3.13: Histograms of the absolute value of all powers from target power with and without BESS [historical and predicted power] with 1000€/kWh installation cost

3.5 Conclusions

This chapter described a Real-Time extension of the methodology proposed in chapter 2. This approach is significative because during the optimization procedure, the BESS aging costs is considered as an optimization criteria. The optimization procedure has been performed on real historical data spanning for one year, and predicted data are computed by means of system identification methods. Real-Time GA-MPOPF optimized the SoC of BESS based on 18 hours of historical data and 6 hours of predicted data with a moving window of one hour (duration of each time step) and total cots of system is minimized for the whole year. The performance of the optimization performed with predicted data is evaluated considering the actual data (i.e perfect knowledge of the future), leading to similar results. Furthermore, a sizing of BESS has been performed during the optimization procedure in order to obtain the most economical capacity of installed BESS. Under the point of view of profit, values in a range between 2.9% and 12.64% are found in the case of predicted data, while the results with actual data improved total system profit in a range between 5.5% and 16.5%. It is also observed that if the size of the BESS is not chosen correctly, profits are significantly reduced and in some cases turn into losses. With regards to energy saving, different BESS sizes and installation costs confirmed that the proposed method produced very good outcomes with most of load peaks shaved especially when considering lower BESS installation cost (as expected in the future BESS market).

Chapter 4

Optimal Positioning of Storage Systems in Microgrids Based on Complex Networks Centrality Measures aiming Voltage Regulation

4.1 Overview of Complex Networks

In the recent years, thanks also to the access to large datasets, there has been an explosion of network models and analysis for the systems that are at the hearth of our society [144]. At the hearth of such models is the old an beautiful field of *graph theory*. The first paper of graph theory was written by Leonhard Euler and goes back by 1736 [145]; however, the first textbook on graph theory is only in 1936, by Dnes Kőnig [146].

Formally, a graph is an ordered pair $G = (V, E)$ where V is the set of vertices (also called nodes) and $E \subseteq V \times V$ is the set of edges (also called arcs or lines). Hence, to each edge $e \in E$ corresponds an ordered couple of vertices $(u, v) \in V \times V$. In the following, it will be considered the case of *undirected* graphs, i.e. $(u, v) \in E \rightarrow (v, u) \in E$; in such a case, an edge can be represented as an unordered pair of vertices $e = \{u, v\}$. Notice that in our notation it is impossible to have multiple edges, i.e. it is not considering the case of *multigraphs*.

The vertices belonging to an edge are called the ends or end vertices of the edge. A vertex may exist in a graph and not belong to an edge. The order of a graph is its number of vertices $|V|$; the size of a graph is its number of edges $|E|$. The degree $d\,(i)$ of a vertex i is the number of incident edges; self edges (i.e. edges of the form $\{v, v\}$) are counted twice.

A graph is called simple when it contains no multi–edges and no self–loops. A graph is complete if there exists one and only one edge between every pair of distinct nodes; is k–regular if all its nodes have the same degree (k) . An undirected graph is connected if every node can be reached from every other node. Finally, a graph $G' = (V', E')$ is a

subgraph of $G = (V, E)$ if $V' \subseteq V$ and $E' \subseteq E$.

A very convenient representation of a graph in terms of characteristic matrices associated with the graph. The most immediate representation of a graph G is its *adjacency matrix* A, i.e. a matrix whose ij^{th} element is 1 if there exists an edge between the $i^{th}$and the j^{th} vertices of G (fig.4.2). Notice that the degree of a node i can be defined in terms of the adjacency matrix as $d(i) = \sum_j A_{ij}$.

A powerful alternative for the matrix representation of the graph $G = (V, E)$ is given by its $|E| \times |V|$ *incidence matrix* B. To define B, let consider any the edges of G: let $e = (u, v)$ be the k^{th}edge, v the i^{th} vertex and u the j^{th} vertex with $i < j$. Then, $B_{ki} = 1$, $B_{kj} = -1$ and all the other elements of the k^{th} row are zero. Notice that the incidence matrix B is the network equivalent of the gradient operator ∇ in continuous spaces: given a vector $\{s_i\}$ of scalar quantities associated with the nodes, the difference $s_u - s_v$ of such scalar at the extremes of the k^{th}edge $e = (u, v)$ is $\sum_i B_{ki} s_i = s_u - s_v$, i.e.

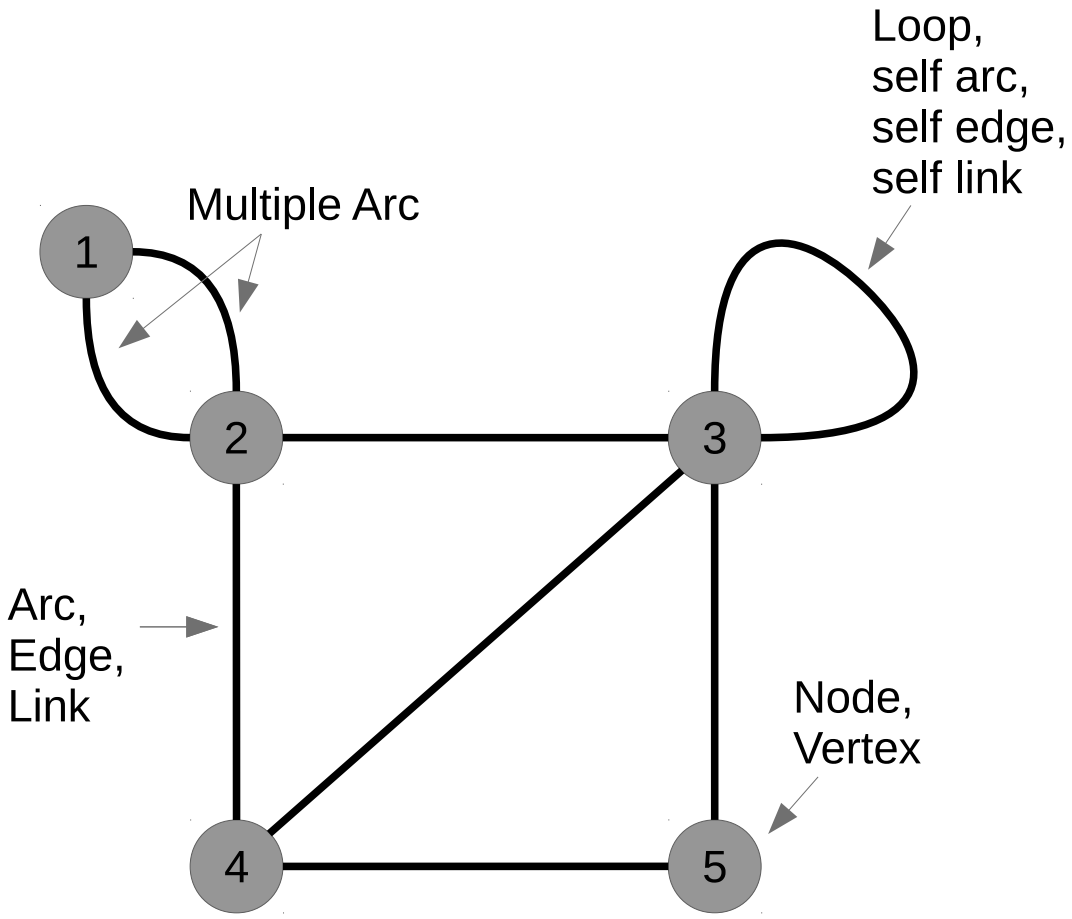

Figure 4.1: Graphical representation of an (undirected) graph. In the following, it will be considered simple graphs, i.e. graphs with no loops or multiple edges.

$$s_u - s_v = (Bs)_e \tag{4.1}$$

The incidence matrix B is very used in the engineering sciences to describe the topology of networks; by multiplying B by its transpose, another very important representation of a graph G is obtained, i.e. its *Laplacian* $L = B^T B$. Notice that, like in the continuous case where the Laplacian is defined as ∇^2, the network Laplacian is also defined as the "square" of the gradient operator B. By explicitly calculating the elements of $B^T B$, it can be seen that the $L_{ij} = -1$ if there is an edge between the $i^{th}$and the j^{th} vertices, L_{ij} is equal to the degree of the i^{th} node if $i = j$ and is $L_{ij} = 0$ otherwise.

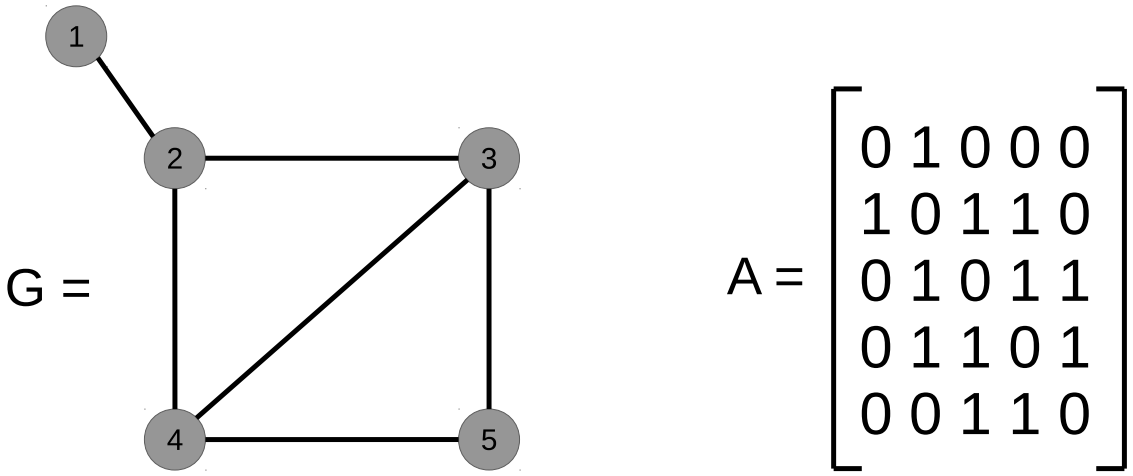

Figure 4.2: A graph G can be represented by its *adjacency matrix* A, i.e. a matrix whose ij^{th} element is 1 if there exists an edge between the $i^{th}$and the j^{th} vertices of G, 0 otherwise.

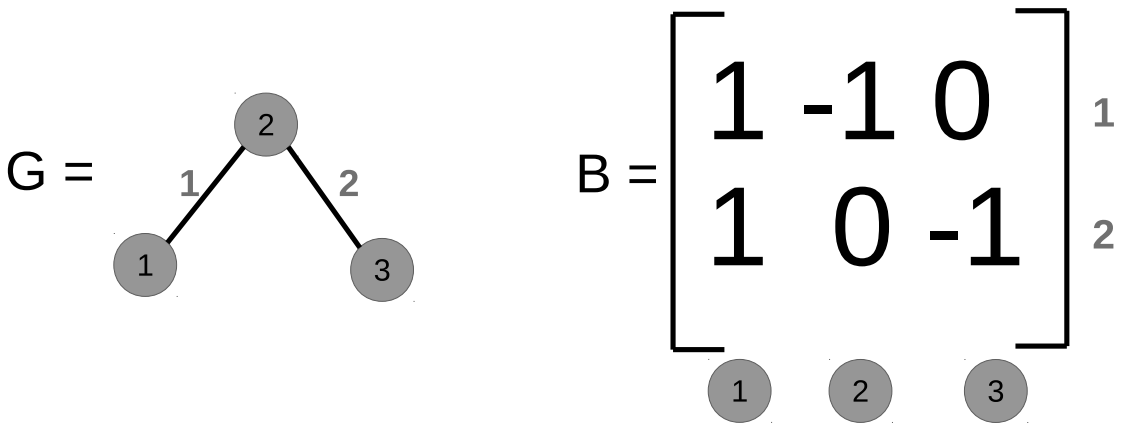

Figure 4.3: An alternative representation of a graph $G = (V, E)$ is given by its $|E| \times |V|$ *incidence matrix* B. Let $e = (u, v)$ be the k^{th}edge, v the i^{th} vertex and u the j^{th} vertex with $i < j$. Then, $B_{ki} = 1$, $B_{kj} = -1$ and all the other elements of the k^{th} row are zero.

Hence, if it is defined by D the diagonal matrix whose ii^{th}element is equal to the degree $d(i)$ of the i^{th} node, it can also be written the Laplacian in terms of the degree matrix D and the adjacency matrix A as $L = D - A$. Notice that the Laplacian matrix is often related to the dynamic properties of systems whose topology can be described as a graph [147].

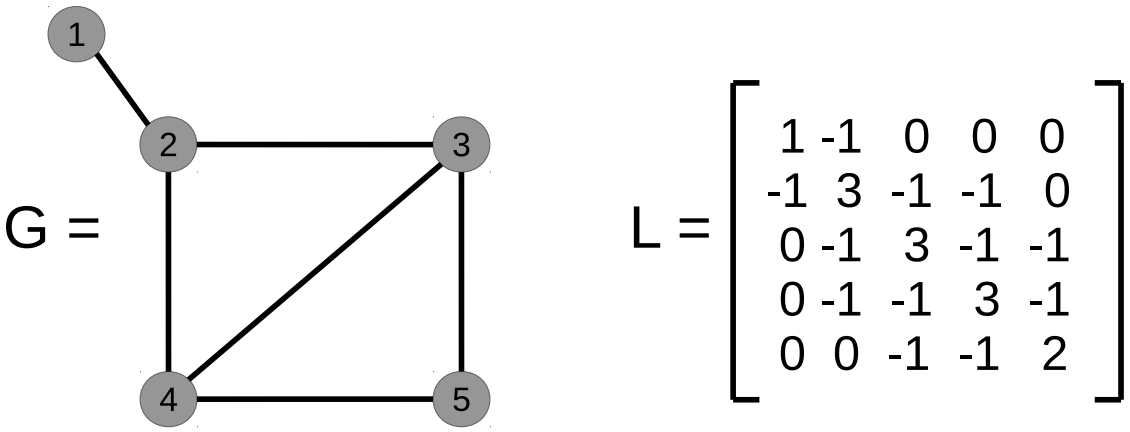

Figure 4.4: The ij^{th} element of the Laplacian matrix associated to a graph G is -1 if there is an edge between the $i^{th}$and the j^{th} vertices, it is equal to the degree of the i^{th} node if $i = j$ and is 0 otherwise.

4.1.1 Weighted Graphs

When graphs describe real systems, it is usual to associate quantities to the edges; in such a case, it is indicated of a *weighted graph*, i.e. a triplet $G = (V, E, W)$ where W is a set of quantities associated to the edges E. For an edge $e = (ij)$, let $w_e = w_{ij}$ the associated weight. The matrix representation of a weighted graph G is consequently modified: in the case of the adjacency matrix, the weighted adjacency matrix becomes

$$A_{ij} = \begin{cases} w_{ij} & \text{if } e = (i,j) \in E \\ 0 & \text{otherwise} \end{cases}$$

and the degree of a node becomes the sum of the weights $d\,(i) = \sum_j A_{ij}$ of the incident edges. Hence, the Laplacian matrix associated to a weighted graph keeps the form

$$L = D - A \tag{4.2}$$

where D is now the diagonal matrix whose ii^{th}element is equal to the weighted degree of the i^{th} node, i.e.

$$D_{ij} = \begin{cases} \sum_k w_{ik} & \text{if } i = j \\ 0 & \text{otherwise} \end{cases}$$

.

In the incidence matrix representation, it is custom NOT to redefine the incidence matrix B, but to describe the system by the couple of matrices (B, Y) where Y is a diagonal $|E| \times |E|$ matrix whose ee^{th}element is equal to the weight of the e^{th} edge, i.e.

$$Y_{ef} = \begin{cases} w_e & \text{if } e = f \\ 0 & \text{otherwise} \end{cases}$$

In the incidence matrix representation, the weighted Laplacian has the form

$$L = B^T Y B \tag{4.3}$$

4.1.2 Networks

While the word *graph* is associated to a very specific concept in mathematics linked to the very well assessed branch of graph theory, the word *network* has been come to assume a different nuance since the birth of of the so called *network science*. Network science takes birth just before the year 2000, first with the paper of Watts and Strogatz [148] and then with the paper of Barabasi and Albert [149]. Watts and Strogatz, to explain several apparently different systems, introduced a stochastic model for a class of graphs – Small World Networks – showing that by adding few random links it is possible to deeply change the properties of the network. Subsequently, Barabasi and Albert showed that a very simple mechanism of growth – preferential attachment – introduced another class of random graphs called Scale Free Networks that are characterized by a power law probability distribution of the degrees. Hence, year 2000 was the birth of *Complex Networks*, a field where Statistical Physics was applied to describe as statistical ensembles systems described by large datasets that could be mapped in a network.

4.2 Introduction and Problem Statement

Recently, energy production is encountering a change in outlook towards all the more clean and stable RESs. Photovoltaic and wind generators will share a large portion of RESs with regards of technical and strategy perspective [110, 150]. Undoubtedly, RESs provide obvious advantages as far as clean energy, energy accessibility, and easiness in the organization of energy generation facilities. Considering these favorable circumstances, this kind of energy sources introduce some drawbacks with respect to discontinuity and uncertainty of power generation, demonstrating difficulties for the common power networks which are based on large fossil-fueled power plants. Moreover, such vulnerability may challenge power quality control, bringing instability in power systems both regarding frequency and voltage stability [151]. Also, uncertainties are raised when the penetration of RESs are more in the power systems [152].

To overcome these issues, two methodologies are proposed: the control of power flows and loads by active approach, and improvement of the grid resilience by passive way [153]. According to the first approach, power systems are encountering massive

technical progress prompting to a smart and online management and control of their working conditions. The developing of the load control characteristics using smart meters, and the online monitoring of the system according of SCADA systems, and growing of the usage of the ESS in the power systems is empowering a high quality control for these systems [154]. ESSs are viewed as essential for the full deployment of RES, due to their ability to mitigate unbalances of grids created by fluctuating RES. On the other hand, the planning of the power networks by considering of passive oriented approaches gets power system planners attention, and, especially in recent years, the complex networks techniques is considered as a strong framework for catching and depicting complex phenomena in the power networks [155, 152, 156]. In particular, complex systems demonstrated how the topology of power networks significantly impacts on the system resilience to outbreaks and failures [157, 158, 153], to the network synchronization [159], to its general voltage stability [152], and to its appropriateness with electric mobility energy requirements[160]. This is in turn showed how the correct planning of power grid topology can improve the system resilience, reducing in this way the costly implementation and maintenance of active control systems.

As indicated by the literature, heuristic approaches for finding the optimal positioning of ESSs in the networks with respects to voltage stability, have been proposed by [161, 162, 32], however, such techniques are limited by the size and topology of the networks, leading to results referred to particular case of studies, and there is the requirement for a strategy able to adapt to complex and large topologies, and to decrease computational time, and bringing more exactness. In this sense, utilizing a multi-disciplinary technique connecting complex networks science and electrical engineering gives off an impression of being promising.

In this study, centrality measure of power network nodes (i.e. measures referring to structure of power network) is proposed and presented how centrality of the power network nodes can be utilized as a model for the optimal location of ESS. Firstly, the method of sec. 2.2 is used for optimization of the active power of the ESS, and then, it is improved with a novel step for the reactive power optimization. The output of the ESS in terms of optimized reactive power profile has been used for enhancing voltage fluctuation, and then, the relation of the centrality measures with optimal placement of the ESS are investigated. The results show that there is a statistically significant correlation between the optimal location of ESS and eigenvector centrality, with a positive impacts on their voltage regulation abilities, and an overall reduction of the voltage fluctuations by a value up to 50%, significantly increasing the power quality.

4.3 Methods

The proposed method is based on the definition of the optimal usage of ESS for active and reactive power control. In particular, ESS is is used for optimizing the system from both technical and economical viewpoint. To achieve this goal, OPF methods widely are used for optimization of power systems in presence of generation facilities [163].

However, the OPF are used mostly for the single period optimization approaches and those methods are not suitable for the optimization of power system including ESS as mentioned in subsec. 3.2, the nature of energy availability of ESS is significantly time dependent and the past and future ESS usage cannot be separated from the real-time optimization. Therefore, MPOPF methods have been presented for the optimization of usage of ESS, and in [164] different type of MPOPF is reviewed. The outcome of the analysis includes the definition of the optimal usage of the generators and ESS of the investigated systems both from economic and technical point of view. Also, this leads to the definition of the system operative parameters such as power flows, losses, and node voltages in the optimal configuration.

GA-MPOPF is used for calculation of voltage distributions and it is described in subsec. 2.2. In this work, a further step of reactive power optimization is added to GA-MPOPF method, for observing the effect of ESS on voltage stability when located on different nodes of the network.

Node centrality

In complex networks science, centrality is a cencept related to the importance that a given node has in the network. There are a number of characteristics, not necessarily correlated, which can be used in determining the importance of a node. These include its ability to communicate directly with other nodes, its closeness to many other nodes, and its indispensability to act as a communicator between different parts of a network. Considering each of these characteristics in turn leads to different centrality measures. For an extensive description of the centrality measures the reader is referred to [165].

The outcomes of the GA-MPOPF have been used to find the optimized reactive power of BESS, and then those reactive power used for finding the best location of the BESS with regards to the voltage regulation. Finally, the correlation of node centrality measure of the network and best location of BESS has been studied from a complex networks perspective. In fact, centrality is an outstanding concept in complex networks hypothesis, and it depends on the meaning of the measures for the quantification of the significance of nodes (or edges) into a given graph. Since the significance of the nodes in a graph is subject to the type of network they belong, different centrality measures have been proposed before. Among them, the most essential centrality measures are the betweenness centrality, the eigenvector centrality and the closeness centrality. These measures have been turned out to be important in a considerable assortment of networks, covering diverse fields like economics and finance, physics, sociology [165]. Likewise, they have been appeared to be imperative measures of significance in different utilizations of complex systems hypothesis to power systems [152], particularly they are considered when their electric correspondents characterized on the base of electric distances.

The proposed optimization process is shown in the flowchart in Fig. 4.6 and it describes the steps of calculation of the correlation between the voltage distributions $V(n)$ and centrality metrics of the tested networks. The flowchart is made by two principle parts. The first part, depicts how the centrality measures are processed beginning from

Table 4.1: Values of the Eigenvector centrality for each node of the IEEE 33 bus network considering the different weights used to model the network

	Eigenvector Centrality			
Nodes	$1/\|R+X\|$	$1/R$	$1/X$	W/o
2	0.40681	0.39342	0.40679	0.10004
3	0.07698	0.07617	0.07697	0.11439
4	0.01786	0.022601	0.01786	0.08411
5	0.00130	0.010768	0.00134	0.07198
6	0.00025	0.001352	0.00026	0.07541
7	3.39E-05	0.000146	3.39E-05	0.04757
8	2.65E-05	6.90E-05	2.65E-05	0.03001
9	9.15E-06	1.63E-05	9.15E-06	0.01893
10	3.56E-07	9.99E-07	3.56E-07	0.01194
11	2.26E-08	1.66E-07	2.26E-08	0.00753
12	1.93E-09	2.50E-08	1.93E-09	0.00474
13	1.59E-10	2.95E-09	1.59E-10	0.00298
14	4.17E-12	2.05E-10	4.17E-12	0.00187
15	3.54E-13	3.46E-11	3.54E-13	0.00116
16	1.02E-13	1.86E-11	1.02E-13	0.00071
17	3.39E-15	1.14E-12	3.39E-15	0.00039
18	3.20E-16	2.44E-13	3.20E-16	0.00018
19	0.09799	0.095891	0.09798	0.06214
20	0.00478	0.012351	0.00478	0.03768
21	0.00071	0.002432	0.00069	0.02135
22	4.41E-05	0.000237	4.41E-05	0.00963
23	0.00490	0.008265	0.00491	0.06935
24	0.00038	0.000996	0.00038	0.03930
25	0.00016	0.000431	0.00016	0.01773
26	1.73E-05	0.000126	1.73E-05	0.04755
27	5.38E-06	3.91E-05	5.38E-06	0.02997
28	2.59E-07	3.29E-06	2.59E-07	0.01886
29	1.71E-08	3.70E-07	1.71E-08	0.01182
30	2.97E-09	6.46E-08	2.97E-09	0.00734
31	1.40E-10	6.37E-09	1.40E-10	0.00445
32	1.75E-11	1.93E-09	1.75E-11	0.00252
33	1.48E-12	4.96E-10	1.48E-12	0.00113

the power network topology: the network is transformed into a graph with weight which the nodes $(1, ..., N)$ serve as the loads and generators of the power grid, as long as the borders demonstrate the electric power transmission lines between two nodes i and j, weighted by the following models:

1. Inverse of reactance (susceptance) weight: $w_{ij} = 1/X_{ij}$
2. Inverse of resistence (conductance) weight: $w_{ij} = 1/R_{ij}$
3. Absolute value of the inverse of impedance (admittance) weight: $w_{ij} = 1/||R_{ij} + jX_{ij}||$
4. No weight: $w_{ij} = 1$ if i, j are connected, otherwise $W_{ij} = 0$.

By considering these weights for each node the following centrality measures are calculated: (1) Closeness, (2) Betweenness, (3) Eigenvector, (4) Pagerank.

The second part of the flowchart, encased in the red box, calculates the $V(n)$, i.e. the distribution of all the voltage values recorded in each bus $(1, ..., N)$ between time t_0 and t_{fin} when the ESS is set in bus n considering a sampling time of one hour. The $V(n)$ is an indicator of the overall quality of voltage in the studied power grids. In this study, the best voltage quality of the system has been considered as 1.0 $p.u.$ and 5% the deviation from 1.0 $p.u.$ positively and negatively $V \in (0.95, 1.05)$ is described as an acceptable quality in means of lower and upper bounds.

The power flow optimization for reactive power Q is the starting point of the procedure. The optimal capacity of ESS in terms of reactive power $Q^*(t)$ for the voltage regulation analysis is the outcome of this step and available capacity of ESS in terms of reactive power Q is calculated from equation 4.4.

$$Q(t) = \pm\sqrt{S^2 - P^2(t)} \tag{4.4}$$

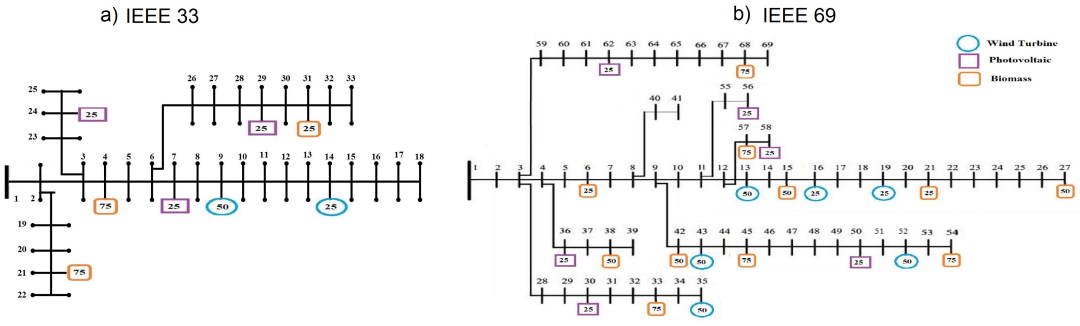

Figure 4.5: The IEEE standard networks used in this work (a) IEEE 33 Bus; (b) IEEE 69 Bus. For both networks the position of loads and generators refers to one of the randomly generated configurations. All power values are given in kW.

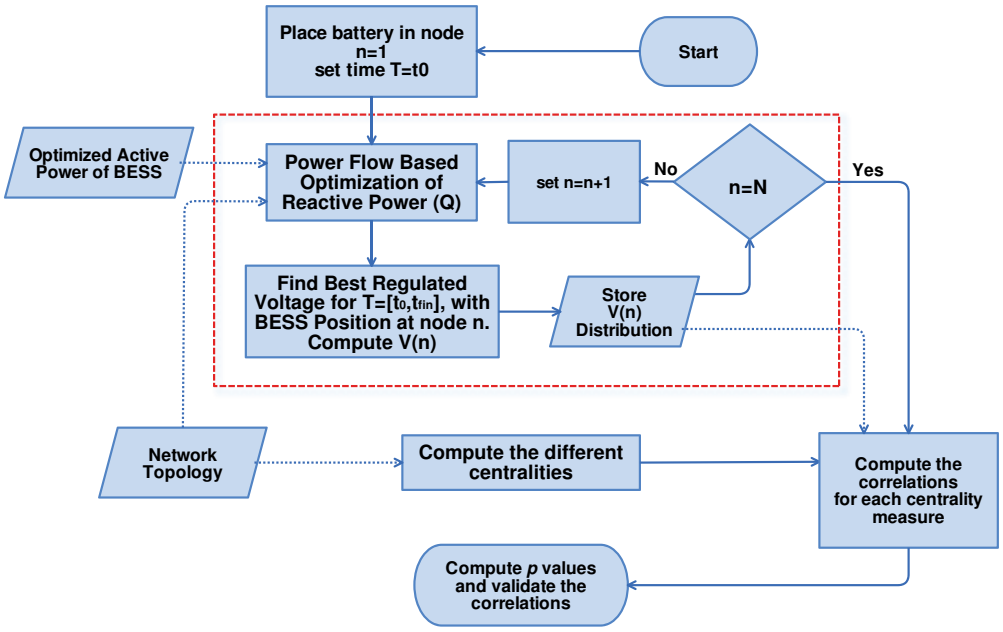

Figure 4.6: Flowchart describing how the computation procedure described in this study works, including the computation of inter-quantile differences Δ_q and the centrality metrics The improved GA-MPOPF method is enclosed in the red box.

Where S is the ESS nominal power, $P(t)$ is optimal active power of ESS and $Q(t)$ is available reactive power of ESS for each time step t. Then for each time $t = [t_0, ..., t_{end}]$ and each node $n = [1, ...N]$ the matrix of the voltage distribution is computed from equation 4.5.

$$V = \begin{pmatrix} v_1(t_0) & \cdots & v_1(t_{end}) \\ \vdots & \ddots & \vdots \\ v_N(t_0) & \cdots & v_N(t_{end}) \end{pmatrix} \tag{4.5}$$

The optimization goal is that to get the optimal reactive power of ESS Q^* with regards to voltage regulation. The optimization of value of Q^* has been performed based on characteristic of a the hierarchical rules described in equation 4.6. Where V_{min} and V_{max} are lower and upper bound of the voltage of the grid, $\#()$ is the counting operator and $\sigma()$ calculates the experimental standard deviation of the sample. The $\min$ values have been considered on the full time steps $t_0 \leq t \leq t_{end}$.

$$\begin{aligned} &1)\ \min \#(V > V_{max} || V < V_{min}) \\ &2)\ \min \#(\max(|1 - V|)) \\ &3)\ \min(\sigma(|1 - V|) \end{aligned} \tag{4.6}$$

By using the hierarchical rules of equation 4.6, the optimal reactive power of ESS Q_p^*

is obtained for all times $t_0, \ldots, t_{end}$ and all node $1, \ldots, N$. Equation 4.7 describes the obtained matrix of Q_p^*.

$$Q_p^* = \begin{pmatrix} Q_1^p(t_0) & \cdots & Q_1^p(t_{end}) \\ \vdots & \ddots & \vdots \\ Q_N^p(t_0) & \cdots & Q_N^p(t_{end}) \end{pmatrix} \tag{4.7}$$

Consequently, a set of n matrix V^p defined in equation 4.8 will be obtained for each location of ESS.

$$V^p = \begin{pmatrix} v_1^p(t_0) & \cdots & v_1^p(t_{end}) \\ \vdots & \ddots & \vdots \\ v_N^p(t_0) & \cdots & v_N^p(t_{end}) \end{pmatrix} \tag{4.8}$$

where $p = 1, ..., N$ are the location of the BESS, and $v_i^p(t_k) = f(Q_p^*(t_k))$.

For each position of the ESS the correlation is calculated starting from the vector of the differences between the 75-th and 25-th quantiles of the $V(n)$ considered as $\Delta_q^n = \left(\Delta_q^1, ..., \Delta_q^N\right)$ and the vector of the centrality measures of each node $C_*^n = (C_*^1, ..., C_*^n)$ figured out for the selected matrix $* = C, B, E, P$ (Closeness, Betweenness, Eigenvector, Pagerank). Correlations are accredit by calculating the p-value and rejecting all the correlations with p-values above 10^{-3}.

The IEEE standard power networks used for this work and they are illustrated in Fig. 4.5, where panel (a) adverts to the 33 bus power network and panel (b) adverts to the 69 bus power grid. Full description of the networks regarding of their parameters and properties can be found in [166, 167]. The generation and consumption data is provided according to subsec. 2.3.

4.4 Results

The examination has been carried out on two prototypical IEEE 33 and 69 Bus medium voltage (MV) networks usually used as a reference in power system studies [166, 134, 167, 168] (see sec. 4.3 and Fig. 4.5 for additional information).

Considering an ESS supplying both active and reactive power, and starting from real generation and consumption data sampled every one hour (for a total length of 720 samples, for a better description of the dataset the reader is referred to 2.3), it has produced for each network 100 random configurations shuffling the loads and generators of each node of the network. This produces different temporal and spatial loads and at the same time keeps constant the total power produced and consumed by the network. The dimension of the ESS has been computed following [168], and is kept constant in all the generated configurations. This progression allows to cover as much as possible the possibility to discover significant loads or generators in various nodes of the grids. The goal has been to ensure the homogeneity of the conceivable power setups both in the

33 and 69 bus networks. In this way, the effects of the factors that are not related to the topology of the network are excluded.

For every setup it is then calculated the optimized effect of the ESS on the voltage regulation of the system according to a novel Genetic Algorithm-based Multi-period Optimal Power Flow (GA-MPOPF) described in sec. 2.2, improved with a reactive power optimization technique introduced in sec.4.3. The impact of the ESS location has been performed by putting it in all the networks buses.

Thus and so, the optimal active and reactive power of the ESS has been calculated for each location. After this progression, the set of observed voltages is computed for the networks amid a whole month, per each possible place of the ESS. At that point, the amplitude of voltage fluctuations amid the tested month have been compared with different centrality metrics (betweenness , eigenvector , closeness and pagerank) of the network nodes. Particularly, the correlation properties are examined between the calculated nodes centrality and the interquartile difference Δ_q of the voltage fluctuation gotten by placing the ESS in each bus (see sec. 4.3 for further details).

Eigenvector centrality is in this way exponentially correlated with the situation of the ESS that maximizes the voltage quality, and this demonstrates the impact of the ESS position on the voltage regulation, demonstrating that situating the ESS in the less central nodes enhances the voltage quality.

Considering the voltage fluctuations and Figure 4.7 reports the histogram of the voltage fluctuation without ESS for the 69 IEEE network, and shows how they are distributed in the range [0.94, 1.1]. By using the ESS in the optimal position, the voltage fluctuation are found in the narrower, better range [0.97, 1.02], as showed in figure 4.8. This last figure also shows that even in non optimal positions (node 2), the ESS still positively affects the voltage quality. In fact, voltage fluctuations are found in the interval [0.97, 1.07].

Table 4.1 illustrates the values of the Eigenvector centrality for the nodes of the 33 bus network for all the weighting models considered in this work. As it can be seen, there is an arrangement of nodes whose centrality is low (e.g. hubs 25 to 33) while the centrality of some nodes (e.g. nodes 2,3 23, 24) are higher. Taking a gander at the voltage distribution in Fig. 4.8 the histogram of the voltage conveyance when the ESS is set in node 2 (higher centrality values) and in node 27 (lower centrality values). Placing the ESS in bus 2 leads to a non ideal selection, since the voltage distribution distributed over the interim [0.97,1.07]. This shows a critically particularly for those qualities going more than 1.05, i.e. the quality upper bound generally considered by the voltage regulation authorities. On the other hand, while considering the ESS is located in node 27, it is found that the location is ideal since the histogram of the voltage distribution contracts inside the interim [0.95,1.02], affirming a significant increase of the voltage quality.

Fig. 4.9 demonstrates the correlation analysis results that carried out on both the IEEE 69 and 33 networks. With regards of the IEEE 33 Bus, panel (a) of Fig. 4.9 shows the boxpolt of correlation between exponential centrality of betweenness , eigenvector , closeness and pagerank for all the weighting models of the network (see sec. 4.3 for the weight definition), and the interquartile difference Δ_q of the voltage fluctuation gotten

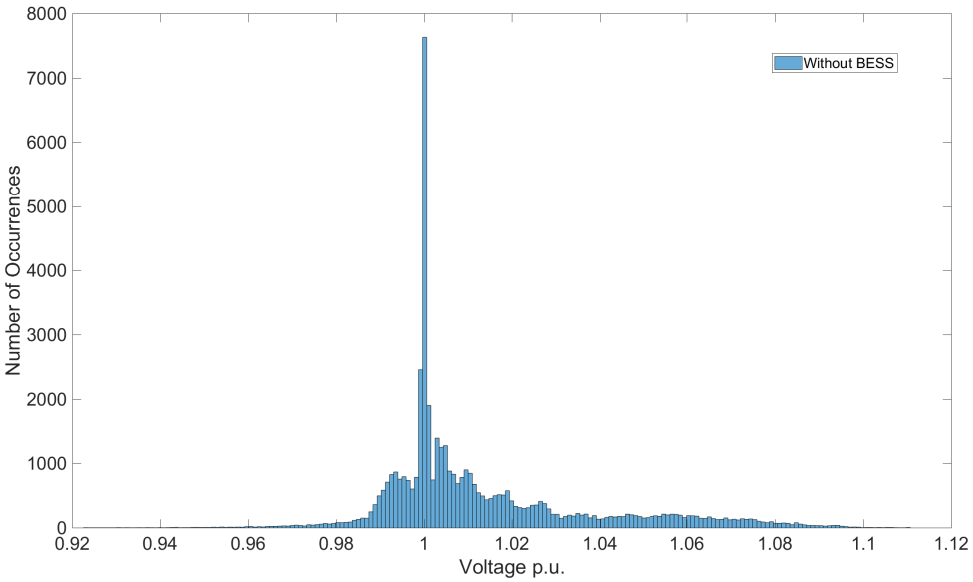

Figure 4.7: Histogram of Voltage fluctuations in case of the system without ESS

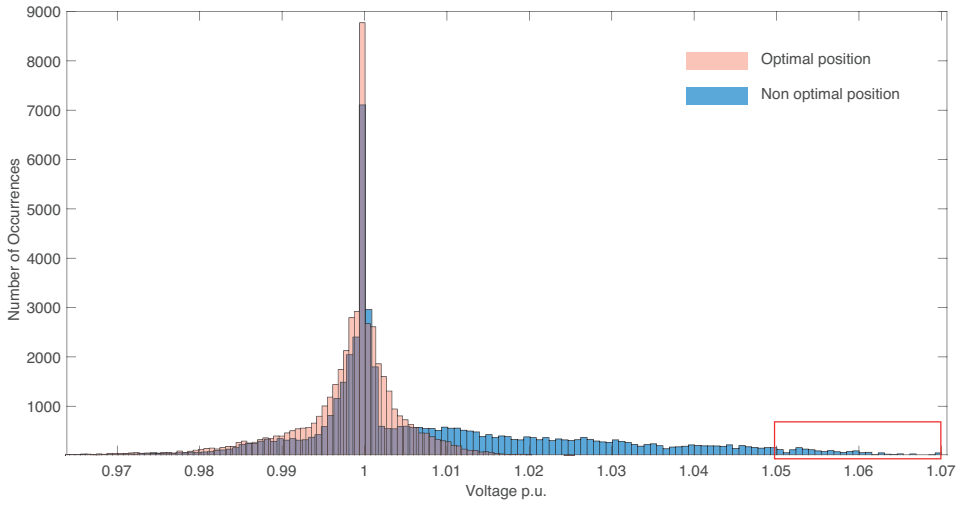

Figure 4.8: Comparison of histograms of voltage fluctuations in case of optimal (i.e. lower centrality) and non optimal (i.e. higher centrality) position of the ESS

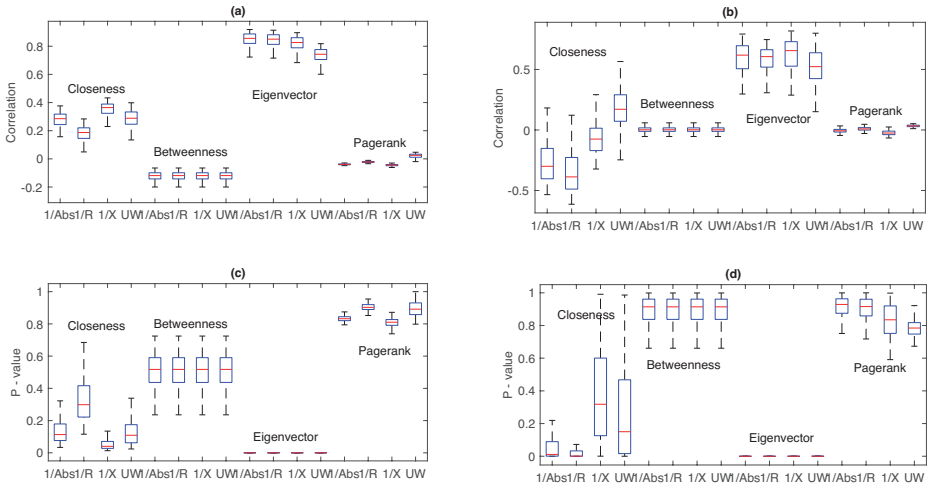

Figure 4.9: Values of correlation functions for the IEEE 33 and 69 bus. (a),(c) IEEE 33 Bus correlations and p-values; (b),(d) IEEE 69 Bus correlations and p-values

by putting the BESS in each bus. While, panel (c) communicates to the p-values whose calculated for validation of the correlations. Results demonstrate that correlation values range from 0.7 to 0.8 on account of Eigenvector centrality, while other measures indicate lower correlations than Eigenvector centrality. With reference to validation from panel (c) that the only suggestive correlation is with Eigenvector centrality, it can be seen the other correlations are rejected under the statistical point of view. A comparable outcome is discovered while examining the outcomes for the IEEE 69 Bus: the Eigenvector correlations are weaker ($\sim$0.6) and the p-values are under the 10^{-3} threshold. The other centrality measures do not give off an impression of being correlated with the quality of the voltage Δ_q.

4.5 Conclusions

Finding a statistically strong correlation between the place of ESS and the node centrality of a power network recommends a simple and significant criterion for the efficient and strong planning of power networks in nearness of fluctuating RES. Since a similar correlation values were discovered considering various weighting strategies, including the unweighted case, one may consider about that the optimal location of ESS (or more generally of active and reactive power compensator) significantly relies upon the topological characteristics of the network. Another important outcome is that when managing voltage fluctuations in power networks, the eigenvector centrality ought to be favored among the available centrality measures.

The findings presents a criterion that is independent from the exact position of loads and generators in the system. Subsequently the outcomes might be valuable amid the

planning procedure of newly or existing power networks, including those for which a further expansion process as far as users and distributed generation is expected. Besides, the outcomes affirm the basic specialized practice to put active and reactive power compensator near or in the end nodes to decrease voltage fluctuations. Future efforts will be dedicated to consist the finding of this work in a bigger structure aiming the passive optimization and resilience of microgrids considering a scenario of full deployed distributed energy sources and microgrids.

Conclusions

This PhD dissertation showed a set of different methods developed for management and planning of power systems with particular attention to microgrids and renewable energy sources (RESs). **Chapter 1** presented the State of the Art of Energy Storage System (ESS) technologies; their properties are compared discussing advantages and drawbacks in power system applications. In **chapter 2** a novel Multi-Period Optimal Power Flow technique based on Genetic Algorithm, called GA-MPOPF has been presented for the optimization of both management and planning of power systems in presence of Battery ESS (BESS) and high penetration of RESs.The presented method introduced a strategy having the capacity to manage complex choice criteria with respect to the optimal management of the cycle aging costs and the State of Charge (SoC) profile of BESS. Results showed the importance of the proposed method when dealing with aging costs during the optimization procedure. In particular, the results demonstrated that including aging costs fundamentally changed the quantitative results of the economic evaluation. In fact, the amortization costs due to BESS aging has been computed in the range between 40 and 60% of the aggregate system costs. Not considering them caused a critical underestimation of the costs.

Chapter 3 described a Real-Time extension of the methodology proposed in chapter 2. This approach is significative because during the optimization procedure, the BESS aging costs is considered as an optimization criteria. The optimization procedure has been performed on real historical data spanning for one year, and predicted data are computed by means of system identification methods. GA-MPOPF optimized the SoC of BESS based on 18 hours of historical data and 6 hours of predicted data with a moving window of one hour (duration of each time step) and total cots of system is minimized for the whole year. The performance of the optimization performed with predicted data is evaluated considering the actual data (i.e perfect knowledge of the future), leading to similar results. Furthermore, a sizing of BESS has been performed during the optimization procedure in order to obtain the most economical capacity of installed BESS. Under the point of view of profit, values in a range between 2.9% and 12.64% are found in the case of predicted data, while the results with actual data improved total system profit in a range between 5.5% and 16.5%. It is also observed that if the size of the BESS is not chosen correctly, profits are significantly reduced and in some cases turn into losses. With regards to energy saving, different BESS sizes and installation costs confirmed that the proposed method produced very good outcomes with most of load peaks shaved es-

pecially when considering lower BESS installation cost (as expected in the future BESS market).

Chapter 4 showed a statistical correlation between the location of the ESS used as reactive power compensator and the network centrality measures of the power system nodes. This correlation suggests a simple and criterion basis for planning of power networks in nearness of fluctuating RES. The finding of the methodology showed that the optimal position of BESS (or more generally of active and reactive power compensator) strongly depend on the topological characteristic of the network. In particular, the eigenvector centrality should be favored among the available centrality measures. The results also showed that the correct position of the active and reactive power compensator does not depend on the position of generators and loads. This findings can be useful during the planning procedure of power systems, as calculation of networks nodes centralities is a simple and faster procedure in comparison with traditional methods based on power flow calculations.

PUBLICATIONS

[1] Korjani, S., Mureddu, M., Facchini, A., Scala, A., Caldarelli, G., Damiano, A. Optimal positioning of storage systems in microgrids based on complex networks centrality measures, Sci. Rep. 2018.

[2] S. Korjani, M. Mureddu, A. Facchini, A. Damiano, Aging cost optimization for planning and management of energy storage systems, Energies 10 (11) (2017) 1916. doi:10.3390/en10111916. URL http://www.mdpi.com/1996-1073/10/11/1916.

[3] C. Buccella, C. Cecati, M.G. Cimoroni, A. Damiano, S. Korjani, M. Porru, A. Serpi, A Cascade Multilevel Configuration for Commercial Transport Aircraft, in the 110th edition of the AEIT Annual Conference (AEIT2018), Bari, Italy, October 2018.

[4] S. Korjani, A. Facchini, M. Mureddu, A. Damiano, A genetic algorithm approach for the identification of microgrids partitioning into distribution networks, in: IECON 2017 - 43rd Annual Conference of the IEEE Industrial Electronics Society, 2017, pp. 21-25. doi:10.1109/IECON.2017.8216008.

[5] S. Korjani, M. Porru, A. Serpi, A. Damiano, A Genetic Algorithm for the Definition of Nodal Load Time Evolutions in Micro Grids Assessment, in 5th ICRERA , Birmingham, U. K., November 2016.

Bibliography

[1] X. Luo, J. Wang, M. Dooner, J. Clarke, Overview of current development in electrical energy storage technologies and the application potential in power system operation, Applied Energy 137 (2015) 511–536. doi:10.1016/j.apenergy.2014.09.081.
URL http://www.sciencedirect.com/science/article/pii/S0306261914010290

[2] I. Hadjipaschalis, A. Poullikkas, V. Efthimiou, Overview of current and future energy storage technologies for electric power applications, Renewable and Sustainable Energy Reviews 13 (6) (2009) 1513–1522. doi:10.1016/j.rser.2008.09.028.
URL http://www.sciencedirect.com/science/article/pii/S1364032108001664

[3] A. Gonzlez, E. Goikolea, J. A. Barrena, R. Mysyk, Review on supercapacitors: Technologies and materials, Renewable and Sustainable Energy Reviews 58 (2016) 1189–1206. doi:10.1016/j.rser.2015.12.249.
URL http://www.sciencedirect.com/science/article/pii/S1364032115016329

[4] S. Vazquez, S. M. Lukic, E. Galvan, L. G. Franquelo, J. M. Carrasco, Energy Storage Systems for Transport and Grid Applications, IEEE Transactions on Industrial Electronics 57 (12) (2010) 3881–3895. doi:10.1109/TIE.2010.2076414.

[5] G. J. May, A. Davidson, B. Monahov, Lead batteries for utility energy storage: A review, Journal of Energy Storage 15 (2018) 145–157. doi:10.1016/j.est.2017.11.008.
URL http://www.sciencedirect.com/science/article/pii/S2352152X17304437

[6] N. Yabuuchi, K. Kubota, M. Dahbi, S. Komaba, Research Development on Sodium-Ion Batteries, Chemical Reviews 114 (23) (2014) 11636–11682. doi:10.1021/cr500192f.
URL http://pubs.acs.org/doi/10.1021/cr500192f

[7] M. Beaudin, H. Zareipour, A. Schellenberglabe, W. Rosehart, Energy storage for mitigating the variability of renewable electricity sources: An updated review, Energy for Sustainable Development 14 (4) (2010) 302–314. doi:10.1016/j.esd.2010.09.007.
URL http://www.sciencedirect.com/science/article/pii/S0973082610000566

[8] Zeitreihen Erneuerbare Energien, Historic data about the development of renewable energies in Germany, Tech. rep., Federal Ministry for Economic Affairs and Energy (2016).

[9] N. Nguyen-Hong, H. Nguyen-Duc, Y. Nakanishi, Optimal Sizing of Energy Storage Devices in Isolated Wind-Diesel Systems Considering Load Growth Uncertainty, IEEE Transactions on Industry Applications 54 (3) (2018) 1983–1991. doi:10.1109/TIA.2018.2802940.

[10] M. H. K. Tushar, A. W. Zeineddine, C. Assi, Demand-Side Management by Regulating Charging and Discharging of the EV, ESS, and Utilizing Renewable Energy, IEEE Transactions on Industrial Informatics 14 (1) (2018) 117–126. doi:10.1109/TII.2017.2755465.

[11] Y. Wang, Y. Xu, Y. Tang, K. Liao, M. H. Syed, E. Guillo-Sansano, G. Burt, Aggregated Energy Storage for Power System Frequency Control: A Finite-Time Consensus Approach, IEEE Transactions on Smart Grid (2018) 1–1doi:10.1109/TSG.2018.2833877.

[12] K. Koiwa, K. Z. Liu, J. Tamura, Analysis and Design of Filters for the Energy Storage System: Optimal Tradeoff Between Frequency Guarantee and Energy Capacity/Power Rating, IEEE Transactions on Industrial Electronics 65 (8) (2018) 6560–6570. doi:10.1109/TIE.2017.2688974.

[13] J. Cao, W. Du, H. Wang, M. McCulloch, Optimal Sizing and Control Strategies for Hybrid Storage System as Limited by Grid Frequency Deviations, IEEE Transactions on Power Systems (2018) 1–1doi:10.1109/TPWRS.2018.2805380.

[14] H. Zhao, M. Hong, W. Lin, K. A. Loparo, Voltage and Frequency Regulation of Microgrid With Battery Energy Storage Systems, IEEE Transactions on Smart Grid (2017) 1–1doi:10.1109/TSG.2017.2741668.

[15] Q. Xu, J. Xiao, X. Hu, P. Wang, M. Y. Lee, A Decentralized Power Management Strategy for Hybrid Energy Storage System With Autonomous Bus Voltage Restoration and State-of-Charge Recovery, IEEE Transactions on Industrial Electronics 64 (9) (2017) 7098–7108. doi:10.1109/TIE.2017.2686303.

[16] M. Zeraati, M. E. H. Golshan, J. M. Guerrero, A Consensus-Based Cooperative Control of PEV Battery and PV Active Power Curtailment for Voltage Regulation in Distribution Networks, IEEE Transactions on Smart Grid (2017) 1–1doi:10.1109/TSG.2017.2749623.

[17] Q. Tabart, I. Vechiu, A. Etxeberria, S. Bacha, Hybrid Energy Storage System Microgrids Integration for Power Quality Improvement Using Four-Leg Three-Level NPC Inverter and Second-Order Sliding Mode Control, IEEE Transactions on Industrial Electronics 65 (1) (2018) 424–435. doi:10.1109/TIE.2017.2723863.

[18] S. Y. Kim, S. Choe, S. Ko, S. K. Sul, A Naval Integrated Power System with a Battery Energy Storage System: Fuel efficiency, reliability, and quality of power., IEEE Electrification Magazine 3 (2) (2015) 22–33. doi:10.1109/MELE.2015.2413435.

[19] S. Bahramirad, W. Reder, A. Khodaei, Reliability-Constrained Optimal Sizing of Energy Storage System in a Microgrid, IEEE Transactions on Smart Grid 3 (4) (2012) 2056–2062. doi:10.1109/TSG.2012.2217991.

[20] P. F. Ribeiro, B. K. Johnson, M. L. Crow, A. Arsoy, Y. Liu, Energy storage systems for advanced power applications, Proceedings of the IEEE 89 (12) (2001) 1744–1756. doi:10.1109/5.975900.

[21] Electricity storage and renewables: Costs and markets to 2030.
URL http://publications/2017/Oct/Electricity-storage-and-renewables-costs-and-markets

[22] K. Agbossou, M. Kolhe, J. Hamelin, T. K. Bose, Performance of a stand-alone renewable energy system based on energy storage as hydrogen, IEEE Transactions on Energy Conversion 19 (3) (2004) 633–640. doi:10.1109/TEC.2004.827719.

[23] A. O. Converse, Seasonal Energy Storage in a Renewable Energy System, Proceedings of the IEEE 100 (2) (2012) 401–409. doi:10.1109/JPROC.2011.2105231.

[24] D. Krishnamurthy, C. Uckun, Z. Zhou, P. R. Thimmapuram, A. Botterud, Energy Storage Arbitrage Under Day-Ahead and Real-Time Price Uncertainty, IEEE Transactions on Power Systems 33 (1) (2018) 84–93. doi:10.1109/TPWRS.2017.2685347.

[25] A. A. Thatte, L. Xie, D. E. Viassolo, S. Singh, Risk Measure Based Robust Bidding Strategy for Arbitrage Using a Wind Farm and Energy Storage, IEEE Transactions on Smart Grid 4 (4) (2013) 2191–2199. doi:10.1109/TSG.2013.2271283.

[26] P. Mercier, R. Cherkaoui, A. Oudalov, Optimizing a Battery Energy Storage System for Frequency Control Application in an Isolated Power System, IEEE Transactions on Power Systems 24 (3) (2009) 1469–1477. doi:10.1109/TPWRS.2009.2022997.

[27] M. Datta, T. Senjyu, Fuzzy Control of Distributed PV Inverters/Energy Storage Systems/Electric Vehicles for Frequency Regulation in a Large Power System, IEEE Transactions on Smart Grid 4 (1) (2013) 479–488. doi:10.1109/TSG.2012.2237044.

[28] H. Fakham, D. Lu, B. Francois, Power Control Design of a Battery Charger in a Hybrid Active PV Generator for Load-Following Applications, IEEE Transactions on Industrial Electronics 58 (1) (2011) 85–94. doi:10.1109/TIE.2010.2062475.

[29] J. Y. Kim, J. H. Jeon, S. K. Kim, C. Cho, J. H. Park, H. M. Kim, K. Y. Nam, Cooperative Control Strategy of Energy Storage System and Microsources for Stabilizing the Microgrid during Islanded Operation, IEEE Transactions on Power Electronics 25 (12) (2010) 3037–3048. doi:10.1109/TPEL.2010.2073488.

[30] R. Tonkoski, L. A. C. Lopes, Voltage Regulation in Radial Distribution Feeders with High Penetration of Photovoltaic, in: 2008 IEEE Energy 2030 Conference, 2008, pp. 1–7. doi:10.1109/ENERGY.2008.4781021.

[31] Y. Wang, K. T. Tan, X. Y. Peng, P. L. So, Coordinated Control of Distributed Energy-Storage Systems for Voltage Regulation in Distribution Networks, IEEE Transactions on Power Delivery 31 (3) (2016) 1132–1141. doi:10.1109/TPWRD.2015.2462723.

[32] S. B. Karanki, D. Xu, B. Venkatesh, B. N. Singh, Optimal location of battery energy storage systems in power distribution network for integrating renewable energy sources, in: 2013 IEEE Energy Conversion Congress and Exposition, 2013, pp. 4553–4558. doi:10.1109/ECCE.2013.6647310.

[33] R. S. Go, F. D. Munoz, J.-P. Watson, Assessing the economic value of co-optimized grid-scale energy storage investments in supporting high renewable portfolio standards, Applied Energy 183 (2016) 902–913. doi:10.1016/j.apenergy.2016.08.134.
URL http://www.sciencedirect.com/science/article/pii/S030626191631234X

[34] A. Bedir, B. Ozpineci, J. E. Christian, The impact of plug-in hybrid electric vehicle interaction with energy storage and solar panels on the grid for a zero energy house, in: IEEE PES T D 2010, 2010, pp. 1–6. doi:10.1109/TDC.2010.5484349.

[35] A. S. A. Awad, T. H. M. EL-Fouly, M. M. A. Salama, Optimal ESS Allocation for Load Management Application, IEEE Transactions on Power Systems 30 (1) (2015) 327–336. doi:10.1109/TPWRS.2014.2326044.

[36] P. Kubalk, S. Mik, J. Stuchl, J. Vramba, M. Uher, Suitable energy storage in Off-Grid systems, in: 2014 14th International Conference on Environment and Electrical Engineering, 2014, pp. 345–349. doi:10.1109/EEEIC.2014.6835891.

[37] L. Guo, Z. Yu, C. Wang, F. Li, J. Schiettekatte, J. C. Deslauriers, L. Bai, Optimal design of battery energy storage system for a wind #x2013;diesel off-grid power system in a remote Canadian community, Transmission Distribution IET Generation 10 (3) (2016) 608–616. doi:10.1049/iet-gtd.2015.0190.

[38] H. Zhao, Q. Wu, S. Hu, H. Xu, C. N. Rasmussen, Review of energy storage system for wind power integration support, Applied Energy 137 (2015) 545–553. doi:10.1016/j.apenergy.2014.04.103.

[39] F. S. Barnes, J. G. Levine, Large Energy Storage Systems Handbook, CRC Press, 2011.

[40] P. T. Moseley, J. Garche, Electrochemical Energy Storage for Renewable Sources and Grid Balancing, Newnes, 2014.

[41] P. Du, N. Lu, Energy Storage for Smart Grids: Planning and Operation for Renewable and Variable Energy Resources (VERs), Academic Press, 2014.

[42] B. Xu, A. Oudalov, A. Ulbig, G. Andersson, D. Kirschen, Modeling of Lithium-Ion Battery Degradation for Cell Life Assessment, IEEE Transactions on Smart Grid (2016) 1doi:10.1109/TSG.2016.2578950.

[43] M. Aneke, M. Wang, Energy storage technologies and real life applications fi?? A state of the art review, Applied Energy 179 (2016) 350–377. doi:10.1016/j.apenergy.2016.06.097.
URL http://www.sciencedirect.com/science/article/pii/S0306261916308728

[44] T. M. Gr, Review of electrical energy storage technologies, materials and systems: challenges and prospects for large-scale grid storage, Energy & Environmental Sciencedoi:10.1039/C8EE01419A.
URL https://pubs.rsc.org/en/content/articlelanding/2018/ee/c8ee01419a

[45] S. Rehman, L. M. Al-Hadhrami, M. M. Alam, Pumped hydro energy storage system: A technological review, Renewable and Sustainable Energy Reviews 44 (2015) 586–598. doi:10.1016/j.rser.2014.12.040.
URL http://www.sciencedirect.com/science/article/pii/S1364032115000106

[46] E. Barbour, I. A. G. Wilson, J. Radcliffe, Y. Ding, Y. Li, A review of pumped hydro energy storage development in significant international electricity markets, Renewable and Sustainable Energy Reviews 61 (2016) 421–432. doi:10.1016/j.rser.2016.04.019.
URL http://www.sciencedirect.com/science/article/pii/S1364032116300363

[47] I. Kougias, S. Szab, Pumped hydroelectric storage utilization assessment: Forerunner of renewable energy integration or Trojan horse?, Energy 140 (2017) 318–329. doi:10.1016/j.energy.2017.08.106.
URL http://www.sciencedirect.com/science/article/pii/S0360544217314822

[48] P. Punys, R. Baublys, E. Kasiulis, A. Vaisvila, B. Pelikan, J. Steller, Assessment of renewable electricity generation by pumped storage power plants in EU Member States, Renewable and Sustainable Energy Reviews 26 (2013) 190–200. doi:10.1016/j.rser.2013.05.072.
URL http://www.sciencedirect.com/science/article/pii/S1364032113003754

[49] C.-J. Yang, R. B. Jackson, Opportunities and barriers to pumped-hydro energy storage in the United States, Renewable and Sustainable Energy Reviews 15 (1) (2011) 839–844. doi:10.1016/j.rser.2010.09.020.
URL http://www.sciencedirect.com/science/article/pii/S1364032110003072

[50] P. Medina, A. W. Bizuayehu, J. P. S. Catalo, E. M. G. Rodrigues, J. Contreras, Electrical Energy Storage Systems: Technologies' State-of-the-Art, Techno-economic Benefits and Applications Analysis, in: 2014 47th Hawaii International Conference on System Sciences, 2014, pp. 2295–2304. doi:10.1109/HICSS.2014.290.

[51] J. I. Prez-Daz, M. Chazarra, J. Garca-Gonzlez, G. Cavazzini, A. Stoppato, Trends and challenges in the operation of pumped-storage hydropower plants, Renewable and Sustainable Energy Reviews 44 (2015) 767–784. doi:10.1016/j.rser.2015.01.029.
URL http://www.sciencedirect.com/science/article/pii/S1364032115000398

[52] R. Madlener, J. Latz, Economics of centralized and decentralized compressed air energy storage for enhanced grid integration of wind power, Applied Energy 101 (2013) 299–309. doi:10.1016/j.apenergy.2011.09.033.
URL http://www.sciencedirect.com/science/article/pii/S0306261911006362

[53] Compressed Air Energy Storage (CAES) | Energy Storage Association.
URL http://energystorage.org/compressed-air-energy-storage-caes

[54] CAES Theory, Resources and Applications for Wind Power.
URL https://webcache.googleusercontent.com/search?q=cache:X-IcuXWiWF8J:https://acee.princeton.edu/wp-content/uploads/2016/10/SuccarWilliams_PEI_CAES_2008April8.pdf+&cd=7&hl=en&ct=clnk&gl=it

[55] The Role of Compressed Air Energy Storage (CAES) in Future Sustainable Energy Systems.
URL http://webcache.googleusercontent.com/search?q=cache:U0dRUpaU5oYJ:people.plan.aau.dk/~lund/Thesis/CAES_ECM-journal-final.pdf+&cd=6&hl=en&ct=clnk&gl=it

[56] C. K. Das, O. Bass, G. Kothapalli, T. S. Mahmoud, D. Habibi, Overview of energy storage systems in distribution networks: Placement, sizing, operation, and power quality, Renewable and Sustainable Energy Reviews 91 (2018) 1205–1230. doi:10.1016/j.rser.2018.03.068.
URL https://www.sciencedirect.com/science/article/pii/S1364032118301606

[57] A. Stodola, Steam and gas turbines : with a supplement on The prospects of thermal prime mover, New York : McGraw-Hill book company, inc, 1927.
URL https://trove.nla.gov.au/version/17902460

[58] J. G. Bitterly, Flywheel technology past, present, and 21st Century projections, in: IECEC-97 Proceedings of the Thirty-Second Intersociety Energy Conversion Engineering Conference (Cat. No.97CH6203), Vol. 4, 1997, pp. 2312–2315 vol.4. doi:10.1109/IECEC.1997.658228.

[59] B. Bolund, H. Bernhoff, M. Leijon, Flywheel energy and power storage systems, Renewable and Sustainable Energy Reviews 11 (2) (2007) 235–258. doi:10.1016/j.rser.2005.01.004.
URL http://www.sciencedirect.com/science/article/pii/S1364032105000146

[60] R. Sebastin, R. Pea Alzola, Flywheel energy storage systems: Review and simulation for an isolated wind power system, Renewable and Sustainable Energy Reviews 16 (9) (2012) 6803–6813. doi:10.1016/j.rser.2012.08.008.
URL http://www.sciencedirect.com/science/article/pii/S1364032112004777

[61] R. Pea-Alzola, R. Sebastin, J. Quesada, A. Colmenar, Review of flywheel based energy storage systems, in: 2011 International Conference on Power Engineering, Energy and Electrical Drives, 2011, pp. 1–6. doi:10.1109/PowerEng.2011.6036455.

[62] S. Lemofouet, A. Rufer, A Hybrid Energy Storage System Based on Compressed Air and Supercapacitors With Maximum Efficiency Point Tracking (MEPT), IEEE Transactions on Industrial Electronics 53 (4) (2006) 1105–1115. doi:10.1109/TIE.2006.878323.

[63] F. A. Farret, M. G. Simes, Integration of Alternative Sources of Energy, John Wiley & Sons, 2006, google-Books-ID: a8BJ3zYYd3MC.

[64] B. Zakeri, S. Syri, Electrical energy storage systems: A comparative life cycle cost analysis, Renewable and Sustainable Energy Reviews 42 (2015) 569–596. doi:10.1016/j.rser.2014.10.011.

[65] R. Boom, H. Peterson, Superconductive energy storage for power systems, IEEE Transactions on Magnetics 8 (3) (1972) 701–703. doi:10.1109/TMAG.1972.1067425.

[66] F. Daz-Gonzlez, A. Sumper, O. Gomis-Bellmunt, R. Villaffila-Robles, A review of energy storage technologies for wind power applications, Renewable and Sustainable Energy Reviews 16 (4) (2012) 2154–2171. doi:10.1016/j.rser.2012.01.029.
URL http://www.sciencedirect.com/science/article/pii/S1364032112000305

[67] D. S. Padimiti, B. H. Chowdhury, Superconducting Magnetic Energy Storage System (SMES) for Improved Dynamic System Performance, in: 2007 IEEE Power Engineering Society General Meeting, 2007, pp. 1–6. doi:10.1109/PES.2007.385739.

[68] M. H. Ali, B. Wu, R. A. Dougal, An Overview of SMES Applications in Power and Energy Systems, IEEE Transactions on Sustainable Energy 1 (1) (2010) 38–47. doi:10.1109/TSTE.2010.2044901.

[69] B. Zakeri, S. Syri, Electrical energy storage systems: A comparative life cycle cost analysis, Renewable and Sustainable Energy Reviews 42 (2015) 569–596. doi:10.1016/j.rser.2014.10.011.
URL http://www.sciencedirect.com/science/article/pii/S1364032114008284

[70] L. Li, S. Kim, W. Wang, M. Vijayakumar, Z. Nie, B. Chen, J. Zhang, G. Xia, J. Hu, G. Graff, J. Liu, Z. Yang, A Stable Vanadium Redox-Flow Battery with High Energy Density for Large-Scale Energy Storage, Advanced Energy Materials 1 (3)

394–400. doi:10.1002/aenm.201100008.
URL https://onlinelibrary.wiley.com/doi/abs/10.1002/aenm.201100008

[71] B. Huskinson, M. P. Marshak, C. Suh, S. Er, M. R. Gerhardt, C. J. Galvin, X. Chen, A. Aspuru-Guzik, R. G. Gordon, M. J. Aziz, A metal-free organic inorganic aqueous flow battery, Nature 505 (7482) (2014) 195–198. doi:10.1038/nature12909.
URL https://www.nature.com/articles/nature12909

[72] D. P. Scamman, G. W. Reade, E. P. Roberts, Numerical modelling of a bromide polysulphide redox flow battery, Journal of Power Sources 189 (2) (2009) 1220–1230. doi:10.1016/j.jpowsour.2009.01.071.
URL http://linkinghub.elsevier.com/retrieve/pii/S0378775309001736

[73] Y. K. Zeng, T. S. Zhao, L. An, X. L. Zhou, L. Wei, A comparative study of all-vanadium and iron-chromium redox flow batteries for large-scale energy storage, Journal of Power Sources 300 (2015) 438–443. doi:10.1016/j.jpowsour.2015.09.100.
URL http://www.sciencedirect.com/science/article/pii/S0378775315303608

[74] Redox flow batteries: a review | SpringerLink.
URL https://link.springer.com/article/10.1007/s10800-011-0348-2

[75] M. Swierczynski, D. I. Stroe, A. I. Stan, R. Teodorescu, Primary frequency regulation with Li-ion battery energy storage system: A case study for Denmark, in: 2013 IEEE ECCE Asia Downunder, IEEE, 2013, pp. 487–492. doi:10.1109/ECCE-Asia.2013.6579141.

[76] A. Joseph, M. Shahidehpour, Battery storage systems in electric power systems, in: 2006 IEEE Power Engineering Society General Meeting, 2006, pp. 8 pp.–. doi:10.1109/PES.2006.1709235.

[77] H. Chen, T. N. Cong, W. Yang, C. Tan, Y. Li, Y. Ding, Progress in electrical energy storage system: A critical review, Progress in Natural Science 19 (3) (2009) 291–312. doi:10.1016/j.pnsc.2008.07.014.
URL http://www.sciencedirect.com/science/article/pii/S100200710800381X

[78] C. J., M. T., C. C., Identification of Community Structure in Networks, 2009 International Joint Conference on Computational Sciences and Optimization.

[79] O. Palizban, K. Kauhaniemi, Energy storage systems in modern gridsfi?!Matrix of technologies and applications, Journal of Energy Storage 6 (2016) 248–259. doi:10.1016/j.est.2016.02.001.
URL http://www.sciencedirect.com/science/article/pii/S2352152X1630010X

[80] N. Kawakami, Y. Iijima, M. Fukuhara, M. Bando, Y. Sakanaka, K. Ogawa, T. Matsuda, Development and field experiences of stabilization system using 34mw NAS batteries for a 51mw wind farm, in: 2010 IEEE International Symposium on Industrial Electronics, 2010, pp. 2371–2376. doi:10.1109/ISIE.2010.5637487.

[81] F. Palone, M. Rebolini, M. D. Simone, S. Gentili, G. M. Giannuzzi, Operating strategies for congestion management of HV lines using NaS batteries, in: 2015 AEIT International Annual Conference (AEIT), 2015, pp. 1–6. doi:10.1109/AEIT.2015.7415242.

[82] M. S. Whittingham, Electrical Energy Storage and Intercalation Chemistry, Science 192 (4244) (1976) 1126–1127. doi:10.1126/science.192.4244.1126.
URL http://science.sciencemag.org/content/192/4244/1126

[83] A. Heller, Electrochemical cell (Nov. 1975).
URL https://patents.google.com/patent/US3922174/en

[84] M. Zanini, S. Basu, J. E. Fischer, Alternate synthesis and reflectivity spectrum of stage 1 lithiumfi?!graphite intercalation compound, Carbon 16 (3) (1978) 211–212. doi:10.1016/0008-6223(78)90026-X.
URL http://www.sciencedirect.com/science/article/pii/000862237890026X

[85] S. Basu, C. Zeller, P. J. Flanders, C. D. Fuerst, W. D. Johnson, J. E. Fischer, Synthesis and properties of lithium-graphite intercalation compounds, Materials Science and Engineering 38 (3) (1979) 275–283. doi:10.1016/0025-5416(79)90132-0.
URL http://www.sciencedirect.com/science/article/pii/0025541679901320

[86] N. A. Godshall, I. D. Raistrick, R. A. Huggins, Thermodynamic investigations of ternary lithium-transition metal-oxygen cathode materials, Materials Research Bulletin 15 (5) (1980) 561–570. doi:10.1016/0025-5408(80)90135-X.
URL http://www.sciencedirect.com/science/article/pii/002554088090135X

[87] K. Mizushima, P. C. Jones, P. J. Wiseman, J. B. Goodenough, LixCoO2 (0, Materials Research Bulletin 15 (6) (1980) 783–789. doi:10.1016/0025-5408(80)90012-4.
URL http://www.sciencedirect.com/science/article/pii/0025540880900124

[88] N. A. Godshall, Lithium transport in ternary lithium-copper-oxygen cathode materials, Solid State Ionics 18-19 (1986) 788–793. doi:10.1016/0167-2738(86)90263-8.
URL http://www.sciencedirect.com/science/article/pii/0167273886902638

[89] R. Yazami, P. Touzain, A reversible graphite-lithium negative electrode for electrochemical generators, Journal of Power Sources 9 (3) (1983) 365–371. doi:10.1016/0378-7753(83)87040-2.
URL http://www.sciencedirect.com/science/article/pii/0378775383870402

[90] A. Yoshino, K. Sanechika, T. Nakajima, Secondary battery (May 1987).
URL https://patents.google.com/patent/US4668595/en

[91] M. Armand, P. Touzain, Graphite intercalation compounds as cathode materials, Materials Science and Engineering 31 (1977) 319–329. doi:10.1016/0025-5416(77)90052-0.
URL http://www.sciencedirect.com/science/article/pii/0025541677900520

[92] P. Novk, K. Mller, K. S. V. Santhanam, O. Haas, Electrochemically Active Polymers for Rechargeable Batteries, Chemical Reviews 97 (1) (1997) 207–282. doi:10.1021/cr941181o.
URL https://doi.org/10.1021/cr941181o

[93] E. Yoo, J. Kim, E. Hosono, H.-s. Zhou, T. Kudo, I. Honma, Large Reversible Li Storage of Graphene Nanosheet Families for Use in Rechargeable Lithium Ion Batteries, Nano Letters 8 (8) (2008) 2277–2282. doi:10.1021/nl800957b.
URL https://doi.org/10.1021/nl800957b

[94] T. Yamabe, K. Tanaka, K. Ohzeki, S. Yata, Electronic structure of polyacenacene. A one-dimensional graphite, Solid State Communications 44 (6) (1982) 823–825. doi:10.1016/0038-1098(82)90282-4.
URL http://www.sciencedirect.com/science/article/pii/0038109882902824

[95] S. Yata, Electrically conductive organic polymeric material and process for production thereof (Jul. 1986).
URL https://patents.google.com/patent/US4601849/en

[96] C. K. Chiang, C. R. Fincher, Y. W. Park, A. J. Heeger, H. Shirakawa, E. J. Louis, S. C. Gau, A. G. MacDiarmid, Electrical Conductivity in Doped Polyacetylene, Physical Review Letters 39 (17) (1977) 1098–1101. doi:10.1103/PhysRevLett.39.1098.
URL https://link.aps.org/doi/10.1103/PhysRevLett.39.1098

[97] C. K. Chiang, C. R. Fincher, Electrical Conductivity in Doped Polyacetylene, PHYSICAL REVIEW LETTERS 39 (17) 4.

[98] A. Franco, Rechargeable Lithium Batteries: From Fundamentals to Applications, 1st Edition, Woodhead Publishing, 2015.

[99] A. Manthiram, An Outlook on Lithium Ion Battery Technology, ACS Central Science 3 (10) (2017) 1063–1069. doi:10.1021/acscentsci.7b00288.
URL https://doi.org/10.1021/acscentsci.7b00288

[100] Y. Mekonnen, A. Sundararajan, A. I. Sarwat, A review of cathode and anode materials for lithium-ion batteries, in: SoutheastCon 2016, 2016, pp. 1–6. doi:10.1109/SECON.2016.7506639.

[101] N. Nitta, F. Wu, J. T. Lee, G. Yushin, Li-ion battery materials: present and future, Materials Today 18 (5) (2015) 252–264. doi:10.1016/j.mattod.2014.10.040.
URL http://www.sciencedirect.com/science/article/pii/S1369702114004118

[102] W. G. Howard, C. L. Schmidt, E. R. Scott, Lithium-ion battery (Oct. 2010).
URL https://patents.google.com/patent/US7807299B2/en

[103] P. G. Bruce, Energy storage beyond the horizon: Rechargeable lithium batteries, Solid State Ionics 179 (21) (2008) 752–760. doi:10.1016/j.ssi.2008.01.095.
URL http://www.sciencedirect.com/science/article/pii/S0167273808001331

[104] H. Popp, J. Attia, F. Delcorso, A. Trifonova, Lifetime analysis of four different lithium ion batteries for (plug fi?? in) electric vehicle 10.

[105] A. R. Armstrong, P. G. Bruce, Synthesis of layered LiMnO2 as an electrode for rechargeable lithium batteries, Nature 381 (6582) (1996) 499–500. doi:10.1038/381499a0.
URL https://www.nature.com/articles/381499a0

[106] A. Eftekhari, LiFePO4/C nanocomposites for lithium-ion batteries, Journal of Power Sources 343 (2017) 395–411. doi:10.1016/j.jpowsour.2017.

01.080.
URL http://www.sciencedirect.com/science/article/pii/S0378775317300915

[107] S. Wang, W. Quan, Z. Zhu, Y. Yang, Q. Liu, Y. Ren, X. Zhang, R. Xu, Y. Hong, Z. Zhang, K. Amine, Z. Tang, J. Lu, J. Li, Lithium titanate hydrates with superfast and stable cycling in lithium ion batteries, Nature Communications 8 (1) (2017) 627. doi:10.1038/s41467-017-00574-9.
URL https://www.nature.com/articles/s41467-017-00574-9

[108] Lithium Secondary - Rechargeable - Cells.
URL https://www.mpoweruk.com/lithiumS.htm

[109] I. Cowie, All About Batteries, Part 12: Lithium Titanate (LTO).
URL https://www.eetimes.com/author.asp?section_id=36&doc_id=1325358

[110] A. Facchini, Distributed energy resources: Planning for the future, Nature Energy 2 (2017) 17129.

[111] A. Marongiu, A. Damiano, M. Heuer, Experimental analysis of lithium iron phosphate battery performances, in: 2010 IEEE International Symposium on Industrial Electronics, IEEE, 2010, pp. 3420–3424. doi:10.1109/ISIE.2010.5637749.

[112] H. Beltran, E. Bilbao, E. Belenguer, I. Etxeberria-Otadui, P. Rodriguez, Evaluation of Storage Energy Requirements for Constant Production in PV Power Plants, IEEE Transactions on Industrial Electronics 60 (3) (2013) 1225–1234. doi:10.1109/TIE.2012.2202353.

[113] G. Haddadian, N. Khalili, M. Khodayar, M. Shahidehpour, Optimal scheduling of distributed battery storage for enhancing the security and the economics of electric power systems with emission constraints, Electric Power Systems Research 124 (2015) 152–159. doi:10.1016/j.epsr.2015.03.002.

[114] M. Ghofrani, A. Arabali, M. Etezadi-Amoli, M. S. Fadali, A Framework for Optimal Placement of Energy Storage Units Within a Power System With High Wind Penetration, IEEE Transactions on Sustainable Energy 4 (2) (2013) 434–442. doi:10.1109/TSTE.2012.2227343.

[115] R. DAgostino, L. Baumann, A. Damiano, E. Boggasch, A Vanadium-Redox-Flow-Battery Model for Evaluation of Distributed Storage Implementation in Residential Energy Systems, IEEE Transactions on Energy Conversion 30 (2) (2015) 421–430. doi:10.1109/TEC.2014.2369437.

[116] M. Mureddu, A. Damiano, A statistical approach for resilience analysis of ESS deployment in RES-based power systems, in: 2017 IEEE 26th International Symposium on Industrial Electronics (ISIE), IEEE, 2017, pp. 2069–2074. doi:10.1109/ISIE.2017.8001574.

[117] D. Gayme, U. Topcu, Optimal power flow with distributed energy storage dynamics, in: Proceedings of the 2011 American Control Conference, IEEE, 2011, pp. 1536–1542. doi:10.1109/ACC.2011.5991460.

[118] J. Warrington, P. Goulart, S. Mariethoz, M. Morari, Policy-Based Reserves for Power Systems, IEEE Transactions on Power Systems 28 (4) (2013) 4427–4437. doi:10.1109/TPWRS.2013.2269804.

[119] A. Gopalakrishnan, A. U. Raghunathan, D. Nikovski, L. T. Biegler, Global optimization of multi-period optimal power flow, in: 2013 American Control Conference, 2013, pp. 1157–1164. doi:10.1109/ACC.2013.6579992.

[120] R. A. Jabr, S. Karaki, J. A. Korbane, Robust Multi-Period OPF With Storage and Renewables, IEEE Transactions on Power Systems 30 (5) (2015) 2790–2799. doi:10.1109/TPWRS.2014.2365835.

[121] A. Rabiee, M. Parniani, Voltage security constrained multi-period optimal reactive power flow using benders and optimality condition decompositions, IEEE Transactions on Power Systems 28 (2) (2013) 696–708. doi:10.1109/TPWRS.2012.2211085.

[122] P. Scott, S. Thiébaux, Distributed Multi-Period Optimal Power Flow for Demand Response in Microgrids, Proceedings of the 2015 ACM Sixth International Conference on Future Energy Systems - e-Energy '15 (2015) 17–26doi:10.1145/2768510.2768534.

[123] J. H. Holland, Adaptation in Natural and Artificial Systems, MIT Press, 1992.

[124] L. Chambers, The Practical Handbook of Genetic Algorithms: Applications, Second Edition, Chapman&Hall/CRC, 2000.

[125] R. D. Zimmerman, C. Murillo Sanchez, R. Thomas, C. Murillo Saffinchez, R. Thomas, MATPOWER: Steady-State Operations, Planning, and Analysis Tools for Power Systems Research and Education, Power Systems, IEEE Transactions on 26 (1) (2011) 12–19. doi:10.1109/TPWRS.2010.2051168.

[126] G. W. Chang, S. Y. Chu, H. L. Wang, An Improved Backward/Forward Sweep Load Flow Algorithm for Radial Distribution Systems, IEEE Transactions on Power Systems 22 (2) (2007) 882–884. doi:10.1109/TPWRS.2007.894848.
URL http://ieeexplore.ieee.org/document/4162583/

[127] C. G. L. (ed.), Atificial Life: An overview, MIT Press, 1997.

[128] J. C. Cebrian, N. Kagan, Reconfiguration of distribution networks to minimize loss and disruption costs using genetic algorithms, Electric Power Systems Research 80 (1) (2010) 53–62. doi:10.1016/j.epsr.2009.08.005.

[129] T. Lu, Z. Wang, Q. Ai, W.-J. Lee, Interactive Model for Energy Management of Clustered Microgrids, IEEE Transactions on Industry Applications 9994 (c) (2017) 1–1. doi:10.1109/TIA.2017.2657628.

[130] P. Georgilakis, N. Hatziargyriou, Optimal distributed generation placement in power distribution networks: models, methods, and future research, IEEE Transactions on Power Systems 28 (3) (2013) 3420–3428. doi:10.1109/TPWRS.2012.2237043.

[131] M. E. Baran, F. F. Wu, Optimal capacitor placement on radial distribution systems, IEEE Transactions on Power Delivery 4 (1) (1989) 725–734. doi:10.1109/61.19265.

[132] S. A. Arefifar, Y. A. R. I. Mohamed, T. H. M. El-Fouly, Supply-adequacy-based optimal construction of microgrids in smart distribution systems, IEEE Transactions on Smart Grid 3 (3) (2012) 1491–1502. doi:10.1109/TSG.2012.2198246.

[133] S. A. Arefifar, Y. A. R. I. Mohamed, T. H. M. El-Fouly, Optimum microgrid design for enhancing reliability and supply-security, IEEE Transactions on Smart Grid 4 (3) (2013) 1567–1575. doi:10.1109/TSG.2013.2259854.

[134] A. R. Malekpour, A. Pahwa, Radial Test Feeder including primary and secondary distribution network, 2015 North American Power Symposium (NAPS) (2015) 1–9doi:10.1109/NAPS.2015.7335222.

[135] IESO, IESO (2017).
URL http://ieso.ca/

[136] Q. Wang, G. Lu, X. Li, Y. Zhang, Z. Yun, D. Bian, Real - time Optimization of Distributed Energy Storage System Operation Strategy Based on Peak Load Shifting, IOP Conference Series: Earth and Environmental Science 108 (2018) 052014. doi:10.1088/1755-1315/108/5/052014.
URL http://stacks.iop.org/1755-1315/108/i=5/a=052014?key=crossref.db1d4ab11d042d1a702cc7229581443d

[137] L. Yao, Z. Damiran, W. H. Lim, Optimal Charging and Discharging Scheduling for Electric Vehicles in a Parking Station with Photovoltaic System and Energy Storage System, Energies 10 (4) (2017) 550. doi:10.3390/en10040550.
URL http://www.mdpi.com/1996-1073/10/4/550

[138] K. Rahbar, J. Xu, R. Zhang, Real-Time Energy Storage Management for Renewable Integration in Microgrid: An Off-Line Optimization Approach, IEEE Transactions on Smart Grid 6 (1) (2015) 124–134. doi:10.1109/TSG.2014.2359004.

[139] K. Rahbar, M. R. V. Moghadam, S. K. Panda, Real-time Shared Energy Storage Management for Renewable Energy Integration in Smart Grid, arXiv:1706.00620 [cs]ArXiv: 1706.00620.
URL http://arxiv.org/abs/1706.00620

[140] J. S. Kim, H. Yang, S. G. Choi, Distributed real-time stochastic optimization based ESS management strategy for residential customers, in: 2017 19th International Conference on Advanced Communication Technology (ICACT), 2017, pp. 321–325. doi:10.23919/ICACT.2017.7890107.

[141] S. Korjani, M. Mureddu, A. Facchini, A. Damiano, Aging cost optimization for planning and management of energy storage systems, Energies 10 (11) (2017) 1916. doi:10.3390/en10111916.
URL http://www.mdpi.com/1996-1073/10/11/1916

[142] S. Paoletti, M. Casini, A. Giannitrapani, A. Facchini, A. Garulli, A. Vicino, Load forecasting for active distribution networks, in: IEEE PES Innovative Smart Grid Technologies Conference Europe, 2011. doi:10.1109/ISGTEurope.2011.6162780.

[143] G. E. P. Box, G. M. Jenkins, G. C. Reinsel, Time series analysis: Forecasting and Control, 2008.

[144] G. D'Agostino, A. Scala, Networks of Networks: The Last Frontier of Complexity, Understanding Complex Systems, Springer International Publishing, 2014. doi:10.1007/978-3-319-03518-5.
URL http://link.springer.com/book/10.1007%2F978-3-319-03518-5

[145] L. Euler, Solutio problematis ad geometriam situs pertinentis, Comment. Acad. Sci. U. Petrop. 8 (1736) 128–140.

[146] D. Konig, Theorie der endlichen und unendlichen Graphen, Lipsia, Akademische Verlagsgesellschaft, 1936.

[147] D'Agostino, G., Scala, A., Zlatić, V., Caldarelli, G., Robustness and assortativity for diffusion-like processes in scale-free networks, Europhys Lett 97 (6) (2012) 68006. doi:doi:10.1209/0295-5075/97/68006.

[148] D. J. Watts, S. H. Strogatz, Collective dynamics of 'small-world' networks., Nature 393 (6684) (1998) 440–2. doi:10.1038/30918.

[149] A. Barabasi, R. Albert, Emergence of scaling in random networks, Science 286 (5439) (1999) 509–512. doi:DOI:10.1126/science.286.5439.509.

[150] C. Kennedy, I. D. Stewart, M. I. Westphal, A. Facchini, R. Mele, Keeping global climate change within 1.5 ^{o}C through net negative electric cities, Curr. Opin. Environ. Sustain. 30 (2018) 18–25. doi:10.1016/j.cosust.2018.02.009.

[151] G. Balaban, G. C. Lazaroiu, V. Dumbrava, C. A. Sima, Analysing Renewable Energy Source Impacts on Power System National Network Code, Inventions 2,23. doi:10.3390/inventions2030023.

[152] G. A. Pagani, M. Aiello, The Power Gridas a complex network: A survey, Physica A: Statistical Mechanics and its Applications 392 (11) (2013) 2688–2700. doi:10.1016/J.PHYSA.2013.01.023.

[153] W.-W. Kim, J.-S. Shin, J.-O. Kim, Operation Strategy of Multi-Energy Storage System for Ancillary Service, IEEE Transactions on Power Systems 8950 (c) (2017) 1. doi:10.1109/TPWRS.2017.2665669.

[154] G. Celli, S. Mocci, F. Pilo, M. Loddo, Optimal integration of energy storage in distribution networks, in: 2009 IEEE Bucharest PowerTech, 2009, pp. 1–7. doi:10.1109/PTC.2009.5282268.

[155] A. Vespignani, Complex networks: The fragility of interdependency, Nature 464 (7291) (2010) 984–985. doi:10.1038/464984a.

[156] S. V. Buldyrev, R. Parshani, G. Paul, H. E. Stanley, S. Havlin, Catastrophic cascade of failures in interdependent networks., Nature 464 (7291) (2010) 1025–8. doi:10.1038/nature08932.

[157] R. Albert, H. Jeong, A. Barabasi, Error and attack tolerance of complex networks, Nature 406 (6794) (2000) 378–82. doi:10.1038/35019019.

[158] I. Dobson, Complex Interacting Infrastructure Systems, in: 2007 40th Annual Hawaii International Conference on System Sciences (HICSS'07), IEEE, 2007, pp. 111–111. doi:10.1109/HICSS.2007.138.

[159] M. Rohden, A. Sorge, D. Witthaut, M. Timme, Impact of network topology on synchrony of oscillatory power grids, Chaos: An Interdisciplinary Journal of Nonlinear Science 24 (1) (2014) 013123. arXiv:arXiv:1305.1634v1, doi:10.1063/1.4865895.

[160] M. Mureddu, A. Facchini, A. Scala, G. Caldarelli, A. Damiano, A Complex Network Approach for the Estimation of the Energy Demand of Electric Mobility, Sci. Rep. 8 (1) (2018) 1–8. doi:10.1038/s41598-017-17838-5.

[161] A. Giannitrapani, S. Paoletti, A. Vicino, D. Zarrilli, Optimal Allocation of Energy Storage Systems for Voltage Control in LV Distribution Networks, IEEE Trans. Smart Grid 8 (6) (2017) 2859–2870. doi:10.1109/TSG.2016.2602480.

[162] M. Sedghi, A. Ahmadian, M. Aliakbar-Golkar, Optimal storage planning in active distribution network considering uncertainty of wind power distributed generation, IEEE Transactions on Power Systems 31 (1) (2016) 304–316. doi:10.1109/TPWRS.2015.2404533.

[163] S. Frank, S. Rebennack, An introduction to optimal power flow: Theory, formulation, and examples, IIE Trans. 48 (12) (2016) 1172–1197. doi:10.1080/0740817X.2016.1189626.

[164] A. Soroudi, Multi-Period Optimal Power Flow, Springer International Publishing, Cham, 2017, pp. 141–173. doi:10.1007/978-3-319-62350-4_6.

[165] E. Estrada, P. Knight, A First Course in Network Theory, 2015. doi:10.1145/2757218.2757223.

[166] J. S. Savier, D. Das, Impact of Network Reconfiguration on Loss Allocation of Radial Distribution Systems, IEEE Transactions on Power Delivery 22 (4) (2007) 2473–2480. doi:10.1109/TPWRD.2007.905370.

[167] M. E. Baran, F. F. Wu, Optimal capacitor placement on radial distribution systems, IEEE Transactions on Power Delivery 4 (1) (1989) 725–734. doi:10.1109/61.19265.

[168] S. Korjani, A. Facchini, M. Mureddu, A. Damiano, A genetic algorithm approach for the identification of microgrids partitioning into distribution networks, in: IECON 2017 - 43rd Annual Conference of the IEEE Industrial Electronics Society, 2017, pp. 21–25. doi:10.1109/IECON.2017.8216008.